BREAKING THE OBESITY-BREAST CANCER LINK: THE ROLES OF INFLAMMATION AND EPIGENETIC REPROGRAMMING

Emily L. Rossi

A dissertation submitted to the faculty of the University of North Carolina at Chapel Hill in partial fulfillment of the requirements for the degree of Doctor of Philosophy in the Department of Nutrition.

Chapel Hill
2017

Approved by:

Stephen D. Hursting

Melinda A. Beck

William B. Coleman

Scott J. Bultman

Sergey Krupenko

©2017
Emily L. Rossi
ALL RIGHTS RESERVED

ABSTRACT

Emily L. Rossi: Breaking the Obesity-Breast Cancer Link: The Roles of Inflammation and Epigenetic Reprogramming
(Under the direction of Stephen D. Hursting)

Obesity-associated adipose tissue remodeling, including adipocyte hypertrophy, contributes to a chronic state of low-grade inflammation that promotes breast cancer growth through multiple signaling pathways. Inflammation is often regulated and perpetuated by epigenetic modifications, including aberrant DNA methylation. However, the precise relationship between obesity-associated inflammation, epigenetic modifications and breast cancer has not been clearly elucidated. Furthermore, the plasticity of obesity-associated DNA methylation and impact on tumor growth after weight loss remains unclear.

We hypothesized that targeting obesity-associated inflammation would be critical to reduce mammary tumor growth. We found that anti-inflammatory supplementation (Resveratrol or Sulindac) in obese mice reduced mammary tumor growth in association with decreased adipocyte size, influx of macrophages, and expression of pro-inflammatory mediators in the mammary tissue. We then tested if obesity-associated inflammation was reversible with weight loss by low-fat diet (LFD) and found that the pro-tumorigenic effects of obesity and aberrant methylation of inflammatory genes persists after weight loss. Considering the substantial evidence demonstrating that weight loss via bariatric surgery reduces cancer risk, we established a surgical sleeve

gastrectomy (SG) protocol in our mouse model of obesity. We demonstrated that weight loss via surgery and LFD was equally effective at reducing body weight, but produced differential effects on tumor growth and systemic inflammation. Mice that lost weight via SG, but not LFD alone, had reduced tumor growth compared to obese mice. Additionally, mice that received SG had more effectively reversed expression of pro-inflammatory mediators and aberrant DNA methylation of metabolism related genes observed in obese mice.

Our results that 1) targeting inflammation reduces mammary tumor growth in obese mice; 2) pro-inflammatory gene expression and aberrant methylation of inflammatory-related genes persists after weight loss by diet; 3) weight loss via surgery, but not LFD, significantly reduces tumor growth and more effectively reverses obesity-induced aberrant methylation. We have identified the critical mechanisms underlying the protective effects of anti-inflammatory supplementation or bariatric surgery as preventing adipocyte hypertrophy and macrophage infiltration, decreasing expression of pro-inflammatory mediators, and normalizing DNA methylation in the mammary tissue. These results could inform the development of mechanism-based strategies to more precisely intervene to prevent obesity-related cancers.

ACKNOWLEDGEMENTS

I would like to thank my mentor, Steve Hursting, for providing me with a research environment where the only failure was not taking risks. His unmatched patience and ability to see the good in others will inspire me indefinitely. I know I will continue to rely on Steve for his advice and I look forward to future collaborations.

I would also like to thank my committee members for their time and service and for their contributions to my development. Dr. Beck encouraged me to design experiments to more closely identify molecular mechanisms at play. Dr. Krupenko consistently provided helpful advice on displaying data. Dr. Coleman instructed my most valuable and enjoyable course at UNC and provided an invaluable translational perspective that has helped keep my research relevant. Dr. Bultman, a fellow Wisconsin native, was instrumental in my research progress and continually contributed to experimental design as well as providing enthusiasm.

I would like to thank all of the current and former members of the Hursting lab, particularly Laura Bowers who regularly engaged in scientific debate with me, resulting in revised experimental design and revisions in writing. Subreen Khatib has made significant contributions to this work and has also inspired me to meet my potential as a cancer researcher and finish strong. Steven Doerstling has also been instrumental in the evolution of my research and I have greatly benefited from his contagious work ethic. I would also like to thank Ciara O'Flanagan, Erika Tlsty, and Emma Allott for their

significant contributions to this work. I would also like to thank Mahmoud Shobair and John Terry for their friendship and relieving me of my dog-mom responsibilities so I could complete this dissertation.

Finally I am forever grateful to all four of my parents Steven and Ingrid Richardson and Bob and Mary Rossi for supporting me during my graduate career. I am thankful that my parents not once laughed at a joke about me dropping out of graduate school in the past five years.

TABLE OF CONTENTS

LIST OF TABLES

LIST OF FIGURES

LIST OF ABBREVIATIONS

13-HODE	13-hydroxyoctadecadienoic acid
5-HETE	5-hydroxyeicosatetraenoic acid
AA	Arachidonic acid
Adig	Adipogenin
AMP	Adenosine monophosphate
AMPK	AMP-activated protein kinase
ATGL	Adipose triglyceride lipase
ATP	Adenosine triphosphate
$ATpO_2$	Adipose tissue partial pressure
Bcl-2	B-cell lymphoma 2
BLBC	Basal-like breast cancer
BMI	Body mass index
Cebp α	CCAAT/enhancer binding protein α
CI	Confidence interval
CLBC	Claudin-low breast cancer
CLS	Crown-like structures
COX-1	Cyclooxygenase 1
COX-2	Cyclooxygenase 2
CR	Calorie restricted
CXCL2	Chemokine (C-X-C motif) ligand 2

DGAT-2	Diacylglycerol O-Acyltransferase 2
DIO	Diet-induced obesity
DNA	Deoxyribonucleic acid
DM	Diabetes mellitus
DMBA	7,12-Dimethylbenzanthracene
EMT	Epithelial-mesenchymal transition
ER	Estrogen receptor
FA	Fatty acid
Fabp4	Fatty acid binding protein 4
FFA	Free fatty acids
Fgf2	Fibroblast growth factor 2
FOb	Formerly obese
Foxc2	Forkhead Box C2
GLUT-4	Glucose transporter type 4
GM-CSF	Granulocyte macrophage colony-stimulating factor
H&E	Hematoxylin and eosin
HER2	Human epidermal growth factor 2
HIF-1α	Hypoxia-inducible factor 1-alpha
HOMA-IR	Homeostatic model assessment of insulin resistance
HPLC	High-performance liquid chromatography
HR	Hormone receptor
HSL	Hormone-sensitive lipase
IFN-γ	Interferon gamma

IGF-1	Insulin-like growth factor-1
IGFBP	Insulin-like growth factor binding protein
IGT	Impaired glucose tolerance
IHC	Immunohistochemistry
IL-6	Interleukin 6
IRS	Insulin receptor substrate
IRS-1	Insulin receptor substrate-1
IRS-2	Insulin receptor substrate-2
LA	Linoleic acid
LC/MS/MS	Liquid chromatography/tandem mass spectroscopy
LFD	Low-fat diet
Lpl	Lipoprotein lipase
M-CSF	Macrophage colony-stimulating factor
MCP	Monocyte chemoattractant protein
MIF	Macrophage inhibitor factor
MMP-9	Matrix metalloproteinase-9
mTORC	Mechanistic target of rapamycin complex
NGT	Normal glucose tolerance
NOS2	Nitric oxide synthase
NR	Nuclear receptor
NSAID	Nonsteroidal anti-inflammatory drug
OR	Odds ratio
PG	Prostaglandin

PPARγ	Proliferator-activated receptor gamma
PR	Progesterone receptor
Prdm16	PR domain containing 16
PUFA	Polyunsaturated fatty acids
qMR	Quantitative magnetic resonance
qPCR	Quantitative polymerase chain reaction
Rb	Retinoblastoma protein
RR	Risk ratio
RT	Room temperature
RT-PCR	Real time polymerase chain reaction
RYGB	Roux-en Y gastric bypass
s.d.	Standard deviation
SERMs	Estrogen-receptor response modulator
SOCS1	Suppressor of cytokine signaling-1
SOS	Swedish Obese Subjects
TICs	Tumor-initiating cells
TNBC	Triple-negative breast cancer
TNF-α	Tumor necrosis factor alpha
TSS	Transcription start site
TXB2	Thromboxane B2
TZD	Thiazolidinediones
Ucp1	Uncoupling protein 1
VAT	Visceral adipose tissue

VEGF	Vascular endothelial growth factor
WAT	White adipose tissue
WHR	Waste-to-hip ratio

CHAPTER I. INTRODUCTION

A. Obesity and breast cancer

The prevalence of obesity, an established risk and prognostic factor for several chronic diseases including many cancers, is at an unprecedented rate [1]. Currently, nearly 40% of adults and 20% of children are considered obese, defined as having a body mass index (BMI) > 30 kg/m^2 [1,2]. The percent of U.S. adults that are at a healthy weight, defined by a BMI of 18.6-24.9 kg/m^2 is only 28%, which has fallen by more than 4% in the past ten years [1,2]. Overall, data from the National Health and Nutrition Examination Survey (NHANES) in 2013-2014 show that Americans are more likely to meet physical activity guidelines and less likely to have high cholesterol and smoke cigarettes than ever before. However, rates of diabetes, metabolic syndrome, and the number of adults that moderately and heavily consume alcohol continues to rise [3]. For the first time since 1986, the average life expectancy has plateaued for three sequential years [1].

Approximately 85,000 new cancer cases per year are attributed to obesity in the United States [4]. A prospective study in the U.S. by Calle et al. found that compared to normal weight women (BMI < 25 kg/m^2) the risk of developing cancer is 8% higher in overweight women (BMI = 25-29.9 kg/m^2), 18% higher in women with Class I obesity (BMI = 30-34.9 kg/m^2), 32% higher in women with Class II obesity (BMI = 35-39.9 kg/m^2), and 62% higher in women who are severely obese (BMI ≥ 40) [5]. In the same

study a significant positive association between BMI and death from cancer of the esophagus, colon and rectum, liver, gallbladder, pancreas and kidney for both men and women. Additionally, the relationship was also observed in stomach and prostate cancer in men and death from cancer of the breast, uterus, cervix and ovary in women. Calle et al. extended their findings by estimating the fraction of deaths due to cancer in the U.S. that are attributable to a BMI ≥ 25 kg/m^2 which was estimated to be 14% of all deaths from cancer in men and 20% of all cancer deaths in women [5].

In its 2007 review The World Cancer Research Fund (WCRF) reported that there is convincing epidemiological and plausible mechanistic evidence for the link between excessive body fatness and postmenopausal breast cancer. However, an inverse relationship was reported between BMI and premenopausal breast cancer. Currently, a substantial amount of literature conflicts with an equally substantial amount of literature on the role of obesity and premenopausal breast cancer. A limitation of several epidemiological studies is the disregard for the five subtypes of breast cancer, which alludes to its complexity as a disease. The relationship between obesity and breast cancer risk is possible to disentangle when comparisons are made with regard to breast cancer subtype, in addition to stratifying by menopausal status and also assessing risk differences by race.

1. Obesity differentially impacts the five major molecular subtypes of breast cancer

Breast cancer is an immensely heterogeneous disease with five molecular subtypes differing in cellular origin, molecular characteristics, and factors that promote growth [6-8]. Breast cancer subtypes are dictated in part by hormone receptor (HR)

status, which is precedent in clinical characteristics and response to treatment. Determining the expression of estrogen receptor (ER), progesterone receptor (PR) and human epidermal growth factor 2 (HER2) and stratifying tumors as either 'positive' (possessing a detectible level) or 'clinically negative' (displaying no to minimal detection, >1%) contributes to the stratification of the five major molecular subtypes (Table 1.1) [9].

Table 1.1. Summary of the five major molecular subtypes of breast cancer

	Luminal A	Luminal B	HER2 - enriched	Triple-negative	Normal breast-like
ER	+	+	-	-	
PR	+ or -	+ or -	-	-	
HER2	-	+	+	-	
Percent of all breast cancers [10]	30-40%	20-25%	10-15%	10-25%	1-5%
Outcome [10]	Good	Intermediate	Poor	Poor	Intermediate
Targeted Therapy	SERMs, Aromatase inhibitors	SERMs, Aromatase inhibitors	Herceptin	-	-
Enrichment of mutations [5,11-14]	GATA3, FOXA1, RUNX1	KCNB2	HER2E, PIK3CA	BRCA1, TP53	
Stage IV patients median overall survival [15]	36 months (95% CI 34.1, 37.9)	44 months (95% CI undetermined)	34 months, (95% CI 27.4, 40.6)	13 months (95% CI 12.2, 13.9)	Data not available
Most common site of distant metastasis [15]	Bone	Bone	Liver	Brain and/or lung	Data not available

In a landmark study, a classification gene list for intrinsic breast tumor subtype was put forth by Hu et al. in 2006 termed the Intrinsic/UNC gene set. The intrinsic list contains over 1,000 genes and gene expression signatures for proliferation and hypoxia that assist in further characterizing the subtypes as well as predicting response to

treatment and prognosis [13]. Molecular characterization using gene expression signatures, also referred to as “molecular taxonomy,” has been especially advantageous for triple-negative breast cancer (TNBC). The claudin-low breast cancer (CLBC) and basal-like breast cancer (BLBC) subtypes, which are both in the triple-negative category, are impacted by dietary energy balance modulation in humans and mice and often confer a worse prognosis, at least in part due to a lack of established mechanistic targets or therapies [16,17]. Several biological features of CLBC and BLBC are better understood in the context of molecular taxonomy characterization. CLBC is the only subtype that displays a gene expression signature enriched in genes associated with tumor-initiating cells (TICs; also referred to as cancer stem cells). CLBC also displays histological stem cell features and the ability to easily undergo epithelial-mesenchymal transition (EMT). Sequencing of CLBC tumors also revealed that they have low expression of genes encoding cell-cell junction proteins and high immune cell infiltrate [18-20]. BLBC express cytokeratins 5, 6, or 17, which are typically exclusively expressed in the basal epithelial layer of the skin and airways, thus earning their name “basal-like” [14]. BLBC are exceedingly proliferative, which is related to the loss of tumor suppressor retinoblastoma protein (Rb), resulting in loss of cell cycle regulation. In vitro silencing of Rb sensitizes cells to cyclooxygenase 2 (COX-2) upregulation [21]. Gauthier et al. found that approximately 50% of all basal-like tumors overexpress COX-2, and vertically all luminal and HER2 positive tumors express low mRNA levels of COX-2 [21]. In 2009 Hu et al. again employed microarrays to analyze breast tumors but built on previous findings to distinguish gene expression patterns to distinguish primary from metastatic tumors. In this study, a 13-gene hypoxia signature was developed. The

hypoxia signature includes eight genes that contain a hypoxia-inducible factor 1-alpha (HIF-1α) binding site, enabling regulation. The hypoxia signature is observed to the greatest extent in BLBC and CLBC out of all breast cancer subtypes interrogated [22].

2. The effects of obesity on breast cancer risk are dependent upon menopausal status

The results of numerous studies consistently show that obesity increases the risk of breast cancer in postmenopausal women and the risk of triple-negative breast cancer in premenopausal women. The results of a meta-analysis of 61 data sets, which included 41,406 cases of breast cancer, suggest that postmenopausal breast cancer cases are largely responsible for the positive association between obesity and breast cancer risk. In the study by Wang et al. the risk ratio (RR) (per 5 kg/m^2 increase) in females for breast cancer was significant (RR = 1.07; 95% CI 1.05, 1.09). There was essentially no effect in premenopausal cases of breast cancer (RR = 0.99; 95% CI 0.97, 1.01) but a stronger effect in postmenopausal breast cancer (RR = 1.11; 95% CI 1.08, 1.14) [23].

The Fred Hutchinson Cancer Research Center conducted a population-based case-case study that included 2,659 women aged 20-69 years diagnosed with invasive breast cancer, designating patients with luminal A breast cancer as the reference group. In their analysis, Chen et al. reported that obese premenopausal women had an 82% increased risk (OR = 1.82; 95% CI 1.32, 2.51) of triple-negative breast cancer compared to normal weight women (BMI < 25 kg/m^2) [24]. In this study, however, authors found that in postmenopausal women obesity was associated with reduced risks of triple-negative and HER2-overexpression breast cancer. These findings were compared to

the luminal A patients, and the authors noted that their results implicated obesity in the etiology of postmenopausal luminal A breast cancer, rather than absolving obesity from contribution to triple-negative breast cancer risk [24]. Analysis on the effects of obesity on postmenopausal breast cancer risk using data from the Women's Health Initiative showed similar associations in both ER-positive and triple-negative postmenopausal breast cancer risk. In fact, the hazard ratio for breast cancer was increased for ER-positive breast cancer in the third BMI quartile (BMI = 26.9 – 31.04 25 kg/m^2; ER-positive OR = 1.17; 95% CI 1.03, 1.33) and for triple-negative (OR = 1.21; 95% CI 0.83, 1.77). Similar results were observed in the fourth BMI quartile in ER-positive (BMI > 31.05 kg/m^2; ER-positive OR = 1.39; 95% CI 1.22, 1.58) and triple-negative breast cancer (OR = 1.35; 95% CI 0.92, 1.99) [25]. Therefore, case-case studies comparing the relationship between obesity and postmenopausal breast cancer risk which utilize luminal A / ER-positive breast cancer as a reference may fail to unveil a positive association of obesity on postmenopausal triple-negative breast cancer risk.

Pierobon et al. conducted a meta-analysis, which pooled multiple studies to investigate the effects of obesity on triple-negative breast cancer risk. In a case-case comparison, obese women were more likely to be diagnosed with triple-negative breast cancer (OR = 1.20; 95% CI 1.03, 1.40) than non-obese women (BMI < 30 kg/m^2). Similar to the results from the Fred Hutchinson Cancer Research Center, this finding was driven by the premenopausal women (OR = 1.43; 95% CI 1.23, 1.65) who were found to have increased breast cancer risk if obese compared to postmenopausal women (OR = 0.99; 95% CI 0.79, 1.24). Five studies were included in the meta-analysis for premenopausal women, which included two studies with significant positive findings

(Millikan et al. (OR = 1.65; 95% CI 1.16, 2.34) and Yang et al. (OR = 1.63; 95% CI 1.31, 2.03)) and three with non-significant findings but an OR greater than 1.0. Of the six studies included in the meta-analysis for postmenopausal women, one study by Yang et al. reported a positive finding (OR = 1.21; 95% CI 1.03, 1.41). Four reported a non-significant effect with three reporting an OR greater than 1.0 and one reporting an OR less than 1.0. Notably only one study in the meta-analysis possessed a significant negative association by Lara-Medina et al. (OR = 0.55; 95% CI 0.38, 0.80), which drove the pooled OR results in postmenopausal women. In the original study, Lara-Medina et al. reported that postmenopausal women who had a healthy BMI (< 25 kg/m^2) *or* were overweight BMI (<30 kg/m^2) were more likely to have triple-negative breast cancer with a much more significant effect in the overweight ($P < 0.001$) than healthy ($P = 0.27$) women [26]. Thus, it appears that a positive relationship in postmenopausal women between being overweight and triple-negative breast cancer contributed to a negative association between obesity and triple-negative breast cancer.

Data from the Nurses Health Study provided insight that weight gain in young adulthood may be a more important determinant of breast cancer risk than obesity at time of diagnosis. Women with above-average weight gain, who were not necessarily obese (RR = 1.19; 95% CI 1.08, 1.31) and consistently obese women (RR = 1.06; 95% CI 0.95, 1.17) were both at increased risk of breast cancer compared to women who were average rate (reference, RR = 1.0) and women who maintained a stable weight (RR = 0.92; 95% CI 0.88, 0.96) [27]. Findings from the European Prospective Investigation into Cancer and Nutrition (EPIC) revealed a positive association between breast cancer risk and changes in weight in postmenopausal but not premenopausal

women [28]. Interestingly, 13% of postmenopausal women in the EPIC study had lost weight between age 20 and age at study entry. The remaining 87% of women had gained an average of 13.5 ± 9.5 kg, resulting in an average gain for postmenopausal women of 11.0 kg during adulthood [28].

3. Obesity negatively impacts breast cancer prognosis

The effects of obesity on breast cancer prognosis are generally more consistent across subtypes, and individuals with breast cancer that are obese are more likely to be resistant to treatment and develop metastases and recurrence [29]. Greater rates of metastatic breast cancer and increased mortality are seen in the obese breast cancer patient population, independent of disease stage at diagnosis [30-32]. A very large meta-analysis of 82 follow-up studies found that each 5 kg/m^2 increment of BMI before diagnosis resulted in a 18% increase in breast cancer mortality [32]. Cakar et al. reported that obesity was associated with a poorer overall survival in postmenopausal TNBC patients, but that effect was lost when all patients (pre and postmenopausal) were evaluated [33]. In a retrospective study on 418 breast cancer patients (124 normal weight, 130 overweight, 164 obese), Ademuyiwa et al. found no association between obesity and recurrence-free survival or overall survival [34]. A recent meta-analysis of 21 studies pooled hazard ratios and found a significant association between obesity and overall survival in breast cancer in hormone receptor-positive (HR = 1.31; 95% CI 1.17, 1.46) and hormone receptor-negative cancer (HR = 1.18; 95% CI 1.06, 1.31). The same association driven by obesity was seen in positive and negative subtypes for breast cancer-specific survival, which was increased in hormone receptor-positive (HR = 1.36;

95% CI 1.20, 1.54) and in hormone receptor-negative breast cancer (HR = 1.46; 95% CI 1.11, 1.71) [17].

In addition to inducing systemic inflammation and altered growth factor signaling, which promotes the aggressive triple-negative breast cancer subtype, obesity also enhances a highly treatable ER-positive subtype of breast cancer (luminal A). Postmenopausal women are more likely to be diagnosed with ER-positive breast cancer, which obesity promotes by enhancing production of non-ovarian estrogen via increased aromatase activity in adipose stromal cells [35,36]. ER-positive breast cancer is highly treatable with hormonal therapy, including selective estrogen-receptor response modulators (SERMs) and aromatase inhibitors. Thus, obesity is strongly associated with decreased overall breast cancer survival in postmenopausal women, with subtype-specific effects including links between obesity and TNBC prognosis, particularly in premenopausal women [5,17].

4. Conflicting results on breast cancer risk after weight loss

The impact of weight loss following chronic obesity on breast cancer risk is poorly understood, and the effects of weight loss interventions on obesity-associated inflammation, epigenetic alternations, and breast cancer are unknown. A recent study by Han et al. eludes to the difficulty in studying weight loss and cancer risk. Using data from the Atherosclerosis Risk in Communities cohort that includes data from 13,901 U.S. adults, researchers reported that 77% of women and 62% of men were normal weight at age 25. However, at study baseline (1987-1989) when participants were 45-64 years old, only 36% of women and 27% of men were within the normal weight range [37]. Both the increasing prevalence of overweight and obesity, and the tendency for

individuals to gain weight with age, renders a study population that lost weight and maintained weight loss difficult to obtain [38-40]. In a study of 124 obese adults, weight loss peaked at month six of the twelve month program, with 54% of participants having lost more than 5% of their initial body weight. At the end of the program (month twelve) only 33% had lost and maintained 5% of their body weight [41]. Mason et al. reported auspicious results in a randomized controlled trial investigating the effects of dietary weight loss and exercise on insulin sensitivity in 439 inactive, overweight or obese postmenopausal women. Women assigned to the dietary weight loss intervention on average lost 9.1 lbs and 9.9% body fat after twelve months, which conferred a 21.8% decrease in insulin levels relative to baseline [42]. Interestingly no additional benefit was observed in the women assigned to the dietary weight loss + exercise (225 minutes/week of aerobic exercise) compared to the diet alone group. While these findings are promising, cancer is a chronic disease, and delineating the exact impact on breast cancer after weight loss is achieved remains a formidable endeavor.

Data from the Iowa Women's Health Study demonstrated that weight loss prior to menopause was potentially effective at decreasing postmenopausal breast cancer risk. The study looked at weight changes during two periods, the first age 18 to 30 years, the second period spanned age 30 years to menopause. The study used the group of women who gained weight during both periods of as a reference group, thus one is not able to discern a decrease in breast cancer risk due to weight loss independent of current weight, as the reference group had a baseline BMI that was obese (BMI = 30.1 kg/m^2). However, the study did find that women who gained weight during the first period from age 18-30 years, but then lost weight from age 30 years to menopause, had

a reduced risk of postmenopausal breast cancer (RR = 0.62; 95% CI 0.47, 0.82) compared to women who gained weight during both periods. Their change in risk is not especially impressive considering that women who gained weight age 18-30 years but then maintained their weight also had a reduced risk compared to women who gained weight during both periods (RR = 0.76; 95% CI 0.66, 0.88). In the same study Harvie et al. also reported that weight loss or maintenance from age 18-30 years, followed by weight gain from age 30 years to menopause had similar risk (RR = 0.91; 95% CI 0.81, 1.03) to women who had gained weight during both periods [43].

Multiple studies have reported that surgical weight loss is overwhelmingly effective at producing significant weight loss and reductions in obesity-associated metabolic perturbations. In one of the most compelling arguments in support of bariatric surgery, the Swedish Obese Subjects (SOS) intervention study reported that 845 surgically treated patients had lost 28 ± 15 kg at two years after baseline, compared to the 845 matched control patients who received conventional obesity treatment and lost 0.5 ± 8.9 kg [44]. A meta-analysis that investigated the outcome of 621 weight loss studies found that 78.1% of diabetic patients had complete resolution of diabetes 2 years after bariatric surgery, and diabetes was improved or resolved in 86.6% of patients [44]. Evidence suggests that surgical weight loss abates metabolic perturbations in part through an epigenetic mechanism. Obese individuals displayed increased methylation in the promoter of inflammatory related genes, including IL-1β, IL-6, and TNF-α , 12 months after Roux-en Y gastric bypass (RYGB) compared to baseline levels [45]. Notably, both gene expression and methylation profiles returned to levels seen in normoweight healthy control subjects that were also analyzed. Barres et al. reported

that by time of discharge the aberrant methylation of regulatory lipid metabolism genes in skeletal muscle biopsies from obese individuals was ameliorated in those that received RYGB by time of discharge [46]. Anveden et al. completed a prospective study matching 1,420 women from the SOS cohort that received bariatric surgery with 1,447 matched controls that received conventional obesity treatment to investigate the effect of bariatric surgery on long-term incidence of female-specific cancer. Women who received bariatric surgery had a reduced risk of overall cancer (HR = 0.71; 95% CI 0.59, 0.85; $P < 0.001$) and a non-significant reduction in breast cancer (HR = 0.75; 95% CI 0.51, 1.10; $P = 0.142$). As a study limitation the researchers cited that the participants in the surgery group had received vertical banded gastroplasty or banding, as the technology of bariatric surgery has advanced and those methods are not currently utilized. Thus, the type of surgical procedure, which likely impacts recovery and adverse side effects, could influence the result towards a non-significant trend. Christou et al. completed a observational 2-cohort study of 1,035 morbidly obese patients that received bariatric surgery at the McGill University Health Centre and 5,746 matched morbidly obese controls that had not been treated surgically. The majority (73.4%) of the bariatric surgery cohort had received Roux-en Y isolated gastric bypass, and 97% of the procedures were performed by four surgeons. The risk of cancer during the five year follow-up in the bariatric surgery cohort was profoundly decreased (RR = 0.22; 95% CI 0.14, 0.35; $P < 0.001$) compared to controls. Furthermore, the risk of breast cancer in the bariatric surgery cohort (RR = 0.17; 95% CI 0.98, 0.31; $P < 0.001$) maintained the significant reduction in risk relative to controls [47].

B. Molecular mechanisms mediating the effects of obesity on breast cancer growth and progression

The driving phenomenon behind the obesity-breast cancer link is the metabolic pertubations often accompanying obesity, notably insulin resistance and a decreased adipogenic capacity, which fuel the growth of cancer cells (Figure 1.1). In obesity, excess energy is converted to triacylglycerol and stored in various adipose tissue depots throughout the body.

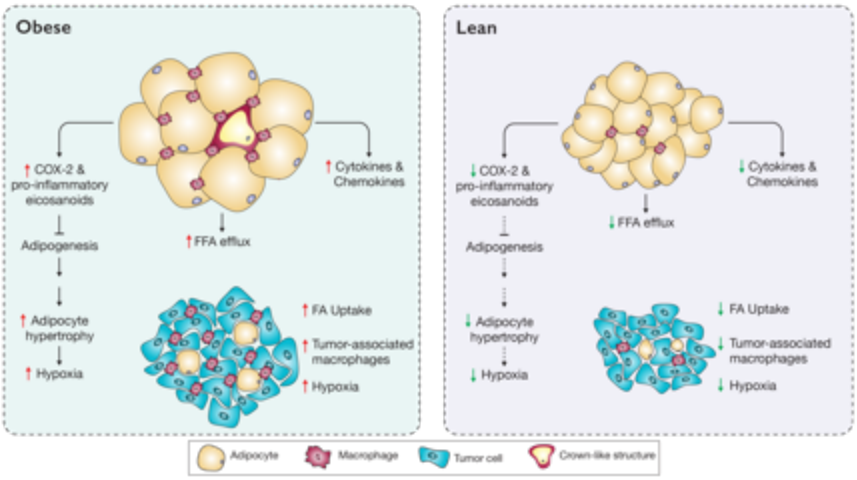

Figure 1.1. Molecular mechanisms mediating the effects of obesity on breast cancer growth and progression. The connection between obesity-associated metabolic dysregulation and inflammation is largely mediated through aberrant adipose tissue remodeling. At a basic level, excess energy balance results in hypertrophied adipocytes which secrete factors recruiting and activating macrophages in amounts proportionate to adipocyte size (i.e. the larger the adipocyte, the greater amount of factors secreted). In addition to directly promoting tumor growth, metabolic dysregulation in obesity contributes to a growth-promoting milieu enhancing cross-talk between tumor cells and macrophages, adipocytes and fibroblasts.

The obese state is thus associated with profound expansion of the adipose tissue, which occurs by adipocyte hyperplasia (increase in adipocyte number) or hypertrophy (increase in adipocyte size). In obese adults, hypertrophy predominates as the mechanism to support the growth in adipose tissue [48]. Adipocyte hypertrophy, and

the associated fatty acid spill over, is strongly implicated in insulin resistance and other obesity-associated metabolic perturbations (Table 1.2.).

Table 1.2. Studies on adipocyte hypertrophy in humans and mice		
	Study population	**General finding**
Human Studies		
Henninger et al. [49]	non-obese subjects with genetic predisposition for type II DM and matched controls (total n = 17)	Subjects with genetic predisposition to type II DM had significantly larger adipocyte cell size despite equivalent age, BMI, and WHR to control subjects without genetic predisposition. In subjects with genetic predisposition to type II DM adipocyte size was associated with fasting insulin (R = 0.69; $P < 0.01$) and HOMA-IR (R = 0.64; $P < 0.02$).
Arner et al. [50]	764 subjects with BMI 18-60 kg/m^2	Occurrence of hyperplasia (negative morphology value) or hypertrophy (positive morphology value) was independent of sex and body weight but correlated with fasting plasma insulin levels and insulin sensitivity.
Weyer et al. [51]	280 Pima Indians with either normal (NGT), impaired (IGT), or diabetic glucose tolerance	Relative to those with NGT, mean subcutaneous abdominal adipocyte size was 19% higher in diabetic subjects and 11% higher in IGT subjects, despite adjusting for age, sex, and percent body fat.
Pasarica et al. [52]	Lean, obese and type II DM subjects (total n = 21)	Mean fat cell size was negatively correlated with VEGF mRNA (R = -0.7; $P < 0.01$) and capillary density (R = -0.67; $P < 0.01$) Insulin suppression of lipolysis correlated with fat cell size (R = 0.53; $P < 0.06$)
Animal Studies		
Balogun et al. [53]	Female and male C57BL/6 mice	Supplementation with Omega-3 PUFA (10% w/w) in male but not female mice, decreased adipocyte area in association with decreased mRNA expression of Fabp4, DGAT-2 and leptin in gonadal fat pads.
Jimenez-Gomez et al. [54]	Rhesus monkeys	In monkeys fed a high-fat, high-sugar diet, adipocyte distribution changed towards larger adipocytes in visceral WAT, with a decrease in the number of small adipocytes, indicative of adipocyte hypertrophy. Presence of large adipocytes was also associated with increased NF-κB activation and decreased IRS-1 and GLUT4 protein levels.

In obesity excess energy intake often results in increased growth factor signaling, in addition to adipocyte hypertrophy [55,56]. Nutrients (glucose, amino acids), growth factors and their receptors (insulin, IGF-1, VEGF) serve as ligands in the mechanistic target of rapamycin complex 1 (mTORC1) pathway. mTORC1 integrates signals from growth factors, hormones, nutrients, and cellular energy and responds by modulating the protein translation of genes which regulate cell growth, proliferation and survival accordingly [57]. An excess of activating ligands and insufficiency of inhibitors (hypoxia, AMPK conferring low energy) results in high levels of mTORC1 activation, which allows for the expression of genes and biosynthetic intermediates which promote cell proliferation and survival. Specifically, mTORC1 activation induces the translation of genes involved in ribosome biogenesis, cell cycle activators (Cyclin D1, cMYC), anti-apoptosis (Bcl-2, survivin), and metastasis (MMP-9) [58,59].

Pre-clinical studies utilizing rapamycin, an inhibitor of mTORC1 but not mTORC2 have implicated deregulated mTORC1 in adipose tissue dysregulation that occurs with obesity. Studies in mice have demonstrated that complete loss of function of mTORC1 reduces adiposity, however partial mTORC1 inhibition with rapamycin resulted in enhanced fat deposition [60,61]. Furthermore, Paschoal et al. showed that rapamycin supplementation in obese mice exacerbated adipose tissue inflammation as evidenced by an increase in activated M1 macrophages and levels of pro-inflammatory cytokines TNF-α, IL-6, and MCP-1 [61]. Mercalli et al. published concordant *in vitro* data in which rapamycin induced apoptosis of M2 macrophages, but not M1 [62].

Insulin resistance, hypoxia, and altered cytokines observed in obesity converge to deregulate mTORC1, which has detrimental consequences on adipose tissue health.

In the adipose tissue, cell fate is often dictated by the integration of cellular signals through mTORC1. Plasma FFA concentrations are approximately 20-40% greater in obese humans and mice compared to their lean counterparts [63,64]. Basal and adrenergic receptor-mediated lipolytic rates are increased in adipocytes obtained from obese women and mice [64,65]. The failure of insulin to successfully signal through the mTORC1 complex decouples nutrient status from the appropriate biological response and can ultimately deregulate the adipose tissue through multiple mechanisms with pathogenic consequences, and render an excess supply of glucose and fatty acids to fuel tumor growth.

1. Altered growth hormones in obesity

After insulin binds to the extracellular ligand binding domain of the insulin receptor, proper insulin signaling is contingent upon the subsequent intracellular phosphorylation of the insulin receptor substrate (IRS) [66]. Serine phosphorylation of IRS proteins by circulating free fatty acids and TNF-α, impairs insulin signal transduction [67]. When insulin signaling is impaired, the requirement for a higher than normal concentration of insulin to elicit a normal response is defined as insulin resistance [68]. The pathological consequence of impaired insulin signaling is the inability for insulin to i.) decrease serum glucose concentrations and ii.) inhibit lipolysis in the adipose tissue. Given that 90% of type II diabetics are obese, the relationship between obesity and impaired insulin signaling is undeniable [69]. Boyle et al. completed a meta-analysis and reported that breast cancer risk is increased by 27% in women with type II diabetes, however adjusting for BMI, the increase was only partially reduced, with a remaining 16% increased risk of breast cancer [70].

Insulin can also increase the bioavailability of insulin-like growth factor 1 (IGF-1) by inhibiting the production of its binding protein, IGFBP-1. A meta-analysis conducted by Shi et al. found a positive significant association between IGF-1 levels and premenopausal breast cancer risk (OR = 1.39; 95% CI 1.16, 1.66) [71]. However, the study did not find a significant association in postmenopausal women (OR = 0.93; 95% CI 0.80, 1.10) [71]. Animal models have demonstrated blunted metabolic and anti-cancer effects of calorie restriction when mice are supplemented with exogenous IGF-1. Calorie restricted (CR) mice that received exogenous IGF-1 displayed intermediate expression of several metabolism and cancer-related genes compared to CR and control mice. These results were in association with restored (to control levels) triple-negative mammary tumor growth in CR mice with exogenous IGF-1 [72].

The adipokines leptin and adiponectin are primarily thought of as regulators of calorie intake and energy expenditure, however they are also involved in modulating inflammation and insulin resistance. Leptin is commonly referred to as the “satiety hormone” and its actions result in activation of mTORC1 [73]. Alternatively, adiponectin activates AMP-activated protein kinase (AMPK), which is a cellular stressor indicative of low ATP stores, which inhibits mTORC1 [74]. Commonly, the onset of obesity causes individuals to become leptin resistant despite excess leptin production by the adipose tissue [75]. In many obese individuals, leptin acts directly on macrophages to stimulate the synthesis of pro-inflammatory cytokines such as TNF-α and IL-6. These effects of leptin differ greatly from those of adiponectin, which increases fatty acid oxidation and glucose uptake in skeletal muscle and decreased hepatic gluconeogenesis [73]. However, TNF-α, IL-6 and other pro-inflammatory mediators suppress adiponectin

secretion from adipocytes, and the obese population typically has low adiponectin levels.

2. Adipocyte hypertrophy and hypoxia

Adipose tissue accommodates the need to store excess triglyceride through expansion of existing adipocytes or through creation of new adipocytes from precursor cells (adipogenesis). Chronic positive energy balance in obesity promotes the aberrant expansion of existing adipocytes, which is characterized by hypertrophic adipocytes. This is in part due to the limited adipogenic capacity observed in obesity, with concordant preadipocyte arrest, as several pro-inflammatory molecules and signaling pathways inhibit adipogenesis [76]. The size of hypertrophic adipocytes exceeds the capacity of the body to supply the tissue with adequate oxygen through vascularization. Therefore, adipocyte hypertrophy promotes adipose tissue hypoxia, oxidative stress and mitochondrial dysfunction [77]. Thus, chronic positive energy balance in obesity results in the remodeling of the adipose microenvironment, resulting in hypertrophic adipocytes and increased hypoxia.

Studies of C57BL/6 mice have established strong correlations between fat pad mass and mean adipocyte size, a measure of hypertrophy [78]. Furthermore, with increasing adipocyte size the adipocyte secretome is enriched in pro-inflammatory adipokines and cytokines, including TNF-α and IL-6 [79]. Adipocyte size also positively correlates with macrophage infiltration in the adipose tissue as well as systemic insulin resistance [80,81]. TNF-α is a potent inhibitor of adipogenesis and can prevent preadipocytes from differentiating into mature adipocytes. Partially transdifferentiated

preadipocytes can possess a macrophage-like phenotype and secrete cytokines similar to macrophages [76]. Isakson et al. harvested preadipocytes from obese and non-obese adipose tissue biopsies and found that the number of preadipocytes that differentiated into adipose cells was negatively correlated with both BMI and adipocyte cell size of the donors [82].

Wueest et al. isolated adipocytes from the epididymal fat pads of C57BL/6J mice after exposure to a low-fat or high-fat diet for eight weeks. Adipocytes were separated by size resulting in small (average diameter 60.9 +/- 3.1 μM) and large (average diameter 83.0 +/- 6.6 μM) adipocytes. The large adipocytes had a basal lipolysis rate that was two-fold higher compared to the small adipocytes. This was accompanied by differences in insulin responsiveness, as insulin did not decrease lipolysis in adipocytes harvested from mice maintained on the high-fat diet, but insulin decreased lipolysis by approximately 30% in adipocytes from mice on the low-fat diet [83].

Adipose tissue hypoxia is implicated as an early event in adipose tissue dysfunction. Obese individuals tend to have a lower expression of angiogneic genes and a lower capillary density in abdominal adipose tissue compared to lean individuals [77,84]. Once activated, HIF-1α dampens metabolic flexibility by reducing the ability for fatty acid oxidation to occur [85]. Pasarica et al. utilized a euglycemic-hyperinsulinemic clamp to measure insulin sensitivity and basal and insulin-suppressed lipolysis in lean and obese human subjects. Abdominal adipose tissue biopsies were obtained to measure fat cell size in addition to assessing *in situ* adipose tissue oxygenation (defined as adipose tissue partial pressure ($ATpO_2$)) to establish associations between hypoxia and the ability of insulin to inhibit lipolysis [52]. Insulin sensitivity correlated positively

with suppression of lipolysis and lipolysis rates in the presence of insulin were significantly higher in obese vs. lean men and women. Furthermore, insulin suppression of lipolysis correlated negatively with fat cell size and positively with $ATpO_2$ [52].

3. Effects of COX-2 and pro-inflammatory eicosanoids

In obesity-induced insulin resistance, excessive adipocyte lipolysis produces pathogenic levels of free fatty acids circulation signal through toll-like receptors, activating the NF-κB pathway, which largely controls inflammation. Additional consequences of pathogenic lipolysis include enhanced cyclooxygenase COX expression and recruitment of inflammatory macrophages [86]. Macrophages that have infiltrated into adipose tissue propagate the recruitment of additional macrophages by secreting chemoattractants, including monocyte chemoattractant protein (MCP)- 1. Macrophages also induce cyclooxygenase-2 (COX-2) expression resulting in high levels of arachidonic acid metabolites including prostaglandins that disrupt fatty acid homeostasis by inhibiting adipogenesis. PGE_2 is the most abundant COX-derived product and exacerbates metabolic dysfunction in obesity by inhibiting adipogenesis, which would alleviate adipocyte hypertrophy and associated insulin resistance. Prostaglandin (PG) F2 alpha ($PGF_{2\alpha}$) and PGE_2 inhibit peroxisome proliferator-activated receptor gamma (PPARγ) [87], a transcription factor regulating adipocyte differentiation and maintenance of insulin sensitivity.

As a negative feedback mechanism, PGE_2 acts on the EP3 receptor which signals through G_i-coupled protein receptors to reduce intracellular cAMP levels to inhibit lipolysis [88]. However, this feedback mechanism is only able to inhibit lipolysis

that results from hormone-sensitive lipase (HSL), which is typically lower in obese individuals than normal weight [89]. Adipose triglyceride lipase (ATGL) is not decreased in obesity and may compensate for the reduced HSL expression [90]. Furthermore adipose tissue also produces PGI_2, a potent lipolytic agent [91].

Pre-clinical studies utilizing celebcoxib, a selective COX-2 nonsteroidal anti-inflammatory drug (NSAID) or genetic deletion of COX-2 heavily implicate COX-2 as a mediator of adipose tissue dysregulation [92]. Mice on a high-fat diet that received celecoxib have shown reduced expression of monocyte chemoattractant protein 1 (MCP-1) and with concurrent decreases in CD68 positive cells in epididymal and subcutaneous fat depots [92]. Adi et al. demonstrated that hematopoietic COX-2 deficiency in mice resulted in reduced inflammatory markers in the visceral adipose tissue (VAT) stromal vascular cells, but increased inflammatory markers in the adipocyte fraction [93]. Furthermore, hematopoietic COX-2 deficient mice experienced weight gain with associated increased VAT mass, which was related to an increase in adipogenesis via loss of inhibition by Wnt signaling [93]. Hu et al. used a combination of in vivo and in vitro techniques to show that adipocytes undergoing lipolysis produce PGE_2, which strongly promotes macrophage migration [94].

COX-2 expression, in association with increased PGE_2 levels, is linked to increased metastasis and reduced breast cancer survival [95,96]. In vitro studies have shown that PGE_2 is a negative regulator of the tumor suppressor p53 in human breast adipose stromal cells [97]. Additional changes in the cellular composition of the mammary tissue provide additional sources of PGE_2. Obesity is associated with extracellular matrix remodeling, resulting in an increase in adipose tissue fibrosis [98].

Hypertrophic adipocytes secrete larger amounts of TNF-α compared to adipocytes that are normal in size. TNF-α is a potent inhibitor of adipogenesis and can prevent preadipocytes from differentiating into mature adipocytes or stimulate dedifferentiation of mature adipocytes into a fibroblast-like cell [99]. Partially transdifferentiated preadipocytes can possess a macrophage-like phenotype and secrete cytokines similar to macrophages [76]. Thus, in the obese mammary stroma, fibroblasts and preadipocytes are rich sources of PGE_2 which drive cancer growth [100].

4. Complementary metabolic pathways between adipocytes, adipose stromal cells and tumor cells

Interplay between the adipose tissue (including adipocytes and adipose stromal cells) and neighboring tumor cells are dynamic. A large body of literature supports the notion that many factors in obesity not only confer advantageous growth to tumor cells, but also propagate to increase the ability to meet the metabolic needs of tumor cells for growth and survival [101]. Several obesity-associated cancers, including breast and pancreas, occur within or in close proximity to adipose depots, which suggests that altered adipose metabolism promotes their growth [102]. The metabolism in the microenvironment contributes to the bioenergetics and necessary substrate to support the rapid growth of proliferating tumor cells.

The free fatty acids released from hypertrophied adipocytes impact metabolic processes in nearby tissue and on a systemic level. The ability of microenvironment metabolism to influence cancer growth was initially put forth by Stephen Paget in 1889. The “seed and soil” hypothesis credits growth of cancer cells and metastasis to a rich supply of nutrients in the microenvironment. The microenvironment of the mammary

tissue (the ‘soil’) differs between lean and obese individuals. Inflammatory and growth promoting factors converge at the adipocyte level, heavily influencing the output of the adipose tissue as an endocrine organ. Particularly, insulin resistance and local inflammation result in the aberrant release of free fatty acids from the adipose tissue, which can recruit and also activate macrophages [103].

Less aggressive luminal subtypes of breast cancer rely on a balance between de novo fatty acid synthesis and β-oxidation to support energy needs and requirements for new growth. However receptor negative subtypes, including BLBC overexpress genes involve in the uptake of exogenous fatty acids, which are increased in obesity [104]. Furthermore, breast cancer cells can alter metabolism in neighboring adipose tissue, enhancing lipase activity in adipocytes to fuel the growth of tumor cells [105]. Adipocytes can also adapt to utilize the lactate produced by tumor cell metabolism [106].

C. Inflammation regulates (and is regulated by) epigenetic modifications

Inflammation is the body’s natural response to injury, which serves to convey the need for changes in gene expression as part of the inflammatory response. These stimulated changes in gene expression can be not only mediated but also perpetuated by epigenetic modifications. Critical enzymes involved in one carbon metabolism, which generate methyl donors, are increased in response to inflammation [107]. DNA methylation of the miR-210 gene is increased in gastric biopsies after Helicobacter pylori infection, which promotes inflammation, compared to non-infected biopsies [108]. Furthermore, the expression of inflammation-related genes, Chemokine (C-X-C motif)

ligand 2 (CXCL2), IL-1β, Nitric oxide synthase, inducible (NOS2) and TNF-α, have been shown to increase in parallel with total DNA methylation levels in gastric tissue, suggesting that DNA methylation serves to regulate and perpetuate the inflammatory response [109].

The inflammatory master regulator NF-κB transcription factor family function as dimeric transcription factors for cytokines and interleukins central to the inflammatory response [110]. In a disease state, NF-κB evades regulation by modulating the epigenetic landscape to silence inhibitors and promote positive feed back loops. Notably, inhibitors of NF-κB, including chemokine (C-X-C motif) ligand 14 (CXCL14), and suppressor of cytokine signaling-1 (SOCS1) are often rendered silent by promoter methylation, a phenomenon observed in macrophages and tumor cells [111,112]. The microRNA let-7 inhibits IL-6 and its expression is decreased in most cancer cells. Activated NF-κB leads to decreased expression of let-7, resulting in increased levels of IL-6, which positively feed back stimulating increased NF-κB activation [113].

Several genes mediating the obesity-associated phenotype, including chronic low-grade inflammation, decreased adipogenic capacity, and hypoxia are dysregulated, in part, through epigenetic mechanisms such as DNA methylation. Fujiki et al. evaluated the methylation status of the promoter of the PPARγ2 gene in 3T3-LI preadipocytes and discovered that it was hypermethylated, but progressively demethylated upon induction of preadipocyte differentiation with corresponding increases in mRNA levels.

CHAPTER II. RESVERATROL INHIBITS OBESITY-ASSOCIATED ADIPOSE TISSUE DYSFUNCTION AND TUMOR GROWTH IN A MOUSE MODEL OF POSTMENOPAUSAL CLAUDIN-LOW BREAST CANCER

A. Chapter Précis

Adipose tissue dysregulation, a hallmark of obesity, contributes to a chronic state of low-grade inflammation and is associated with increased risk and progression of several breast cancer subtypes, including claudin-low breast tumors. Unfortunately, mechanistic targets for breaking the links between obesity-associated adipose tissue dysfunction, inflammation and claudin-low breast cancer growth have not been elucidated. Ovariectomized female C57BL/6 mice were randomized (n=15/group) to receive a control diet, a diet-induced obesity (DIO) diet, or a DIO + resveratrol (0.5% wt/wt) diet. Mice consumed these diets ad libitum throughout study and after six weeks were orthotopically injected with M-Wnt murine mammary tumor cells, a model of estrogen receptor (ER)-negative claudin-low breast cancer. Compared with controls, DIO mice displayed adipose dysregulation and metabolic perturbations including increased mammary adipocyte size; cyclooxygenase (COX)- 2 expression; inflammatory eicosanoid levels; macrophage infiltration; and prevalence of crown-like structures (CLS). DIO mice (relative to controls) also had increased systemic inflammatory cytokines and decreased adipocyte expression of PPARγ and other adipogenesis-regulating genes. Supplementing the DIO diet with resveratrol prevented obesity-associated increases in mammary tumor growth, mammary adipocyte

hypertrophy, COX-2 expression, macrophage infiltration, CLS prevalence, and serum cytokines. Resveratrol also offset the obesity-associated downregulation of adipocyte PPARγ and other adipogenesis genes in DIO mice. Our findings suggest that resveratrol may inhibit obesity-associated inflammation and claudin-low breast cancer growth by preventing adipocyte hypertrophy and associated adipose tissue dysregulation that typically accompanies obesity.

B. Introduction

The prevalence of obesity, an established risk and prognostic factor for several subtypes of breast cancer, has increased dramatically in the US and globally over the past 35 years [114]. Obese, relative to normal weight, postmenopausal women with estrogen receptor (ER)-negative breast cancer are more likely to have poorer response to treatment and higher rates of recurrence [115]. This includes the ER-negative claudin-low (CL) subtype of breast cancer, which is energy balance-responsive in humans and mice and often confers a poor prognosis due to a current lack of targeted therapies [16,116]. While obesity-associated inflammation is implicated in the generally poor response to therapy and increase in mortality in obese women compared with their lean counterparts, the mechanism by which inflammation promotes ER-negative claudin-low breast cancer growth is unknown [117,118].

Chronic positive energy balance in obesity results in the remodeling of the adipose microenvironment and results in hypertrophic adipocytes. Studies of C57BL/6 mice have established strong correlations between fat pad mass and mean adipocyte size, a measure of hypertrophy [78]. Furthermore, with increasing adipocyte size the

adipocyte secretome is enriched in pro-inflammatory adipokines and cytokines, including tumor necrosis factor alpha (TNF-α) and interleukin (IL)-6 [79]. Adipocyte size also positively correlates with macrophage infiltration in the adipose tissue as well as systemic insulin resistance [80,81]. TNF-α is a potent inhibitor of adipogenesis and can prevent preadipocytes from differentiating into mature adipocytes. Partially transdifferentiated preadipocytes can possess a macrophage-like phenotype and secrete cytokines similar to macrophages [76]. Isakson et al. harvested preadipocytes from obese and non-obese adipose tissue biopsies and found that the number of preadipocytes that differentiated into adipose cells was negatively correlated with both BMI and adipocyte cell size of the donors [82].

The crosstalk between hypertrophied adipocytes and macrophages promote and sustain a pro-inflammatory environment in adipose tissue, manifested by an influx of immune cells and metabolic dysfunction. Macrophages that have infiltrated into adipose tissue propagate the recruitment of additional macrophages by secreting chemoattractants, including monocyte chemoattractant protein (MCP)- 1. Macrophages also induce cyclooxygenase-2 (COX-2) expression resulting in high levels of arachidonic acid metabolites such as prostaglandins that disrupt fatty acid homeostasis by inhibiting adipogenesis. Prostaglandin (PG) F2 alpha ($PGF_{2\alpha}$) and PGE_2 inhibit peroxisome proliferator-activated receptor gamma (PPARγ) [87], a transcription factor regulating adipocyte differentiation and maintenance of insulin sensitivity. A higher ratio of PPARγ to COX-2, as achieved by COX-2 inhibition via non-steroidal anti-inflammatory drugs (NSAIDs) or PPARγ-agonists such as thiazolidinediones (TZD), is associated with decreased macrophage infiltration and adipocyte insulin sensitivity [119-

121]. Although not well studied in the context of cancer, pharmacologic strategies that have been successful in resolving obesity-associated inflammation in diabetes were dependent on restoring adipogenesis and adipocyte turnover [122,123].

Resveratrol is a natural polyphenolic compound produced in several species of plants in response to pathogens [124]. Resveratrol supplementation increases PPARγ expression in vivo in the adipose tissue of obese mice and in vitro in cultured macrophages and cancer cells [125-127]. Furthermore, resveratrol has demonstrated potential as a cancer chemopreventive agent due to its established ability to attenuate the pro-inflammatory effects of obesity [128,129]. Specifically, resveratrol decreases TNF-α production [130], NF-κB activation [131] and COX-2 activity [132,133], targets critical to perpetuating the cancer-promoting effects of adipose dysfunction in obesity.

The present study evaluated the ability of resveratrol to offset the effects of obesity on adipose tissue dysfunction, inflammation and claudin-low breast cancer growth. We and others have demonstrated success in disrupting the obesity-cancer link in a variety of cancer types by targeting inflammation with omega-3 fatty acids, NSAIDs or selective COX-2 inhibitors [134-136]. Here we hypothesized that resveratrol, via its ability to remodel adipose tissue and inhibit pro-inflammatory cytokine production, would protect against the pro-tumorigenic effects of obesity in our murine model of claudin-low breast cancer.

C. Materials and methods

In vivo studies

All animal studies and procedures were approved and monitored by the University of Texas Institutional Animal Care and Use Committee. As summarized in Figure 2.1A, eight-week-old ovariectomized female C57BL/6 mice were randomized (n=15 per group, based on sample size calculations) to receive one of the following three dietary regimens: i) control diet (catalog # D12450B; 10% kcal from fat); ii) diet-induced obesity (DIO) regimen (catalog # D12492; 60% kcal from fat), or DIO regimen supplemented with resveratrol (5 g resveratrol/kg DIO diet). All mice were fed *ad libitum* and diets were purchased from Research Diets, Inc. (New Brunswick, NJ). Diets were stored at 4°C in sealed bags and replaced biweekly to prevent oxidation. After five weeks on diet mice underwent a retro-orbital bleed for serum collection. One week later, mice received an orthotopic injection of 25,000 M-Wnt murine mammary tumor cells. These cells were clonally derived from the Wnt-1 transgenic mouse model of mammary cancer, display transcriptional profiles that closely align with human claudin-low breast tumors, and when orthotopically transplanted into syngeneic C57BL/6 mice generate claudin-low mammary tumors that are sensitive to energy balance modulation [16]. Transplanted tumor growth was monitored for five weeks, and tumors were measured weekly with calipers. At study endpoint (week 11), mice were euthanized by CO2 inhalation followed by cervical dislocation and tumors and mammary fat pad were excised and divided in portions to be formalin fixed or flash frozen in liquid nitrogen and stored at -80°C until further analysis. *Ex vivo* tumor volume was calculated using the

ellipsoid formula $1/6\pi \times D_1 \times D_2 \times D_3$ where D_1, D_2, and D_3 indicate three distinct diameter measurements in millimeters.

Quantitative magnetic resonance analysis

Body composition was measured on all mice at end of study by quantitative magnetic resonance (qMR) (Echo Medical Systems, Houston, TX). Measurements included lean mass, fat mass and total water mass. Percent body fat was calculated by dividing fat mass by total body weight.

Serum hormone, adipokine and cytokine measurement

After five weeks on diet, blood was collected from mice fasted 4-6 hours by retro-orbital bleed, allowed to clot for 30 minutes at room temperature, and serum was collected and flash frozen for subsequent analyses. Insulin and leptin were measured using mouse adipokine LINCOplex®Multiplex Assays (Millipore, Inc., Billerica, MA). Insulin-like growth factor 1 (IGF-1) concentrations were measured using a Millipore Milliplex Rat/Mouse IGF-1 Single Plex Assay and adiponectin concentrations were measured using a Milliplex Mouse Adiponectin Single Plex (Millipore, Inc.). Serum concentrations of mouse cytokines, including IL-1β, IL-6, IL-10, IL-17A, interferon (IFN)-γ, TNF-α, and MCP-1, were measured using a Bio-Plex Pro™ Mouse Cytokine 7-Plex Assay (Bio-rad, Inc., Hercules, CA). All assays were completed and analyzed on a BioRad Bio-Plex 200 analysis system (Bio-rad, Inc., Hercules, CA).

Histopathology and immunohistochemical staining

Paraffin embedded mammary and tumor tissue were cut into 4 μm thick sections for either hematoxylin and eosin (H&E) staining or immunohistochemical analysis. Slides were deparaffinized and processed as previously described [137]. Mammary tissues were stained with the following primary antibodies (source, dilution, and incubation conditions presented parenthetically): COX-2 (Cayman catalog #160126, 1:500, 1 hour at room temperature (RT)) and PPARγ (Abcam #ab59256, 1:250, overnight at 4°C). Tumor tissues were stained with the following primary antibodies: Macrophage Marker (RM0029-11H3), a pan-macrophage antibody (Santa Cruz sc-101447, 1:100, overnight at 4°C) and F4/80 (Abcam #ab6640, 1:200, 2 hours at RT). Slides were incubated with Dako EnVision™ labeled polymer for 30 minutes at RT, followed by incubation with Dako diaminobenzidine to develop the antibody stain then by a hematoxylin counterstain to visualize nuclei. Slides were scanned and digitized using the Aperio CS2 Digital Pathology Scanner (Leica Biosystems, Wetzlar, Germany). Quantification was performed using Aperio Digital Pathology platform. Briefly, three representative areas / tissue (mammary or tumor) were viewed at 20-40X magnification and scored based upon the percentage of cells with positive staining using individually developed scoring algorithms [134].

Analysis of mammary and intratumoral adipocyte size

H & E staining on sections from formalin-fixed, paraffin-embedded mammary fat pad tissue from 12-15 mice/group was processed, scanned and imaged at 40X

magnification. Representative areas (n=3/mouse) were viewed at 8.8X magnification (300 μm) and the size of mammary fat pad adipocytes (calculated as two-dimensional area) was quantified using ImageJ Version 1.51e (National Institute of Health, Bethesda, Maryland). An adipocyte tool macro (MRI Adipocyte Tools.txt) was downloaded from (http://dev.mri.cnrs.fr/projects/imagej-macros/wiki/Adipocytes_Tool) and imported into ImageJ. A preprocessing and simple segmentation algorithm was run on each digital image. The output generated gave squared area in pixels and number of adipocyte counts. Area in pixels was converted to μm^2 using a Moticam Aperio scanned image of a 0.15 mm calibration slide. The area values from the representative three digital images yielded between 345-1991 measurements for each mouse, which were then compiled to calculate the 10^{th}, 50^{th} and 90^{th} percentile of adipocyte area. Resultant percentiles were then averaged by group.

Quantitative RT-PCR

Total RNA was extracted from the flash-frozen mammary fat pad samples collected at end of study using TRI-Reagent (Sigma-Aldrich, St.Louis, MO) according to manufacturer's instructions. RNA concentration was spectrophotometrically determined using a nanodrop (Thermo Scientific, Logan, UT). RNA was reverse transcribed with Multiscribe RT (Applied Biosystems, Carlsbad, CA). Resulting cDNA from tissue samples were assayed in triplicate for PCR using Taqman® Gene Expression Assays for interleukin-6 (IL-6), serum amyloid A 3 (Saa3), monocyte chemoattractant protein-1 (MCP-1), c-x-c motif chemokine ligand 12 (CXCL12), granulocyte macrophage colony-stimulating factor (GM-CSF), macrophage colony-stimulating factor (M-CSF), tumor

necrosis factor-alpha (TNF-α), macrophage migration inhibitory factor (MIF), EGF-like module receptor 1 (Emr1), and peroxisome proliferator-activated receptor gamma (PPARγ) (Applied Biosystems). PCR reactions were completed using a ViiA^{TM} 7 Real time PCR system (Applied Biosciences). Gene expression data were normalized to the housekeeping gene β-actin and analyzed using the delta delta C_T cycle threshold method.

Crown-like structure analysis

The formation of crown-like structures (CLS) was assessed from hematoxylin and eosin staining of 4 μm thick sections prepared from formalin-fixed paraffin embedded mammary fat pad tissue. Briefly, the total number of CLS were counted in a blinded fashion. CLS density measures were achieved by dividing CLS by the total slide area used for analysis using ImageScope Viewing Software Version 12.0 (Leica Biosystems). Values expressed as CLS/area of tissue in cm^2.

Eicosanoid analysis

Eicosanoids in the mammary adipose tissues were extracted and analyzed by liquid chromatography/tandem mass spectroscopy (LC/MS/MS) using the modified method described previously [138]. LC/MS/MS analyses were performed using an Agilent 6460 triple quadrupole mass spectrometer (Agilent Technologies) equipped with an Agilent 1200 binary pump high-performance liquid chromatography (HPLC) system as described previously [139].

Adipogenesis PCR array

RNA was extracted from the mammary fat pad of control, DIO, and DIO + resveratrol mice (n = 6/group) as described above. RNA was reverse transcribed using a cDNA conversion kit according to the manufacturer's instructions. The cDNA was plated on the real-time Mouse Adipogenesis PCR Array (Qiagen, Hilden, Germany, RT^2 Profiler PCR Array catalog # PAMM-049Z) in combination with RT^2 SYBR® Green qPCR Mastermix (catalog # 330529). C_T values were uploaded to the Qiagen data analysis web portal at http://www.qiagen.com/geneglobe and fold change/regulation was calculated using the delta delta C_T method.

Tissue resveratrol analysis

The wet weight of each tumor tissue sample was individually determined. One mL of an extraction solvent consisting of 20% 0.1 M Sodium Acetate buffer (pH 3.8) and 80% methanol was added to each tissue sample. Piceatannol (Sigma) was added to the samples as an internal standard to a final concentration of 0.5 µg/mL. The sample was disrupted using a sonic dismembrator for one minute, then centrifuged at 10,000 x g for 10 minutes. An aliquot of 600 µL was taken from the supernatant and dried using a Speed-Vac system. The samples were then resuspended in 100µL of the mobile phase and aliquots were injected into a Waters Acquity UPLC H-Class (Waters Corporation, Milford, MA). Analysis was accomplished using the peak area of the fluorescence response of resveratrol and piceatannol, with the lower limit of detection at 5 ng/mL (0.005 µg/mL). The results are reported as an average of two technical replicates.

Statistical analyses

A priori sample size calculations were completed to determine the required number of mice/treatment group (n=15) to provide >90% power to detect at least 25% differences in the primary study outcome, which is mean tumor volume between treatment groups [140]. Values are presented as group mean ± standard deviation (s.d.). For all tests, GraphPad Prism software was used (La Jolla, CA), and $P < 0.05$ was considered statistically significant. Differences between groups in body weight and calorie intake were analyzed by two-way analysis of variance (ANOVA) followed by Tukey's post hoc test. Differences between groups in body fat percentage, serum hormones, adipokines, cytokines, adipocyte size, gene expression, CLS, IHC staining, and tumor volume, were analyzed by one-way ANOVA followed by Tukey's post hoc test. Differences in gene expression detected using the Adipogenesis Array were calculated using Student's t-test using Qiagen data analysis web portal.

D. Results

Resveratrol supplementation does not impact the establishment of diet-induced obesity

The DIO (alone or with resveratrol supplementation) and control regimens generated obese and normoweight phenotypes, respectively (Figure 2.1B and 2.1C). Significant differences in body weight were observed after three weeks on diet and continued throughout the remainder of study between control mice and DIO mice. No statistically significant differences in body weight or calorie intake were detected between DIO and DIO + resveratrol mice throughout study. Average body weight is

shown prior to tumor implantation for the first six weeks on diet (Figure 2.1B). DIO + resveratrol mice consumed on average 2.9 – 5.1 mg resveratrol/body weight (g) per week (Table 2.1). Percent body fat, obtained at end of study, was significantly lower in control mice (30.1 ± 3.6%) vs. both DIO (49.3 ± 3.0%; $P < 0.0001$) and DIO + resveratrol mice (46.2 ± 4.7%; $P < 0.0001$), with no statistical differences between DIO and DIO + resveratrol mice (Figure 2.1C).

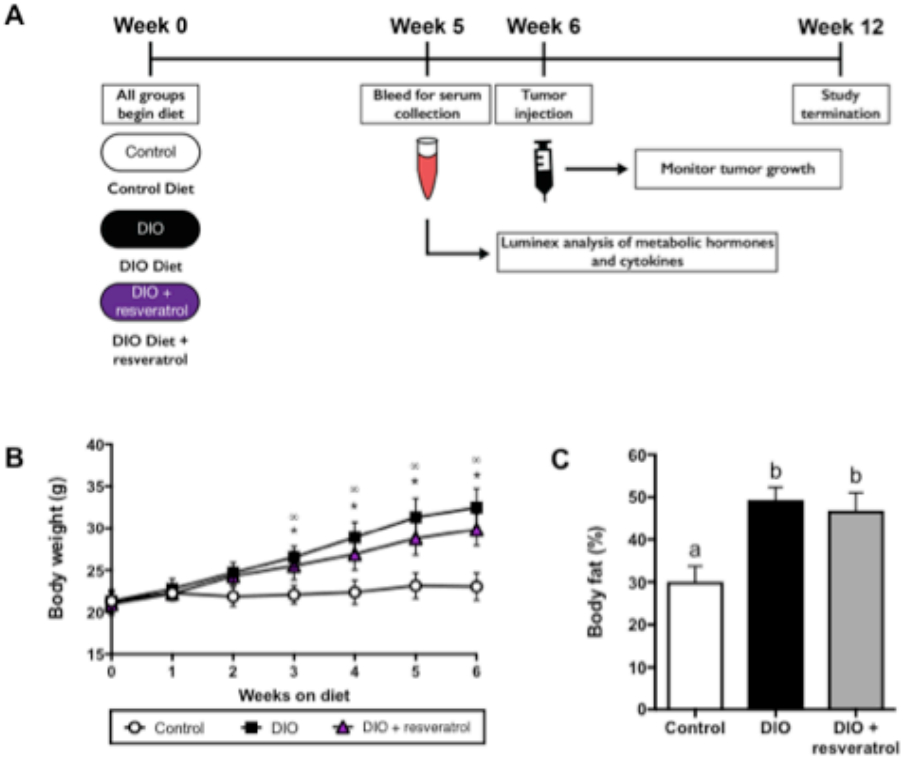

Figure 2.1. Resveratrol supplementation does not impact the establishment of diet-induced obesity (A) Mice began resveratrol supplementation at baseline and continued throughout study. The DIO and control regimens effectively generated obese and normal weight (NW) phenotypes, with significant differences in (B) body weight beginning after three weeks on diet (DIO vs. control, $P < 0.0001$ denoted by ∞; DIO + resveratrol vs. control $P < 0.05$ denoted by *; DIO vs. DIO + resveratrol *NS*). After six weeks on diet and when mammary tumor cells were injected, DIO and DIO + resveratrol had significantly greater body weights than control mice (DIO vs. control, $P < 0.0001$; DIO + resveratrol vs. control $P < 0.0001$; DIO vs. DIO + resveratrol *NS*). (C) Percent body fat, obtained at end of study, was significantly lower in control mice vs. both DIO ($P < 0.0001$) and DIO + resveratrol ($P < 0.0001$), with no differences between DIO and DIO + resveratrol mice. Data presented as mean ± s.d. For percent body fat differences in significance denoted by different letters (a,b).

Table 2.1. Average weekly calorie and resveratrol intake				
	kcal intake/week			Resveratrol intake (mg)/ body weight (kg)/day
Week	**Control**	**DIO**	**DIO + resveratrol**	**Resveratrol**
1	85.6±4.2[a]	114.8±4.3[b]	110.2±3.5[b]	656.1
2	78.7±4.9[a]	102.9±3.7[b]	95.5±5.9[b]	653.6
3	76.1±3.4[a]	104.6±4.5[b]	94.4±7.2[b]	552.9
4	74.0±3.6[a]	96.6±2.5[b]	85.8±4.6[b]	493.8
5	76.0±4.7[a]	96.9±5.2[a]	87.6±11.1[a]	420.4
6	80.7±9.5[a]	90.1±8.4[b]	85.6±7.2[b]	417.9

Values are displayed per mouse as an average of mice from each group. kcal: kilocalories. Statistical significance among groups denoted by different letters (a,b).

Resveratrol supplementation protects against serum metabolic and inflammatory perturbations in DIO mice

DIO mice had significantly higher serum levels of IGF-1, insulin and leptin compared with control mice ($P < 0.01$ for each analyte). DIO + resveratrol mice displayed an intermediate level of IGF-1 and insulin which was not significantly different from DIO or control mice. Leptin was significantly increased in both DIO and DIO + resveratrol mice compared with control mice (DIO vs. control $P < 0.0001$; DIO + resveratrol vs. control $P < 0.0001$). No differences in serum adiponectin levels were detected between groups, but control mice on average had a significantly lower leptin to adiponectin ratio compared with DIO and DIO + resveratrol mice (Table 2.2).

Furthermore, DIO mice, relative to control mice, had significantly increased serum levels of IL-6, IFN-γ, TNF-α, and MCP-1 ($P < 0.05$ for each analyte). DIO + resveratrol mice displayed significantly lower serum IL-6, IFN-γ and TNF-α compared with DIO mice ($P < 0.05$ for each analyte), to levels not statistically different than controls. DIO + resveratrol mice had an intermediate level of MCP-1 which was not significantly different from DIO or control mice. No significant differences were observed between groups in serum IL-1β, IL-10 and IL-17A (Table 2.2).

Table 2.2. Serum hormones, adipokines, and cytokines

	Control	DIO	DIO + resveratrol
Serum Hormones and Adipokines (ng/mL)			
Insulin	0.3 ± 0.2[a]	1.0 ± 0.8[b]	0.5 ± 0.2[a,b]
IGF-1	250.9 ± 85.3[a]	406.6 ± 102.8[b]	323.4 ± 71.3[a,b]
Leptin	1.2 ± 0.5[a]	7.6 ± 2.7[b]	6.2 ± 2.6[b]
Adiponectin	6.2 ± 3.1[a]	4.8 ± 2.2[a]	4.1 ± 2.3a
Leptin: Adiponectin	0.5 ± 0.9[a]	1.9 ± 1.5[b]	2.0 ± 1.4[b]
Serum Cytokines (pg/mL)			
IFN-γ	7.2 ± 5.7[a]	25.4 ± 7.3[b]	11.4 ± 9.9[a]
IL-1β	98.5 ± 45.0[a]	161.1 ± 87.6[a]	95.2 ± 49.2[a]
IL-6	9.2 ± 3.3[a]	14.2 ± 3.3[b]	9.5 ± 4.6[a]
IL-10	49.8 ± 17.0[a]	47.7 ± 21.1[a]	47.6 ± 15.9[a]
IL-17A	19.3 ± 1.4[a]	22.8 ± 6.0[a]	18.4 ± 2.9[a]
MCP-1	195.0 ± 76.2[a]	304.1 ± 57.8[b]	245.9 ± 24.4[a,b]
TNF-α	204.7 ± 178.0[a]	576.5 ± 307.8[b]	203.6 ± 261.9[a]

IFN-γ: interferon-gamma; IL-1β: interleukin-1 beta; IL-6: interleukin-6; IL-10: interleukin-10; IL-17A: interleukin-17A; MCP-1: monocyte chemoatrractant protein-1; TNF-α: tumor necrosis factor-alpha. Statistical significance among groups denoted by different letters (a,b).

Resveratrol prevents adipocyte hypertrophy in the mammary fat pad of DIO mice

We measured the two-dimensional area of each adipocyte using stained H&E sections of mammary fat pad tissue from 12-15 mice/group (Figure 2.2A). The 10^{th} percentile of adipocyte area for DIO mice (1614 ± 627.7 μm^2) was significantly greater than the average 10^{th} percentile of control (336.7 ± 133 μm^2) and DIO + resveratrol mice (399.2 ± 197.1 μm^2; Figure 2.2B and 2.2C). The average median (50^{th} percentile) adipocyte area for the DIO group (4891 ± 1097 μm^2) was significantly greater compared with control (1334 ± 494.2 μm^2) and DIO + resveratrol (2081 ± 540 μm^2). However, DIO + resveratrol mice had a median adipocyte area that was also significantly greater than controls (Figures 2.2B and 2.2D). This trend was also seen in the 90^{th} percentile of adipocyte area, with the largest values in DIO mice (8940 ± 1560 μm^2), intermediate values in DIO + resveratrol mice (5415 ± 578.7 μm^2), and the lowest values in controls (3311 ± 1004 μm^2; Figure 2.2B and 2.2E). All statistical differences were at $P < 0.0001$. These findings on diet-dependent effects on adipocyte area provide additional support that the DIO mice possessed hypertrophied adipocytes, and supplementation of the DIO diet with resveratrol inhibited the pathogenic increase in adipocyte size.

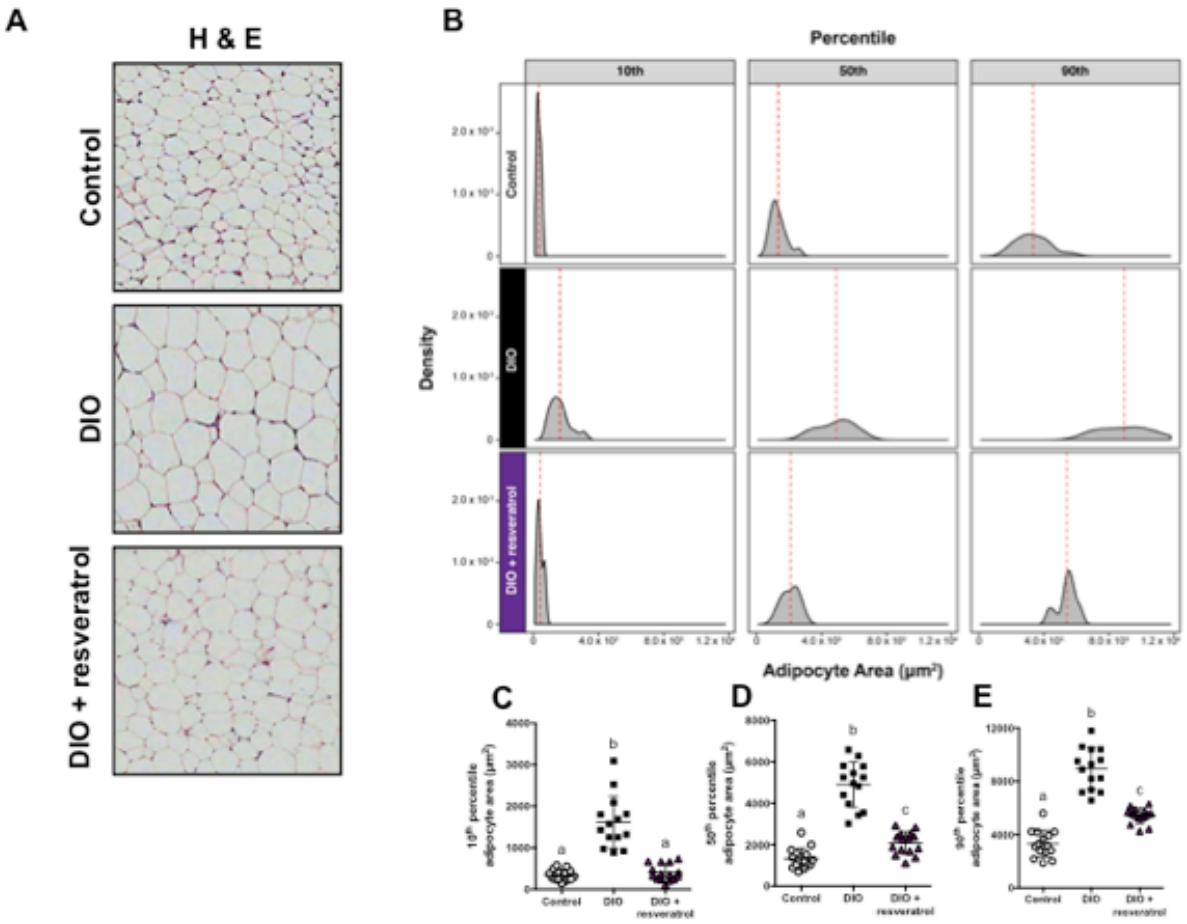

Figure 2.2. Resveratrol prevents adipocyte hypertrophy in the mammary fat pad of DIO mice. We measured the two-dimensional area of each adipocyte (n = 14-15/group) in the mammary fat pad using a stained H&E section, (A) representative image shown. (B) Histogram distribution of the adipocyte area of the 10th, 50th and 90th percentile is shown for control, DIO and DIO + resveratrol. Red dashed lines indicate the median of each percentile. DIO mice had significantly higher adipocyte area for the (C) 10th percentile compared to both control and DIO + resveratrol (DIO vs. control $P < 0.0001$; DIO vs. DIO + resveratrol $P < 0.0001$; control vs. DIO + resveratrol *NS*). DIO mice had significantly higher adipocyte area for the (D) 50th percentile compared to control and DIO + resveratrol (DIO vs. control $P < 0.0001$; DIO vs. DIO + resveratrol $P < 0.0001$). However, DIO + resveratrol mice also had significantly higher adipocyte area for the 50th percentile compared to control ($P < 0.05$). Similarly, DIO mice had significantly higher adipocyte area for the 90th percentile compared to control and DIO + resveratrol (DIO vs. control $P < 0.0001$; DIO vs. DIO + resveratrol $P < 0.0001$). Additionally, DIO + resveratrol mice also had significantly higher adipocyte area for the 90th percentile compared to control ($P < 0.0001$). Data presented as mean ± s.d Differences in significance denoted by different letters (a,b).

Resveratrol protects against inflammatory and macrophage gene signaling in DIO mice

We measured gene expression in the mammary fat pad of mice for mediators of inflammation and genes implicated in macrophage recruitment, proliferation and secretory products of activated macrophages. DIO mice had significantly increased gene expression of the pro-inflammatory mediators IL-6 (DIO vs. control $P < 0.01$; DIO vs. DIO + resveratrol $P < 0.05$) and Saa3 (DIO vs. control $P < 0.01$; DIO vs. DIO + resveratrol $P < 0.01$; Figure 2.3A). DIO mice displayed increased gene expression of MCP-1 ($P < 0.05$) compared with DIO + resveratrol, but not control mice. CXCL12 expression was increased in DIO mice compared with both control ($P < 0.01$) and DIO + resveratrol ($P < 0.01$; Figure 2.3B). DIO mice, relative to control mice and DIO + resveratrol mice, also displayed increased expression of GM-CSF (DIO vs. control $P < 0.01$; DIO vs. DIO + resveratrol $P < 0.01$) and M-CSF (DIO vs. control $P < 0.05$; DIO vs. DIO + resveratrol $P < 0.01$; Figure 2.3C), which promote macrophage proliferation. Gene expression of TNF-α and MIF, which are both predominantly secreted by macrophages in the adipose tissue, were significantly increased in DIO mice compared with control mice ($P < 0.05$) and DIO + resveratrol mice ($P < 0.01$; Figure 2.3D).

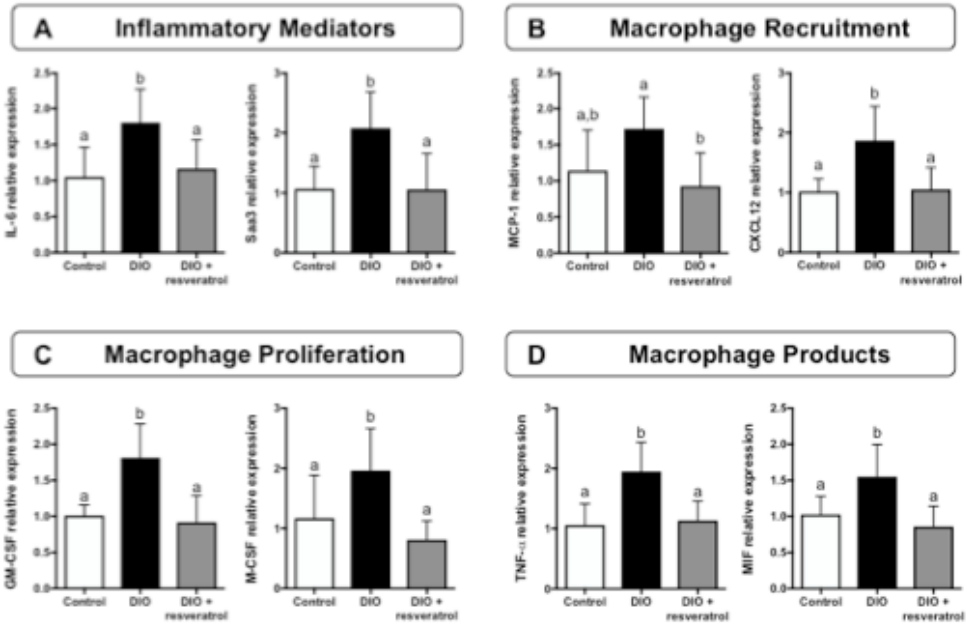

Figure 2.3. Resveratrol protects against inflammatory and macrophage gene signaling in DIO mice. DIO mice had significantly increased gene expression of the pro-inflammatory mediators (A) IL-6 and Saa3 relative to both control and DIO + resveratrol mice. DIO mice also had significantly increased gene expression of (B) macrophage signaling molecules monocyte chemoattractant protein (MCP)-1 and CXC Ligand (CXCL) compared to DIO + resveratrol mice. DIO mice had significantly increased expression of DIO mice had significantly increased gene expression of (C) GM-CSF and M-CSF, which promote macrophage proliferation, compared to both control and DIO + resveratrol mice. Gene expression of secretory products of activated macrophages, including (D) TNF-α and macrophage inhibitor factor (MIF) were significantly increased in DIO mice compared to both control and DIO + resveratrol mice. Data presented as mean ± s.d Differences in significance denoted by different letters (a,b).

Resveratrol blunts mammary gland crown-like structure formation and COX-2 protein expression in DIO mice

To extend our findings from mammary gene expression profiles suggesting resveratrol supplementation modulated macrophage activity, we measured the number of crown-like structures (CLS) in the mammary fat pads of 14-15 mice/group. CLS are indicative of macrophages surrounding dead or dying adipocytes. The density of CLS (expressed as CLS / area of tissue in cm^2) in the mammary fad pad was significantly increased in DIO mice (15.5 ± 5.6 CLS/cm^2) relative to control (9.6 ± 4.0 CLS/cm^2; $P < 0.01$) and DIO + resveratrol mice (11.2 ± 3.5 CLS/cm^2; $P < 0.05$; Figure 2.4A and 2.4B).

Gene expression of Emr1, which is specific to macrophages, was also increased in DIO mice compared to both control ($P < 0.05$) and DIO + resveratrol ($P < 0.05$; Figure 2.4C).

We also quantified COX-2 protein expression using immunohistochemistry analysis on formalin-fixed, paraffin-embedded tissue from the mammary fat pads of mice fed the control, DIO, and DIO + resveratrol diets. DIO mice displayed approximately a two-fold increase in COX-2 protein expression relative to control ($P < 0.0001$) and DIO + resveratrol mice ($P < 0.0001$; Figure 2.4A and 2.4D).

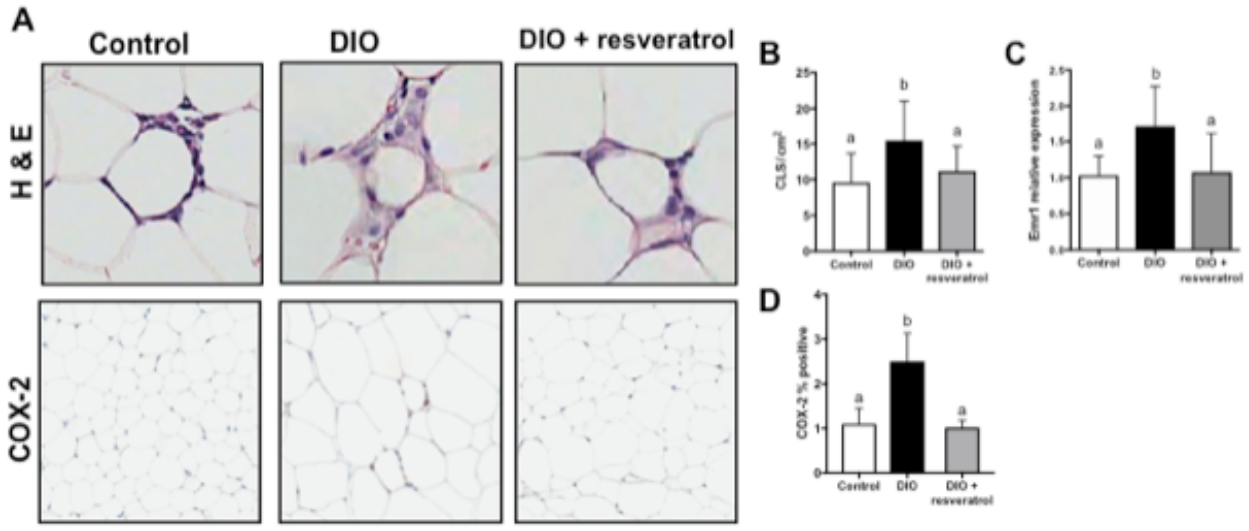

Figure 2.4. Resveratrol blunts mammary gland crown-like structure formation and COX-2 protein expression in DIO mice. We measured the number of crown-like structures (CLS) (n = 14-15/group) in the mammary fat pad using a stained H&E section, representative image shown (A). The prevalence of (B) CLS (expressed as CLS / area of tissue in cm^2) in the mammary fad pad was significantly increased in DIO mice relative to control and DIO + resveratrol mice (DIO vs. control $P < 0.005$; DIO vs. DIO + resveratrol $P < 0.05$; control vs. DIO + resveratrol *NS*). Gene expression of EGF-like module receptor 1 (Emr1), a macrophage-specific marker, was significantly increased in DIO mice compared with control and DIO + resveratrol mice. (D) COX-2 protein expression, representative image shown (A) was significantly increased in DIO mice compared with both control and DIO + resveratrol mice (DIO vs. control $P < 0.0001$; DIO vs. DIO + resveratrol $P < 0.0001$; control vs. DIO + resveratrol *NS*). Data presented as mean ± s.d. Differences in significance denoted by different letters (a,b).

Resveratrol modulates mammary tissue levels of eicosanoids and other inflammatory lipid derivatives in DIO mice

To test if modulation of COX-2 expression in the mammary fat pad resulted in corresponding effects in levels of downstream metabolites, we analyzed the 4th mammary fat pad from each of 4 mice/group for levels of inflammatory lipid derivatives. DIO mice had significantly increased levels of arachidonic acid (AA) pro-inflammatory mediators $PGF_{2\alpha}$ ($P < 0.05$ vs. control; $P < 0.05$ vs. DIO + resveratrol), PGE_2 ($P < 0.05$ vs. control; $P < 0.05$ vs. DIO + resveratrol), $13PGE_2$, as well as linoleic acid (LA) derived 13-hydroxyoctadecadienoic acid (13-HODE) compared with DIO + resveratrol mice. Relative to DIO mice, control mice had significantly decreased $PGF_{2\alpha}$ and 13-HODE but intermediate levels of PGE_2 and $13PGE_2$. No substantial differences between the diet treatment groups were observed in the anti-inflammatory intermediates PGE_1 and PGE_3 or the pro-inflammatory intermediates $6ketoPGF_{1\alpha}$, PGD_2, thromboxane B2 (TXB2), 5-hydroxyeicosatetraenoic acid (5-HETE), 12-HETE and 15-HETE (Table 2.3).

Table 2.3. Eicosanoid intermediates in mouse mammary tissue			
Metabolite	**Control**	**DIO**	**DIO + resveratrol**
5-HETE	1.5 ± 0.8[a]	2.3 ± 1.4[a]	1.2 ± 0.5[a]
12-HETE	62.6 ± 40.1[a]	34.5 ± 31.3[a]	24.1 ± 8.1[a]
15-HETE	5.2 ± 3.3[a]	4.9 ± 3.2[a]	5.0 ± 1.4[a]
13-HODE	69.9 ± 19.7[a]	328.4 ± 124.7[b]	98.8 ± 79.8[a]
PGD_2	43.6 ± 19.0[a]	110.8 ± 69.5[a]	52.0 ± 34.6[a]
PGE_1	3.3 ± 1.7[a]	3.8 ± 2.0[a]	1.9 ± 1.3[a]
PGE_2	27.2 ± 13.4[a,b]	54.4 ± 12.0[a]	16.0 ± 7.8[b]
$PGF2_\alpha$	7.4 ± 3.5[a]	15.0 ± 4.3[b]	8.1 ± 2.3[a]
PGE_3	0.3 ± 0.1[a]	0.4 ± 0.2[a]	0.9 ± 0.8[a]
$13PGE_2$	1.6 ± 0.6[a,b]	2.4 ± 0.8[a]	0.8 ± 0.2[b]
$6ketoPGF1_\alpha$	32.3 ± 7.9[a]	35.5 ± 35.0[a]	13.7 ± 8.2[a]
TXB_2	9.8 ± 5.4[a]	11.4 ± 7.9[a]	8.2 ± 6.2[a]

HETE: hydroxyeicosatetraenoic acid; PG: prostaglandin; TX: thromboxane. Statistical significance among groups denoted by different letters (a,b).

Resveratrol maintains mammary tissue PPARγ expression in DIO mice

COX-2 metabolites $PGF_{2\alpha}$ and PGE_2 are known to inhibit PPARγ, a key regulator of adipogenesis [87], and these interactions could explain the differences in adipocyte size observed between DIO and DIO + resveratrol mice despite both groups having equivalent body fat percentage. Accordingly, we performed immunohistochemistry analysis on paraffin embedded mammary tissue for protein levels of PPARγ. Relative to DIO mice, control and DIO + resveratrol mice had significantly increased staining of

positive nuclei for PPARγ in the mammary fat pad (DIO vs. control $P < 0.0001$; DIO vs. DIO + resveratrol $P < 0.0001$; Figure 2.5A and 2.5B). Furthermore, DIO mice had significantly decreased PPARγ gene expression compared with DIO + resveratrol mice ($P < 0.01$); control mice displayed intermediate gene expression, not statistically different from DIO or DIO + resveratrol mice (Figure 2.5C).

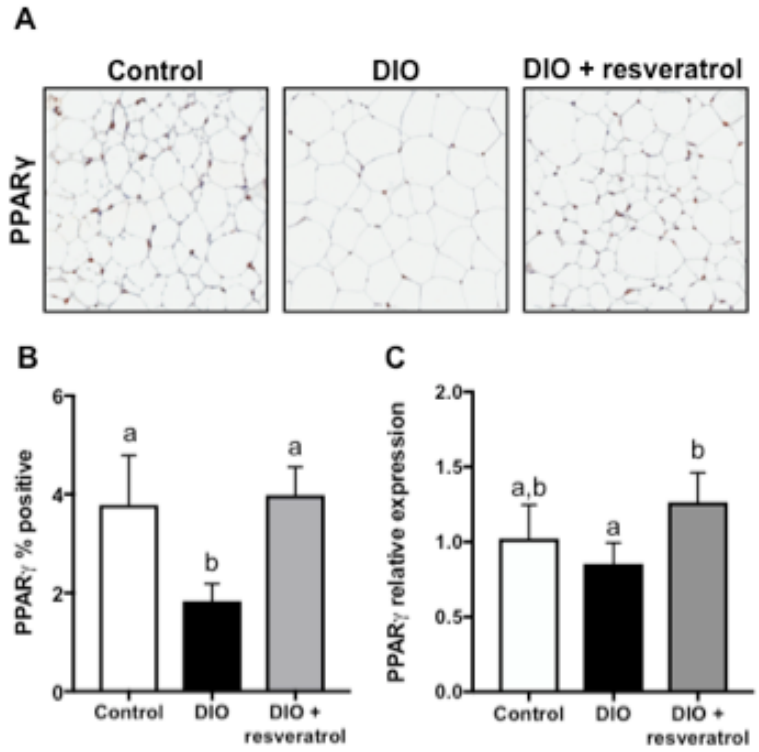

Figure 2.5. Resveratrol maintains mammary tissue PPARγ expression in DIO mice
PPARγ protein expression (B), representative image shown (A), was significantly decreased in DIO mice compared to both control and DIO + resveratrol mice (DIO vs. control $P < 0.0001$; DIO vs. DIO + resveratrol $P < 0.0001$; control vs. DIO + resveratrol *NS*). Similarly, DIO mice had significantly decreased (C) PPARγ gene expression compared to DIO + resveratrol mice, however control mice displayed intermediate gene expression, (DIO vs. control NS; DIO vs. DIO + resveratrol $P < 0.01$; control vs. DIO + resveratrol *NS*). Data presented as mean ± s.d. Differences in significance denoted by different letters (a,b).

Resveratrol protects against obesity-induced dysregulated expression of adipogenesis-related genes in DIO mice

To further characterize the effects of maintained PPARγ expression in DIO + resveratrol mice, we performed a quantitative real-time Adipogenesis PCR array on mammary fat pad tissue for genes involved in preadipocyte commitment, differentiation and adipocyte maturation. Differential expression data (Figure 2.6) demonstrate that DIO mice display patterns of decreased gene expression of targets across the spectrum of adipogenesis compared with control and DIO + resveratrol mice. Furthermore, DIO + resveratrol mice displayed a unique increase in expression of genes implicated in the beiging of adipocytes, relative to both control and DIO mice.

Generally, DIO mice, relative to controls, had significantly decreased expression of factors promoting stem cell differentiation to preadipocytes, including Adipogenin (Adig), fibroblast growth factor 2 (Fgf2), and nuclear receptor subfamily 0 group B member (Nr0b2). DIO + resveratrol mice generally had intermediate expression levels of these preadipocyte differentiation factors that did not significantly differ from either control or DIO mice. Genes which facilitate adipogenesis, including the master regulators PPARγ and CCAAT/enhancer binding protein α (Cebpα), were similarly expressed in control and DIO + resveratrol mice; both groups displayed expression levels of these adipogenesis regulators that were generally higher than in DIO mice. Furthermore, downstream targets of PPARγ, including insulin receptor 2 (Irs2), fatty acid binding protein 4 (Fabp4) and lipoprotein lipase (Lpl) that are known to promote a mature adipocyte phenotype, were decreased in DIO mice compared with control and DIO + resveratrol mice.

The expression of the transcriptional regulator PRD1-BF1-RIZ1 homologous PR domain containing 16 (Prdm16) and Forkhead Box C2 (Foxc2), which both promote the beiging of adipose tissue, was significantly increased in DIO + resveratrol mice compared with both control and DIO mice. The expression of uncoupling protein 1 (Ucp1), a specific marker of adipose browning, was decreased in DIO mice compared with control and DIO + resveratrol mice (Figure 2.6).

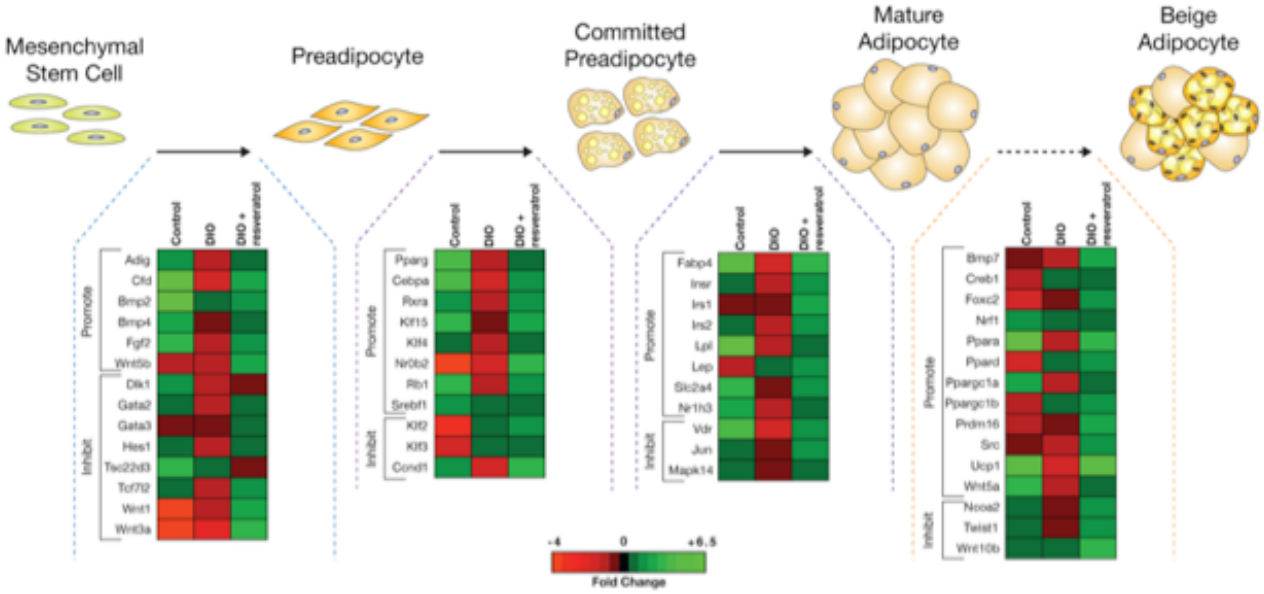

Figure 2.6. Resveratrol protects against obesity-induced dysregulated expression of adipogenesis-related genes in DIO mice. We performed a quantitative real-time Adipogenesis PCR array on mammary fat pad tissue for genes involved in preadipocyte commitment, differentiation, adipocyte maturation and adipocyte beiging. Heatmap representation of log2 fold change (log2 (experimental group) – log2 (average of all groups)) of control, DIO and DIO + resveratrol mice (n = 4-5/group). Black indicates a $\log_2$ fold change of zero, representing a lack of change between the experimental group and the the average of all groups. Increasing brightness of green indicates an increase in expression (log2 fold change >0). Increasing brightness of red indicates a lower level of the expression in the experimental group in comparison to the average of all groups (log2 fold change <0).

Resveratrol protects against enhanced M-Wnt murine mammary tumor size, infiltrating adipocyte size, and tumor associated macrophages in DIO mice

To characterize the effects of obesity with and without adipose tissue dysfunction (the latter achieved in DIO + resveratrol mice) on mammary tumor growth, we orthotopically injected mice with M-Wnt mammary tumor cells, which model claudin-low breast cancer [16]. DIO mice had significantly increased mean *ex vivo* tumor volume (364.5 ± 98.1 mm^3) compared with DIO + resveratrol mice (224.8 ± 113.0 mm^3; $P < 0.05$) and control mice (159.8 ± 115.1 mm^3; $P < 0.01$). Furthermore, the mean *ex vivo* tumor volume of DIO + resveratrol mice and control mice did not statistically differ (Figure 2.7A). We confirmed the presence of resveratrol in tumor tissue by HPLC (Table 2.4). H&E staining of 10 randomly selected tumors/group revealed a markedly increased accumulation of adipocytes within the tumor tissue of DIO mice compared with control and DIO + resveratrol mice. We measured intratumoral adipocyte size via two-dimensional area analysis of each adipocyte present in the tumor. The median adipocyte area for DIO mice was statistically significantly higher than control ($P < 0.01$) and DIO + resveratrol mice ($P < 0.05$; Figure 2.7B and 2.7E).

We also quantified the presence of intratumoral macrophages by utilizing immunohistochemistry on sections of tumor tissue with two different markers: i) Macrophage marker RM0029-11H3 (n = 3 randomly selected tumors/group), a pan-macrophage marker; and ii) F4/80 (n = 5-7 randomly selected tumors/group), a stain more specific to tumor-associated macrophages [141,142]. Tumors from DIO mice displayed nearly a three-fold increase in positive staining for both Macrophage marker (RM0029-11H3) compared with control ($P < 0.01$) and DIO + resveratrol mice ($P < 0.01$; Figure 2.7C and 2.7E). Similarly, DIO tumors had significantly increased positive

staining for F4/80 compared with control ($P < 0.01$) and DIO + resveratrol mice ($P < 0.01$; Figure 2.7D and 2.7E). The tumors from DIO + resveratrol mice did not statistically differ from control tumors in their positivity for Macrophage marker and F4/80 (Figure 2.7D and 2.7E).

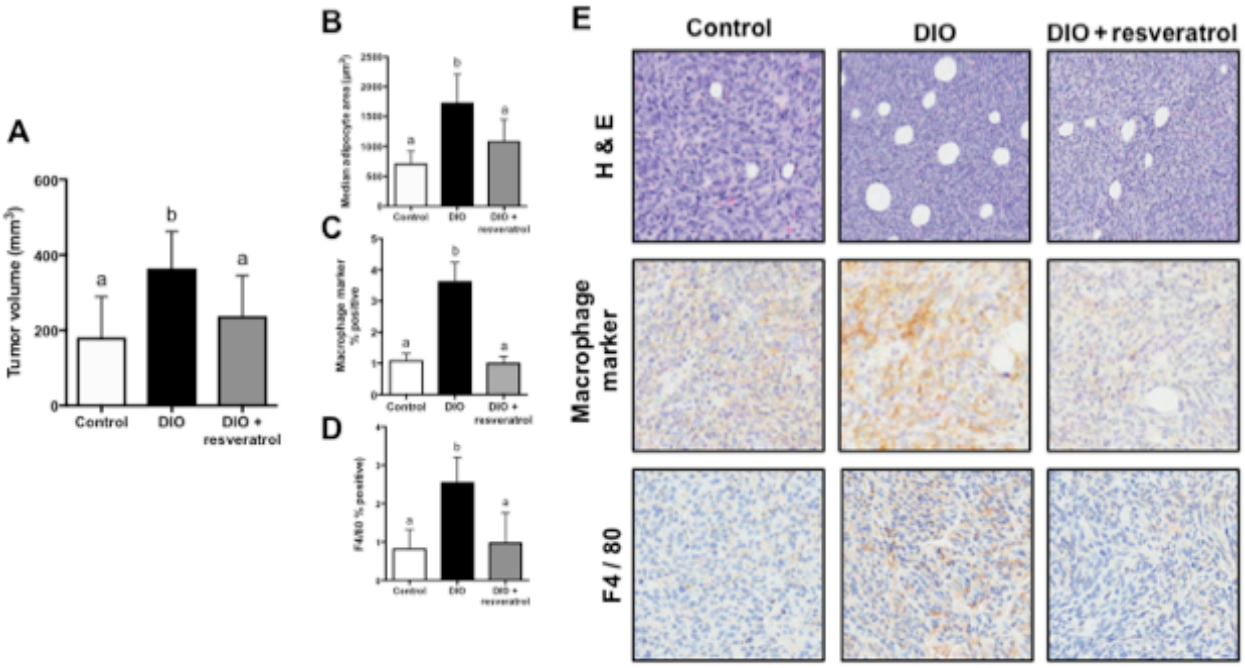

Figure 2.7. Resveratrol protects against enhanced M-Wnt murine mammary tumor size, infiltrating adipocyte size, and tumor associated macrophages in DIO mice. DIO mice had significantly increased (A) *ex vivo* tumor volume compared to DIO + resveratrol ($P < 0.01$) and control ($P < 0.0001$). To detect differences in (B) intratumoral adipocytes we analyzed tumor H&E section on a subset of mice (n = 10/group) and measured the two-dimensional area of each adipocyte. The (C) median adipocyte size in tumors from DIO mice was significantly increased compared to both control ($P < 0.001$) and DIO + resveratrol ($P < 0.0001$). The abundance of (D) F4/80 positive staining was significantly higher in DIO mice compared with control and DIO + resveratrol mice. Representative image shown in (E). Data presented as mean ± s.d. Differences in significance denoted by different letters (a,b).

Table 2.4. Resveratrol levels detected in tumors		
Resveratrol ng/μg wet weight		
Control	**DIO**	**DIO + resveratrol**
n=4 tumors	**n=4 tumors**	**n=7 tumors**
0	0	100
0	0	59
0	1	51
0	0	48
-	-	151
-	-	58
-	-	36

E. Discussion

We report that resveratrol supplementation prevents obesity-induced adipose tissue dysfunction, chiefly adipocyte hypertrophy, and reduces tumor growth in obese mice orthotopically transplanted with an aggressive claudin-low subtype of breast cancer. The anticancer effects of resveratrol in DIO mice were associated with: 1) smaller mammary adipocyte size; 2) lower expression of genes (normalized to control levels) involved in promoting inflammation, macrophage recruitment and signaling; 3) decreased mammary CLS; 4) lower expression of COX-2 and pro-inflammatory eicosanoids; and 5) maintenance of mammary expression of pro-adipogenic genes, notably PPARγ.

This study contributes vital knowledge about the impact of resveratrol supplementation on obesity-associated metabolic dysfunction and mammary tumor progression. Our findings are in agreement with several other studies demonstrating

that resveratrol supplementation in the context of a DIO diet favorably modulates measures of insulin sensitivity and adipose tissue inflammation to levels comparable to lean, metabolically healthy counterparts [54,130,143]. Furthermore, the anticancer benefits we observed on claudin-low mammary tumor growth are consistent with findings investigating the effects of resveratrol in lung, skin, ovarian, colon, and prostate cancer studies [144-149]. The observation that resveratrol exerts potent anticancer effects in obese mice supports the hypothesis suggested by several reports that resveratrol primarily exerts beneficial effects in the face of metabolic perturbations or inflammation (as occurs with obesity). For example, Kang et al. showed that resveratrol improved insulin signaling only in the face of an insulin resistant state in vitro and in vivo [150]. Carreras et al. demonstrated that resveratrol supplementation in male mice reduced visceral white adipose tissue macrophages under conditions of intermittent hypoxia in a mouse model of sleep apnea, but not under normal conditions in wild-type mice [151]. One apparent exception to the notion that resveratrol exerts anticancer effects primarily in the context of a pro-inflammatory state is from 7,12-Dimethylbenzanthracene (DMBA)-induced mammary carcinogenesis studies in which resveratrol enhanced cell-mediated immune response and apoptosis and reduced epithelial carcinogenesis in lean mice [152]. However, even though the mice in this study were lean, topical DMBA treatment is well known to increase cutaneous oxidative stress and inflammation regardless of body weight or adiposity [132,133].

Inflammation reprograms the cellular composition of adipose tissue, including an influx of macrophages and other immune cells that secrete factors to propagate additional macrophage recruitment. TNF-α is produced by macrophages and is the

predominant cytokine contributor to insulin resistance in the adipose tissue. TNF-α inhibits adipogenesis, reduces the expression of genes in mature adipocytes that enable an adequate insulin response, and directly interferes with insulin-induced glucose metabolism by downregulating glucose transporter (GLUT)-4 as well as the activity of IRS-1 [153,154]. In our study, we demonstrated that resveratrol supplementation decreased serum TNF-α as well as mammary TNF-α gene expression. Our findings are consistent with Kang et al. which showed that resveratrol inhibited TNF-α release from macrophages and adipocytes after exposure to conditioned media from macrophages treated with resveratrol [155]. Adipose tissue inflammation, including high levels of TNF-α, drives adipose-derived stem cells towards an endothelial cell or fibroblast fate rather than differentiation into a mature adipocyte [156]. The anti-inflammatory activity of resveratrol, including the decreased TNF-α expression and prevention of macrophage infiltration into the adipose tissue, supports adipogenesis. This is consistent with the findings of Hu et al., who examined the in vitro effects of resveratrol supplementation in 3T3-L1 preadipocytes at varying doses and found that resveratrol treatment at physiologically relevant levels (1 and 10 μM) enhanced 3T3-L1 adipocyte differentiation while doses above 10 μM resveratrol induced cell death [157].. Other groups have shown that deleterious levels of TNF-α, prevalent in obesity, can stimulate the dedifferentiation of adipocytes, which delipidate and take on a fibroblast-like phenotype and lack the ability to respond to insulin and store triglyceride [158]. The apparent dose-dependent effects on preadipocyte fate is supported by several reports showing that resveratrol at very high concentrations inhibits PPARγ, adipocyte differentiation and adipocyte viability in vitro [159,160]. In addition to impacting

preadipocyte fate, resveratrol has also been shown to inhibit breast cancer stem cells by suppressing the Wnt/β-Catenin signaling pathway, which is involved in tumor growth and metastasis and can also regulate adipogenesis [161].

We report here that supplementation of resveratrol in the diet (0.5% w/w) resulted in an average intake/kg body weight/day of 532.4 mg/kg/day, which is in the upper half of the range of doses shown to have anticancer effects in multiple preclinical cancer studies [162]. We found that this pharmacologic level of resveratrol supplementation in DIO + resveratrol mice relative to DIO mice did not impact body weight or body fat percentage, but did impart considerable protection against obesity-associated inflammation. Preventing adipocyte hypertrophy and the associated shift in pro-inflammatory cytokines (including TNF-α and IL-6) produced by hypertrophied adipocytes may explain why DIO + resveratrol mice, relative to DIO mice, had lower gene expression of cytokines associated with recruitment of macrophages, as well as lower COX-2 expression. Notably, our adipogenesis array in the mammary fat pad revealed that resveratrol offset the obesity-induced decrease of pro-adipogenic gene signaling (Figure 2.6), with a shift in gene expression in DIO + resveratrol towards that observed in control rather than DIO mice. Konings et al. reported that resveratrol supplementation (at 150 mg/day, ~ 1.5 mg/kg body weight/day) for 30 days in obese men significantly decreased abdominal subcutaneous adipocyte size [130], [163]. Similar to our findings, Konings et al. also completed a microarray analysis, which indicated a downregulation in Wnt signaling. Additionally, Jimenez-Gomez et al. observed that rhesus monkeys on a high-fat, high-sugar diet supplemented with resveratrol (80 mg/day in year 1; 480 mg/day in year 2) displayed an increase in the

number of small adipocytes in visceral white adipose tissue and a significant difference in mean adipocyte size between the animals on the high-fat, high-sugar diet vs. high-fat, high-sugar diet + resveratrol [54].

From our adipogenesis array, we observed that DIO + resveratrol mice displayed Pgc1α and Fabp4 expression levels that were not statistically different from control mice, while DIO mice had significantly lower expression of both genes. Pgc1α and Fabp4, which facilitate adipose beiging and fatty acid uptake, respectively, are downstream targets of PPARγ [164]. Prevention of the aberrant decrease in gene expression of adipogenesis-related and beiging-related genes observed in DIO mice may also contribute importantly to the protective effects of resveratrol against tumor growth in DIO + resveratrol mice. Enrichment of beige/brown adipose tissue relative to white adipose tissue could change the adipose secretome and limit lipids and other nutrients available to the tumor. Previous reports provided additional evidence that resveratrol enhances beige adipocyte development. For example, Zou et al. found white adipose tissue browning in the male offspring of obese mothers supplemented with resveratrol in the diet (0.2% w/w) during pregnancy [165]. Resveratrol also induced adipose browning when added to an obesogenic diet [166].

There were several limitations to our study. First, we attempted to measure levels of resveratrol metabolites in the serum but had a limited number of samples pass the threshold of detection. Thus, we are unable to report the serum levels that our dose achieved. However, we were successful in measuring resveratrol levels in our tumors and found a range from 157.7 nmol/g to 661.5 nmol/g (Supplementary Table 2.3). This is comparable to the levels in the murine prostate reported by Narayanan et al. that

range from 175.2 nmol/g to 416.2 nmol/g [149]. To our knowledge tissue resveratrol concentrations in human tumors following resveratrol supplementation have not been reported so we unfortunately cannot compare the levels observed in our preclinical studies to human studies. Another limitation of our study is the lack (due to funding restrictions) of a normal weight control group supplemented with resveratrol, which could have more clearly delineated the effects (if any) of resveratrol in the absence of obesity. We also found no effect of resveratrol on the sirtuin pathway in our study. In vitro studies and some in vivo studies have reported that the anticancer effects of resveratrol may involve SIRT1 activation, although this may be dose-dependent [167].

Given the high prevalence of obesity in the US and many other countries, the emerging association between obesity and the development and progression of several breast cancer subtypes (including the deadly claudin-low breast cancer subtype), and the current lack of targeted therapies for this and other subtypes of triple-negative breast cancer, our findings have several important implications. Our preclinical data is the first to establish that resveratrol supplementation prevents obesity-associated increases in claudin-low mammary tumor growth, mammary adipocyte hypertrophy, COX-2 expression, macrophage infiltration, adipose CLS enrichment, and serum cytokines. Resveratrol supplementation also ameliorates downregulation of adipocyte PPARγ and other adipogenesis genes in DIO mice. We conclude that preventing obesity-associated adipose tissue dysregulation can be achieved with resveratrol supplementation and may represent an effective intervention strategy for breaking the links between obesity and breast cancer, including the claudin-low subtype.

CHAPTER III: TARGETING OBESITY-ASSOCIATED INFLAMMATION TO DECREASE MURINE BASAL-LIKE MAMMARY TUMOR BURDEN

A. Chapter Précis

Adipose tissue dysregulation, a hallmark of obesity, contributes to a chronic state of low-grade inflammation, which can promote cancer growth through multiple signaling pathways. We tested the hypothesis that anti-inflammatory supplementation with the non-steroidal anti-inflammatory drug (NSAID) Sulindac or Omega-3 ethyl esters can reduce chronic obesity-associated inflammation, which may function as a critical driver of the enhanced basal-like breast cancer (BLBC) growth observed in obesity. 120 female 6-8 week old C57BL/6 mice were administered a control diet (10% kcal from fat) or diet-induced obesity regimen (DIO, 60% kcal from fat) resulting in normal weight (NW) Control or Obese phenotypes, respectively. After 15 weeks, mice on each diet were randomized to receive no supplement (Control), Sulindac (160 ppm) or Omega-3 ethyl esters (25 ppm) in the diet, resulting in n=20/group. Ten weeks later, all mice were orthotopically injected with E0771 cells, a model of BLBC. Five mice/group were euthanized at a 4-week intermediate time-point after injection, while 15 mice/group continued in a survival study. Mammary median adipocyte size was lower in DIO+Sulindac mice compared to DIO and DIO+Omega-3 mice, though neither anti-inflammatory supplement affected body weight or total body fat percentage. Sulindac supplementation in DIO mice (but not in NW Control mice) significantly reduced mean tumor volume at the 4-week intermediate time point and increased tumor latency in the

survival arm of the study, in comparison to non-supplemented counterparts. Omega-3 supplementation in DIO mice produced an intermediate reduction in tumor volume but did not significantly affect survival. DIO+Sulindac mice also displayed significantly decreased levels of pro-inflammatory eicosanoids in the tumor compared to DIO and DIO+Omega-3, including PGE_2, $PGF_{2\alpha}$ and 13 PGE_2. Furthermore, Sulindac supplementation inhibited adipose tissue dysregulation in DIO mice, significantly reducing mammary CLS density and modulating expression of pro-inflammatory genes and genes involved in lipid metabolism. Our findings demonstrate that Sulindac was a more effective anti-tumor agent than Omega-3 in our mouse model of basal-like breast cancer, possibly via superior anti-inflammatory activity. Mechanism-based anti-inflammatory interventions within the diet may help to suppress obesity-induced inflammation and break the obesity-cancer link.

B. Introduction

Obesity is characterized by an upregulation in inflammatory pathways and dysregulated metabolism [103]. The excessive adipocyte lipolysis that typically accompanies obesity produces pathogenic levels of free fatty acids (FFA), which are increased by 20-40% in the plasma of obese humans and mice compared to their lean counterparts [63,64]. These FFA activate the NF-κB pathway, a key regulator of inflammation, and enhance cyclooxygenase 2 (COX-2) expression and recruitment of inflammatory macrophages [86]. In addition, adipocyte lipolysis preferentially releases eicosapentaenoic acid and arachidonic acid, precursors for the 3- and 2- series of prostaglandins, respectively [168]. COX and LOX produce anti-inflammatory eicosanoid

products from Omega-3 PUFAs, whereas proliferative and pro-inflammatory eicosanoid mediators are produced from arachidonic acid [169]. PGE_2 is the most abundant COX-derived product, and it exacerbates metabolic dysfunction in obesity in part by inhibiting adipogenesis. Hu et al. used a combination of in vivo and in vitro techniques to show that adipocytes undergoing lipolysis produce PGE_2, which also strongly promotes macrophage migration [94].

Pre-clinical studies utilizing celebcoxib, a selective COX-2 nonsteroidal anti-inflammatory drug (NSAID), or genetic deletion of COX-2 heavily implicate COX-2 as a mediator of adipose tissue dysregulation [92]. Mice on a high-fat diet that received celecoxib have shown reduced expression of monocyte chemoattractant protein 1 (MCP-1) with concurrent decreases in macrophage infiltration in epididymal and subcutaneous fat depots [92]. Michaud et al. demonstrated that enhanced lipolytic responsiveness significantly correlated with adipocyte size and expression of macrophage markers CD68 and CD11b. However, the correlation remained significant after adjusting for adipocyte size, rendering macrophages more responsible for high lipolytic responsiveness [170].

Changes in the cellular composition of the mammary tissue in obese women further enhance PGE_2 production. Hypertrophic adipocytes secrete larger amounts of pro-inflammatory cytokines such as TNF-α and Hif-1α compared to adipocytes that are normal in size. TNF-α is a potent inhibitor of adipogenesis and can prevent preadipocytes from differentiating into mature adipocytes or stimulate dedifferentiation of mature adipocytes into a fibroblast-like cell [99]. Hif-1α binds to a hypoxia-responsive element on the COX-2 promoter, resulting in an upregulation of COX-2 and its

metabolite PGE_2 during hypoxia [171]. Thus, in the obese mammary stroma, fibroblasts and preadipocytes are rich sources of PGE_2 [100].

COX-2 expression, in association with increased PGE_2 levels, has also been linked to increased metastasis and reduced breast cancer survival [95,96]. Zhou et al. found that triple-negative breast cancer (TNBC) patients and non-TNBC patients expressed similar levels of COX-2 (32.3% and 38.6%, respectively). However, positive COX-2 expression only correlated with TNBC patient survival [172]. Sulindac is an NSAID that inhibits both COX-1 and COX-2. Preclinical studies utilizing sulindac have shown an anti-cancer benefit related to pro-apoptotic and insulin sensitizing effects as well as a favorable modulation of bioactive lipids and subsequent effects on the immune response [173-175]. Omega-3 ethyl esters have also been shown to inhibit COX-2 and blunt the pro-tumorigenic effects of obesity by reducing inflammatory signaling [134,176]. We tested the hypothesis that supplementation of the anti-inflammatory compounds sulindac or Omega-3 ethyl esters would blunt the protumorigenic effects of obesity in a model of basal-like breast cancer, the most common form of TNBC.

C. Materials and Methods

In vivo studies

All animal studies and procedures were approved and monitored by the University of North Carolina at Chapel Hill Institutional Animal Care and Use Committee.120 female 6-8 week old C57BL/6 mice were administered a control diet (10% kcal from fat) or diet-induced obesity regimen (DIO, 60% kcal from fat) resulting in normal weight (NW) Control or Obese phenotypes respectively. After 15 weeks, mice on

each diet were randomized to receive no supplement, Sulindac (160 ppm) or Omega-3 ethyl esters (25 ppm) in the diet, resulting in n=20/group. All mice were fed *ad libitum* and diets were purchased from Research Diets (New Brunswick, NJ). Diets were stored at 4°C in sealed bags and replaced biweekly to prevent oxidation. Nine weeks after initiating anti-inflammatory supplementation, all mice underwent a submandibular bleed for serum collection. One week later, mice received an orthotopic injection of 30,000 E0771 cells, a model of basal-like breast cancer. Five mice/group were killed, and their tissue collected and stored at an intermediate time-point four weeks after injection, while 15 mice/group continued in a survival study; these mice were killed when tumor size reached 1.2 cm in diameter in any direction. Transplanted tumor growth was monitored daily and tumors were measured biweekly with calipers. At study endpoint (interim or survival sac) mice were euthanized by CO_2 inhalation followed by cervical dislocation and tumors and mammary fat pad were excised and weighed, then divided in portions to be formalin fixed or flash frozen in liquid nitrogen and stored at -80°C until further analysis. *Ex vivo* tumor volume was calculated using the ellipsoid formula $1/6\pi \times D_1 \times D_2 \times D_3$ where D_1, D_2, and D_3 indicate three distinct diameter measurements in millimeters.

Quantitative magnetic resonance analysis

Body composition was measured on all mice at end of study by quantitative magnetic resonance (qMR) (Echo Medical Systems, Houston, TX). Measurements included lean mass, fat mass and total water mass. Percent body fat was calculated by dividing fat mass by total body weight.

Serum hormone and adipokine and measurement

Nine weeks after initiating the anti-inflammatory supplementation, blood was collected from mice fasted 4-6 hours by submandibular bleed, allowed to clot for 30 minutes at room temperature, and serum was collected and flash frozen for subsequent analyses. Serum hormones and adipokines including insulin, leptin, adiponectin, and resistin were measured using Bio-Plex Pro™ Mouse Diabetes Panel 8-Plex, Mouse Diabetes Adiponectin Assay, respectively (Bio-Rad Laboratories; Hercules, California). Insulin-like growth factor 1 (IGF-1) concentrations were measured using R & D systems IGF-1 Bead-Based Single-plex Luminex assay (Minneapolis, MN).

Histopathology and analysis of mammary and intratumoral adipocyte size

Paraffin embedded mammary and tumor tissue were cut into 4 μm thick sections for hematoxlin and eosin (H&E) staining. Slides were deparaffinized and processed as previously described [137]. Slides were scanned and digitized using the Aperio CS2 Digital Pathology Scanner (Leica Biosystems, Wetzlar, Germany). Quantification was performed using Aperio Digital Pathology platform. Briefly, three representative areas / tissue (mammary or tumor) were viewed at 8.8X magnification (300 μm) and the size of mammary fat pad adipocytes (calculated as two-dimensional area) was quantified using ImageJ Version 1.51e (National Institute of Health, Bethesda, Maryland). An adipocyte tool macro (MRI Adipocyte Tools.txt) was downloaded from (http://dev.mri.cnrs.fr/projects/imagej-macros/wiki/Adipocytes_Tool) and imported into ImageJ. A preprocessing and simple segmentation algorithm was run on each

snapshot. The output generated gave squared area in pixels and number of adipocyte counts. Area in pixels was converted to μm^2 using a Moticam Aperio scanned image of a 0.15 mm calibration slide. The area values from the representative three digital images yielded between 345-1991 measurements for each mouse, which were then compiled to calculate the 10^{th}, 50^{th} and 90^{th} percentile of adipocyte area. Resultant percentiles were then averaged by group.

Crown-like structure analysis

The formation of crown-like structures (CLS) was assessed from hematoxylin and eosin staining of 4 μm thick sections prepared from formalin-fixed paraffin embedded mammary fat pad tissue. Briefly, the total number of CLS were counted in a blinded fashion. CLS density measures were achieved by dividing CLS by the total slide area used for analysis using ImageScope Viewing Software Version 12.0 (Leica Biosystems). Values expressed as CLS/area of tissue in cm^2.

Quantitative RT-PCR

Total RNA was extracted from the flash-frozen mammary fat pad samples collected at end of study using TRI-Reagent (Sigma-Aldrich, St.Louis, MO) according to manufacturer's instructions. RNA concentration was spectrophotometrically determined using a nanodrop (Thermo Scientific, Logan, UT) and quality was confirmed using an Agilent 2100 Bioanalyzer (Santa Clara, CA). RNA was reverse transcribed with Multiscribe RT (Applied Biosystems, Carlsbad, CA). Resulting cDNA from tissue samples were assayed in triplicate for PCR using Taqman® Gene Expression Assays.

PCR reactions were completed using a ViiA™ 7 Real time PCR system (Applied Biosciences). Gene expression data were normalized to the housekeeping gene β-actin and analyzed using the delta delta cycle threshold method.

Eicosanoid analysis

Eicosanoids in the tumor tissues were extracted and analyzed by liquid chromatography/tandem mass spectroscopy (LC/MS/MS) using the modified method described previously [138]. LC/MS/MS analyses were performed using an Agilent 6460 triple quadrupole mass spectrometer (Agilent Technologies) equipped with an Agilent 1200 binary pump high-performance liquid chromatography (HPLC) system as described previously [139].

Cytokine Antibody Array

Analysis of inflammatory proteins was assessed using RayBio® C-Series Custom Cytokine Antibody Array. Serum was pooled (n = 3/group) and diluted (1:20) in blocking buffer. Membranes were placed into each well and incubated for 30 minutes in blocking buffer at room temperature. Blocking buffer was then aspirated and all samples were added to a designated well and incubated overnight at 4°C. Next, each membrane was thoroughly washed with wash buffer then incubated with a biotinylated antibody cocktail for 1.5 hours at room temperature. After the addition of the cocktail, 1X HRP-Steptavidin was added to each well and incubated for 2 hours at room temperature. Membranes were then washed again and transferred, printed side up, onto a sheet of

blotting paper. Detection buffer was added to each membrane and chemiluminescence signals were assessed using a ChemiDoc™XRS+ System.

In Vitro studies

Cell viability

E0771 murine breast cancer cell line was maintained in RPMI 1640 medium (GIBCO Life Technologies, Waltham, MA), supplemented with 10 mmol/L HEPES and 10% fetal bovine serum (FBS). For PGE_2 and Sulindac coculture viability assays, cells were seeded at a density of $3x10^3$ in a 96 well plate. The next day cells were then exposed to vehicle (DMSO), or one of three PGE_2 levels (250 ng/mL, 50 ng/mL, or 5 ng/mL) and/or one of two Sulindac doses (500 μM, 50 μM) for 48 hours. Cells were treated with CellTiter-Glo (Promega). For experiments utilizing Sulindac over a time-course, cells were then seeded at a density of $5x10^3$ in a 96 well plate. After 24 hours of growth in the 10% FBS media, the cells were then exposed to either a low (50 μM) or high dose (500 μM) of Sulindac (Sigma Aldrich, St. Louis, MO) diluted in 1.0% of dimethyl sulfoxide (DMSO, Sigma Aldrich). After 24 hours of treatment, the wells were aspirated, washed, and trypsinized into a microcentrifuge tube containing a 1:1 ratio of trypan blue (Thermo Fisher Scientific, Waltham, MA. Cell viability was assessed using a TC20^{TM} Automated Cell Counter (Bio-Rad, Hercules, CA). All experimental conditions were repeated in triplicates over the course of seven days.

Statistical Analysis

All values are represented as mean ± standard deviation (s.d.). One-way analysis of variance (ANOVA) using Tukey's multiple comparisons correction was used to assess the effects of diet regiment on body weight and fat percentage, mean tumor volume, serum hormone concentrations and mammary fat pad gene expression. Results were analyzed using GraphPad Prism software (Graphpad Software Inc., La Jolla, CA) and $P \leq 0.05$ was considered statistically significant.

D. Results

Anti-inflammatory supplementation does not impact body weight in NW Control or DIO mice

The DIO and control regimens effectively generated obese and normoweight (NW) phenotypes, respectively (Figure 3.1). At week 15, the average weight of mice on the DIO regimen was 32.9 ± 4.3g, which was statistically higher than the average weight of mice on the control regimen, 21.8 ± 1.2g ($P < 0.0001$). Approximately ten weeks of anti-inflammatory supplementation did not significantly impact body weight of mice on the DIO regimen (DIO: 43.8 ± 4.0g; DIO+Sulindac: 41.6 ± 5.8g; DIO+Omega-3: 46.4 ± 7.2g; *NS*) or the control regimen (NW Control: 21.8 ± 1.2g; NW Control+Sulindac: 21.8 ± 1.6g; NW Control+Omega-3: 21.6 ± 1.4g; *NS*). No statistically significant differences in body weight or calorie intake were detected within NW Control ± anti-inflammatory and DIO ± anti-inflammatory mice throughout study. NW Control and DIO mice supplemented with Sulindac consumed on average 16.8 ± 0.5 and 11.9 ± 0.7 mg sulindac/body weight (g)/day, respectively. NW Control and DIO mice supplemented

with Omega-3 consumed on average 271.4± 16.7 and 180.2 ± 7.0 mg Omega-3/body weight (g)/day, respectively.

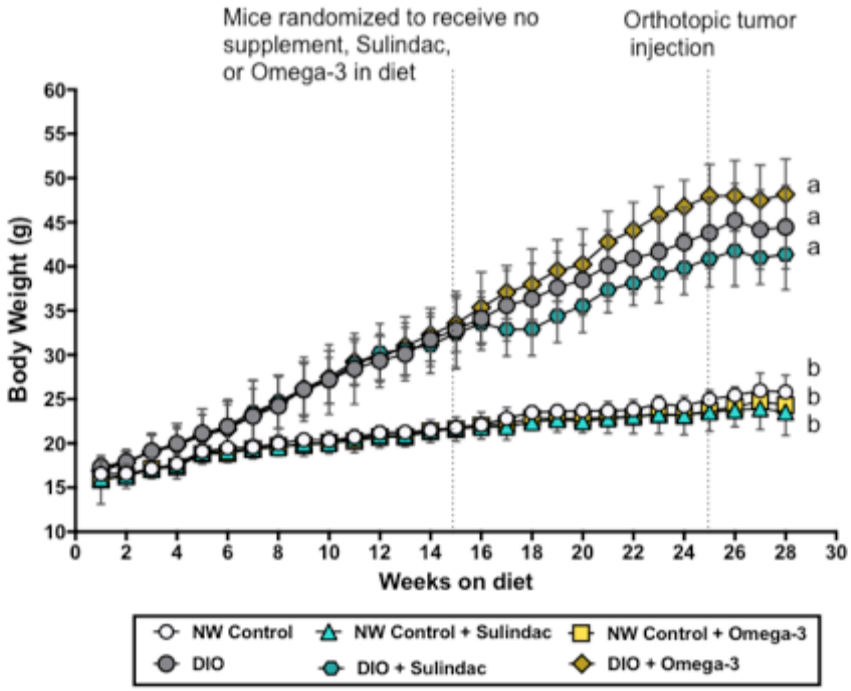

Figure 3.1. Anti-Inflammatory supplementation does not impact body weight in NW Control or DIO mice. Sulindac or Omega-3 supplementation in NW Control and DIO mice does not impact body weight. Data presented as mean ± s.d. Differences in significance noted by different letters (a,b); *P* value < 0.05.

Anti-inflammatory supplementation minimally impacts total adiposity and adipose distribution

Percent body fat, (Figure 3.2A) obtained at end of study, was significantly lower in all control mice (NW Control: 20.1 ± 8.3%; NW Control+Sulindac: 17.6 ± 4.6%; NW Control+Omega-3: 18.0 ± 9.8%) compared with all DIO mice (DIO: 53.9 ± 4.2%; DIO+Sulindac: 45.5 ± 5.7%; DIO+Omega-3: 52.4 ± 8.3%). *P* < 0.001 for all comparisons NW Control ± anti-inflammatory vs. DIO ± anti-inflammatory. Additionally, we measured *ex vivo* weight of adipose depots to investigate changes in adipose distribution in mice. We collected and measured mouse visceral white adipose tissue (VWAT), defined as

adipose tissue internal to and surrounding the abdominal wall; interscapular fat (IF), defined as the adipose lying dorsal to the scapular region; and mammary fat pad (MFP), defined as the 9th mammary fat pad completed removed. DIO mice had greater *ex vivo* fat depot weights compared to NW Control mice with few distinctions. VWAT weight was highest in DIO+Omega-3 mice, with intermediate weights in DIO mice, statistically greater than DIO+Sulindac (Figure 3.2B). IF weight was similar among all DIO mice ± anti-inflammatory (Figure 3.2C). DIO+Sulindac mice had significantly lower *ex vivo* weight of the mammary fat pad distal to the tumor at end of study compared to DIO alone and DIO+Omega-3 mice (Figure 3.2D).

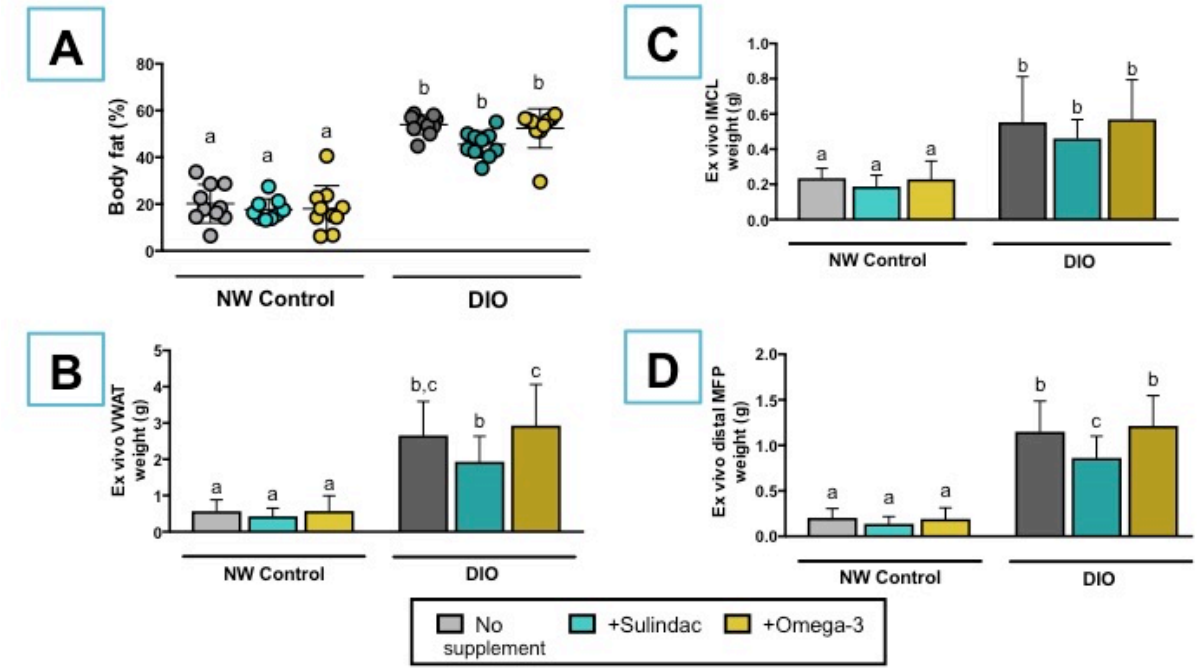

Figure 3.2. Anti-Inflammatory supplementation minimally impacts total adiposity and adipose distribution. Sulindac or Omega-3 supplementation in NW Control and DIO mice does not impact (A) body fat percentage, however DIO+Sulindac mice had lower ex vivo weight of (B) visceral white adipose tissue compared to DIO+Omega-3 mice. No differences were observed between DIO mice ± anti-inflammatory in interscapular fat (IF) however DIO+Sulindac mice had significantly decreased (D) mammary fat pad (MFP) weight distal to tumor compared to DIO and DIO+Omega-3 mice. Data presented as mean ± s.d. Percent body fat was assessed using quantitative magnetic resonance spectroscopy. Differences in significance noted by different letters (a,b); *P* value < 0.05.

Anti-inflammatory supplementation minimally impacts serum metabolic hormones

Mice on the DIO regimen generally had increased serum levels of insulin, IGF-1, resistin, leptin, and PAI-1 compared to NW Control mice (Table 3.1). However, DIO+Sulindac mice displayed intermediate levels of serum insulin, which were not statistically different from NW Control or DIO mice. The insulin levels of DIO+Omega-3 mice remained statistically higher than NW Control mice. Serum levels of IGF-1, Resistin, and PAI-1 were intermediate in both DIO+Sulindac and DIO+Omega-3 mice, statistically equivalent to both NW Control and DIO mice.

Table 3.1. Effects of anti-inflammatory supplementation on serum metabolic hormones

	NW Control	NW Control + Sulindac	NW Control + Omega-3	DIO	DIO + Sulindac	DIO + Omega-3
Insulin (ng/mL)	416.1 ± 116.9^{a,c}	256.3 ± 121.6^{a}	329.2 ± 169.7^{a,c}	712.8 ± 252.8^{b}	581.3 ± 134.3^{b,c}	722.7 ± 182.3^{b}
IGF-1 (ng/mL)	87.0 ± 19.3^{a,b}	74.7 ± 16.1^{b}	87.4 ± 18.6^{a,b}	124.9 ± 27.0^{c}	107.5 ± 14.2^{b,c}	116.0 ± 12.2^{b,c}
Resistin (ng/mL)	1.4 x 10^{5} ± 6.8 x 10^{4a}	1.2 x 10^{5} ± 6.3 x 10^{4a}	1.1 x 10^{5} ± 5.7 x 10^{4a}	3.0 x 10^{5} ± 1.4 x 10^{5b}	2.1 x 10^{5} ± 6.8 x $10^{4a,b}$	2.2 x 10^{5} ± 9.7 x $10^{4a,b}$
Leptin (ng/mL)	2593.0 ± 2243.0^{a}	584.9 ± 769.7^{a}	792.5 ± 1173.0^{a}	28337.0 ± 20346.0^{b}	20055.0 ± 14688.0^{b}	31114.0 ± 10191.0^{b}
Adiponectin (µg/mL)	1.1 x 10^{7} ± 2.2 x 10^{6}	1.2 x 10^{7} ± 4.6 x 10^{6}	1.2 x 10^{7} ± 2.3 x 10^{6}	9.8 x 10^{6} ± 2.2 x 10^{6}	1.2 x 10^{7} ± 2.7 x 10^{6}	1.1 x 10^{6} ± 2.6 x 10^{6}
PAI-1 (ng/mL)	841.0 ± 205.0^{a}	859.4 ± 203.7^{a}	772.2 ± 189.7^{a}	1511.0 ± 526.0^{b}	1251.0 ± 385.3^{a,b}	1340 ± 440.4^{a,b}

Sulindac more effectively decreases tumor volume and extends tumor latency compared to Omega-3 supplementation in DIO mice

At the interim sac, the ex vivo tumor volume of DIO mice (894.4 ± 289.4 mm^3) was significantly greater than all other groups except for DIO+Omega-3 (757.0 ± 282.7 mm^3). The ex vivo tumor volume of DIO+Sulindac (495.6 ± 142.9 mm^3) mice was not statistically different from NW Control (328.2 ± 192.5 mm^3), NW Control+Sulindac (203.4 ± 129.1 mm^3) or NW Control +Omega-3 (287.2 ± 120.5 mm^3) mice (Figure 3.3A). Furthermore, in the survival arm of the study, DIO mice survived significantly less days (25.9 ± 4.2 days) after tumor injection (a proxy of tumor latency) than all other groups except for DIO+Omega-3 (28.5 ± 3.6 days). Alternatively, the average number of days after tumor injection DIO+Sulindac mice survived (31.2 ± 4.3 days) was not statistically different from NW Control (33.8 ± 3.3 days), NW Control+Sulindac (33.3 ± 3.0 days), or NW Control +Omega-3 (32.0 ± 2.9 days) (Figure 3.3B). Furthermore, H&E staining of tumors displayed a significant accumulation of large adipocytes in DIO mice but not DIO+Sulindac or DIO+Omega-3 mice, representative images shown (Figure 3.3C and 3.3D).

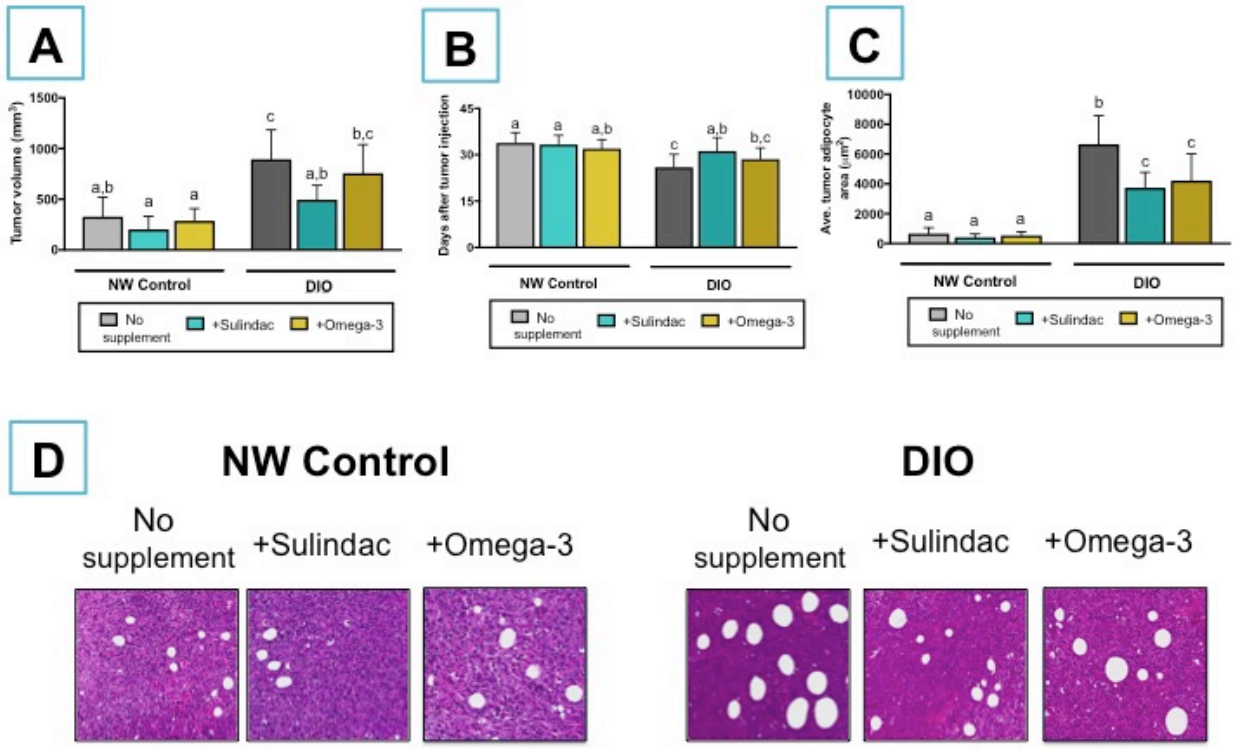

Figure 3.3. Sulindac more effectively decreases tumor volume and extends tumor latency compared to Omega-3 supplementation in DIO mice. (A) At the interim sac, the ex vivo tumor volume of DIO mice was significantly greater than all other groups except for DIO+Omega-3. Similarly, (B) DIO mice survived significantly less days after tumor injection (a proxy of tumor latency) than all other groups except for DIO+Omega-3. (C) DIO mice displayed significantly increased accumulation of large tumoral adipocytes compared to all other groups, (D) representative tumor H&E images shown. Data presented as mean ± s.d. Differences in significance noted by different letters (a,b); *P* value < 0.05.

Sulindac more effectively reduces eicosanoid levels in the tumor compared to Omega-3 supplementation in NW Control and DIO mice

NW Control and DIO mice supplemented with Sulindac demonstrated significant reductions in COX-2 metabolites (A) Prostaglandin E_2 (PGE_2); (B) Prostaglandin D_2 (PGD_2); (C) Prostaglandin $F_{2\alpha}$ ($PGF_{2\alpha}$); (D) 13 PGE_2; and (E) Thromboxane B_2 (TXB_2) compared to DIO mice without supplementation. However, mice supplemented with Sulindac also displayed reduced concentration of anti-inflammatory (F) Prostaglandin E_1

(PGE_1). DIO mice supplemented with Omega-3 displayed intermediate reductions in PGE_2 but not $PGF_{2\alpha}$, PGD_2 and 13 PGE_2.

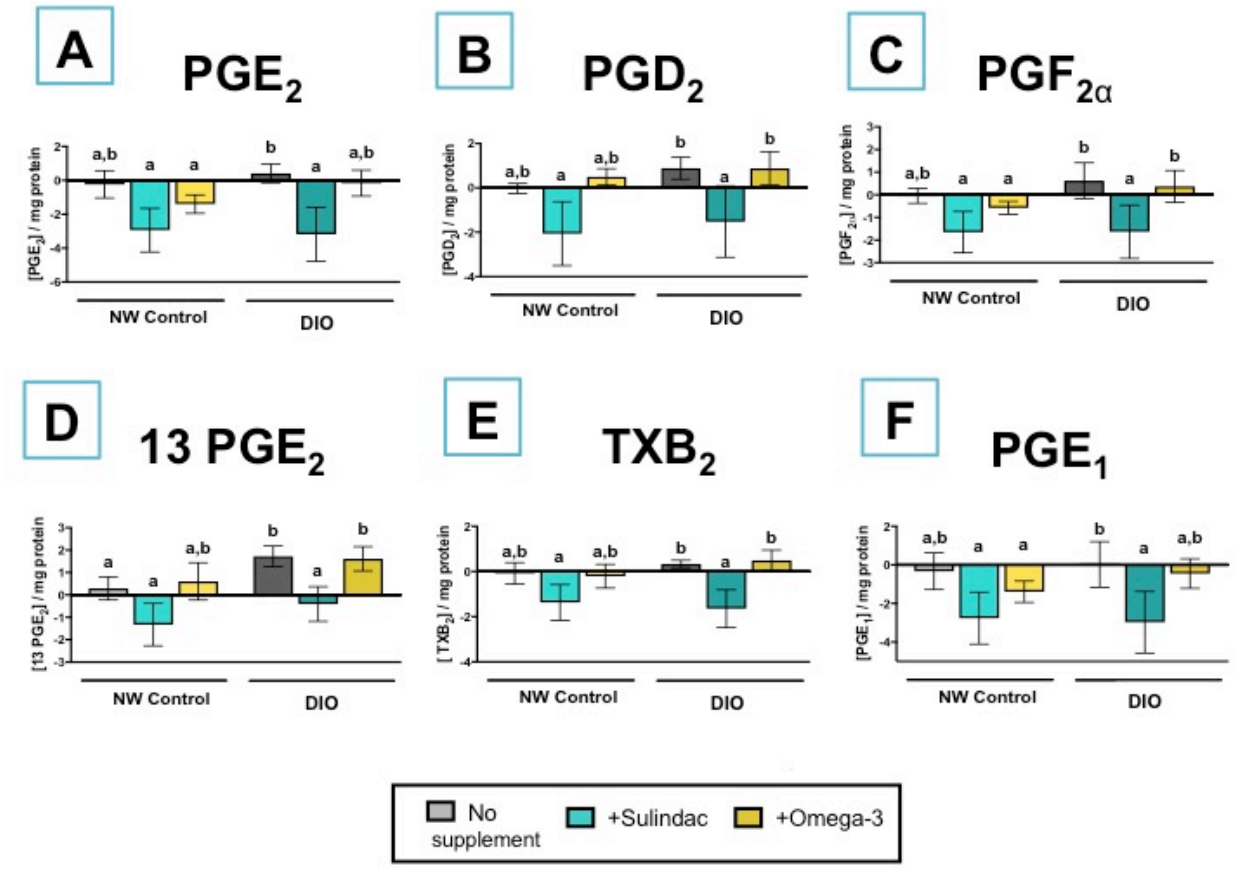

Figure 3.4. Sulindac more effectively reduces eicosanoid levels in the tumor compared to Omega-3 supplementation in NW Control and DIO mice. Eicosanoid levels were measured with liquid chromatography–mass spectrometry (LC-MS), reported concentration is normalized to mg tumor tissue and relative to NW Control without supplementation for (A) Prostaglandin E_2 (PGE_2); (B) Prostaglandin D_2 (PGD_2); (C) Prostaglandin $F_{2\alpha}$ ($PGF_{2\alpha}$); (D) 13 PGE_2; and (E) Thromboxane B_2 (TXB_2); and (F) Prostaglandin E_1 n= 4-6/group. Data presented as mean ± s.d. Differences in significance noted by different letters (a,b); *P* value < 0.05.

Sulindac more effectively protects against adipose tissue dysfunction compared to Omega-3 supplementation in DIO mice

DIO mice displayed significantly increased crown-like structure (CLS) density in the mammary fat pad (Figure 3.5A) compared to NW Control mice, with no differences

detected between NW Control mice ± anti-inflammatory. However, DIO+Sulindac mice displayed a CLS density that was significantly lower than DIO mice, and not statistically different from NW Control mice (Figure 3.5B). DIO+Omega-3 mice displayed an intermediate CLS density, which was not significantly different from DIO or NW Control mice (Figure 3.5B). We measured the two-dimensional area of each adipocyte using stained H & E sections of mammary fat pad tissue from 12-15 mice/group (Figure 3.5A and 3.5C). The median adipocyte size for DIO (4054 ± 790.4 μm^2) and DIO+Omega-3 (3833 ± 486.1 μm^2) was significantly higher than the median adipocyte size for DIO+Sulindac (2467 ± 594.6 μm^2), NW Control (1041 ± 356.3 μm^2), NW Control+Sulindac (868.2 ± 315.4 μm^2) and NW Control+Omega-3 (1005 ± 675.9 μm^2) (Figure 3.5C). Furthermore we plotted the frequency distribution of area of adipocytes (Figure 3.6) and found that DIO and DIO+Omega-3 mice had a shifted frequency towards larger adipocytes, an effect that was not observed in DIO+Sulindac mice. Minimal differences in the distribution of adipocyte among NW Control, NW Control+Sulindac, and NW Control+Omega-3 was detected (Figure 3.6)

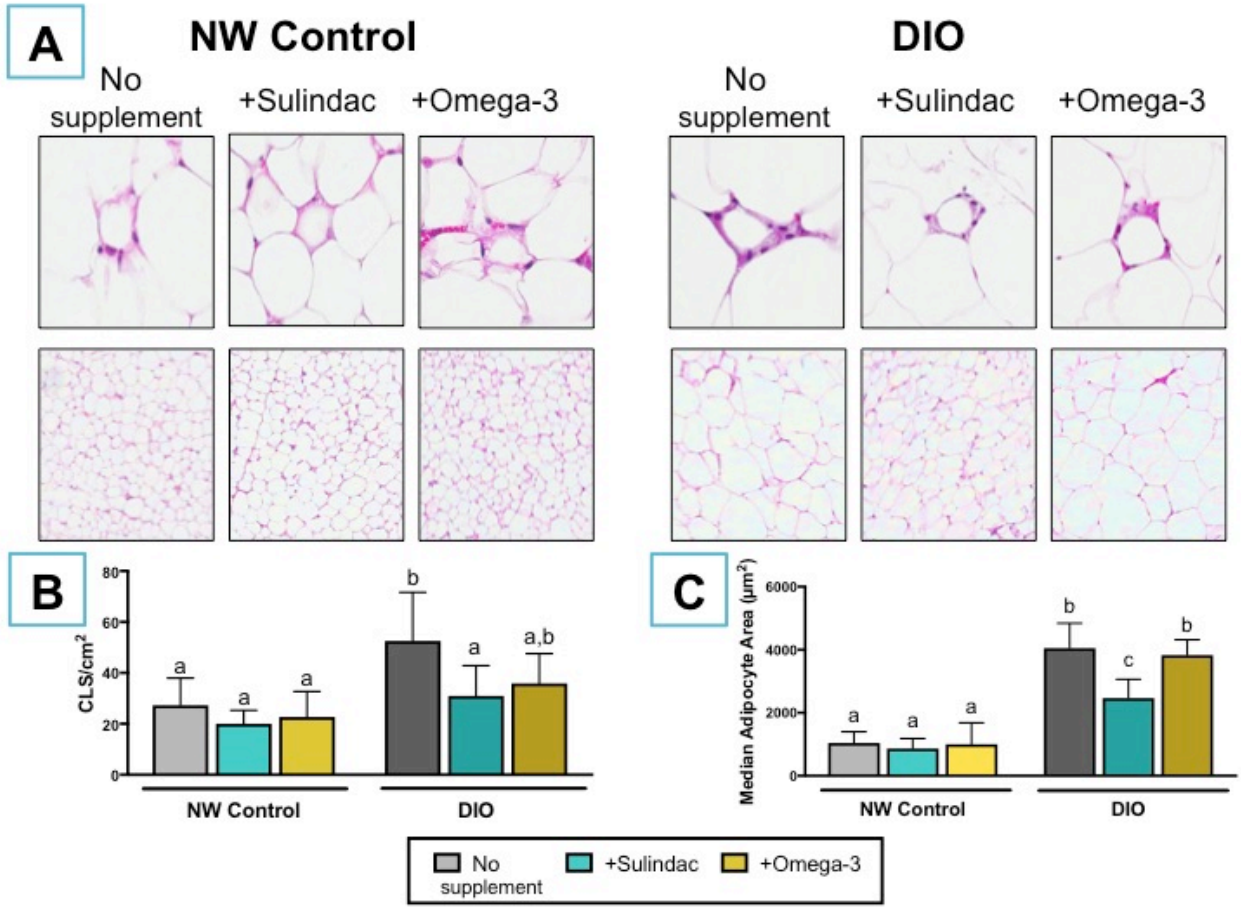

Figure 3.5. Sulindac more effectively protects against adipose tissue dysfunction compared to Omega-3 supplementation in DIO mice. NW Control mice had significantly decreased (A, C) crown-like structure (CLS) density and (C) median adipocyte area compared to DIO mice, regardless of supplementation. However, in DIO mice, Sulindac supplementation significantly decreased CLS density and median adipocyte area vs. DIO mice without supplementation. CLS and adipocyte area were analyzed using H & E sections of mammary fat pad, n = 10-12/group. Data presented as mean ± s.d. Differences in significance noted by different letters (a,b); *P* value < 0.05.

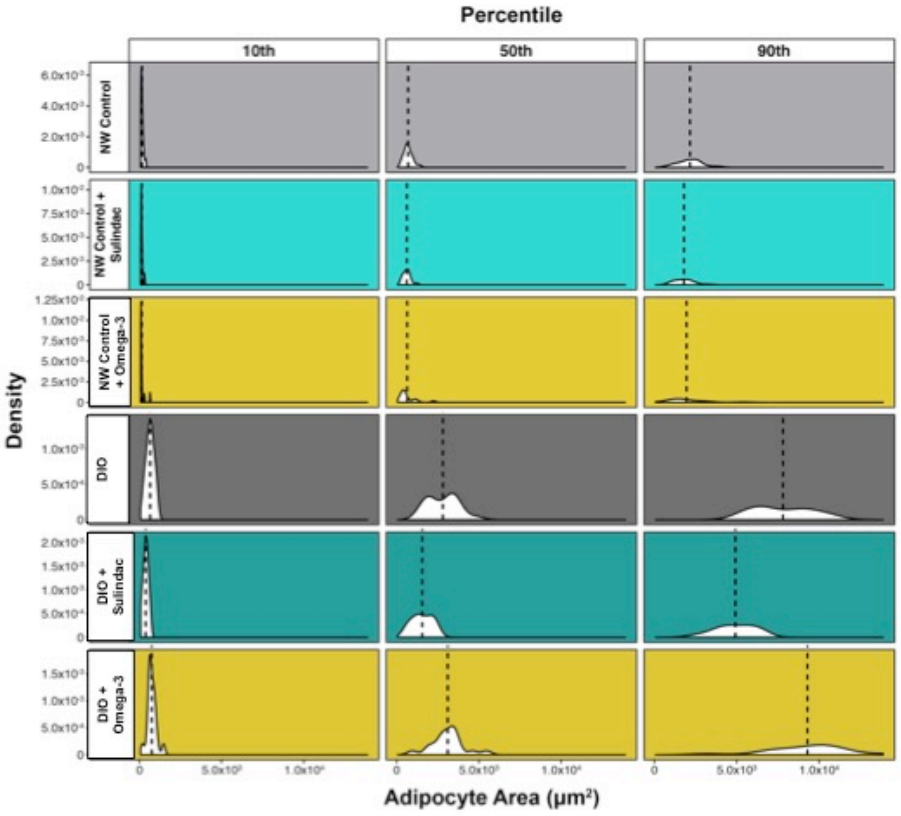

Figure 3.6. Sulindac, but not Omega-3 supplementation prevents changes in frequency distribution of adipocyte size in DIO mice. Anti-inflammatory supplementation in NW Control mice did not significantly impact the 10th, 50th, and 90th percentile of adipocyte area, indicative of adipocyte size. However, DIO+Sulindac mice displayed significantly reduced 50th and 90th percentile adipocyte size, suggesting that Sulindac supplementation in DIO mice prevents the adipocyte hypertrophy that occurred in DIO mice without supplementation and DIO+Omega-3 mice. Data presented as mean ± s.d. Differences in significance noted by different letters (a,b); *P* value < 0.05.

Sulindac more effectively protects against aberrant inflammatory and metabolism related gene expression in the mammary fat pad compared to Omega-3 supplementation in DIO mice

To investigate effectiveness as anti-inflammatory compounds, we quantified mRNA levels (mammary and tumor tissue) and protein expression (mammary tissue) for genes regulating in inflammatory and metabolic processes in mice. The mammary fat pad gene expression of monocyte chemoattractant protein 1 (MCP-1), interleukin 6 (IL-

6), toll like receptor 4 (TLR4), serum amyloid A3 (Saa3) and tumor necrosis factor α (TNF-α) were all significantly increased in DIO mice compared to both DIO+Sulindac and NW Control mice (Figure 3.7). DIO+Omega-3 mice displayed unchanged (relative to DIO) expression of MCP-1, intermediate expression (not significantly different from DIO or DIO+Sulindac) in IL-6, TLR4, Saa3 and TNF-α. Sulindac in DIO mice was also more effective at decreasing pertubations in expression of genes related to lipid metabolism. DIO mice had significantly lower mammary expression of peroxisome proliferator-activated receptor gamma (PPARγ), peroxisome proliferator-activated receptor gamma coactivator 1 (PGC-1α), and fatty acid synthase (Fasn) compared to NW Control mice, however DIO+Sulindac mice displayed normalized expression of these genes, not statistically different from NW Control (Figure 3.7). DIO+Omega-3 mice had intermediate expression of PPARγ, however mammary expression of PGC-1α and Fasn remained significantly decreased relative to NW Control. DIO mice had significantly increased of genes involved in lipolysis, monoacylglycerol lipase (Mgll) and hormone sensitive lipase (HSL) relative to NW Control mice, indicative of an impaired ability for insulin to inhibit lipolysis. DIO+Sulindac but not DIO+Omega-3 mice displayed normalized mammary gene expression of Mgll and HSL (not significantly different from NW Control mice). Analysis of inflammatory genes at the protein level (Table 3.2) supported the notion that DIO increased protein expression of pro-inflammatory mediators, which was prevented with sulindac supplementation in DIO mice. At the protein level, DIO+Sulindac and DIO+Omega-3 was both similarly effective at reducing levels of pro-inflammatory mediators. Notable exceptions include basic fibroblast growth

factor (bFGF) and macrophage colony-stimulating factor (M-CSF), and IL-4, which were increased in DIO+Omega-3 but not DIO+Sulindac.

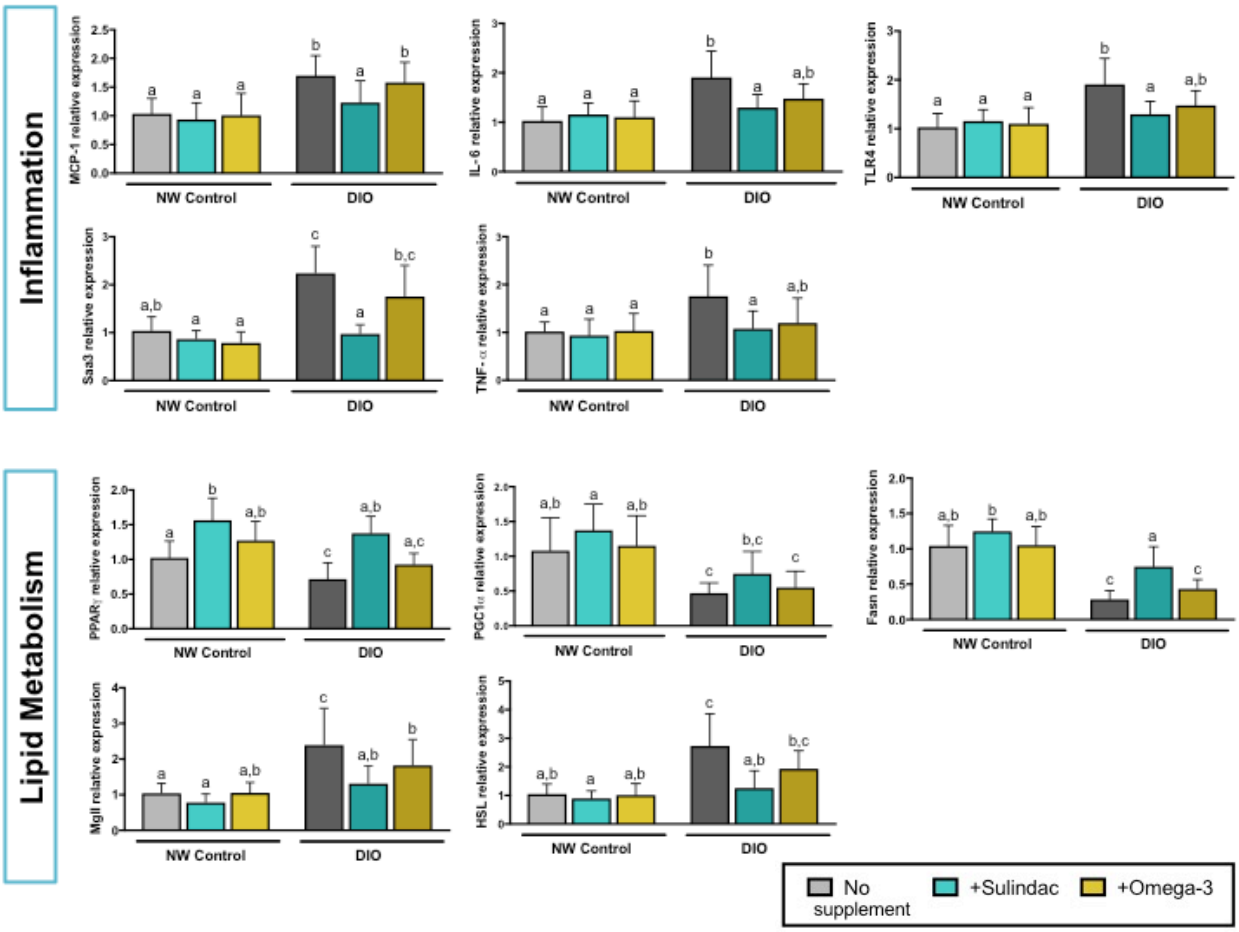

Figure 3.7. Sulindac more effectively protects against obesity-induced dysregulated expression of genes involved in inflammation and adipocyte metabolism in the mammary fat pad. Sulindac supplementation in DIO mice favorably modulated markers of inflammation monocyte chemoattractant protein 1 (MCP-1), IL-6, toll like receptor 4 (TLR4), serum amyloid A3 (Saa3), and tumor necrosis factor α (TNF- α). DIO mice had decreased gene expression of peroxisome proliferator-activated receptor gamma (PPARγ), peroxisome proliferator-activated receptor gamma coactivator 1-alpha (PGC-1α), and fatty acid synthase (Fasn) relative to NW Control mice. DIO mice had increased expression of monoacylglycerol lipase (Mgll) and hormone sensitive lipase (HSL) relative to NW Control mice. The expression of all genes (with the exception of PGC-1α, which was intermediate) was significantly different between DIO+Sulindac and DIO. Differences in significance noted by different letters (a,b); *P* value < 0.05.

Table 3.2 Inflammatory Protein Array Results in Mammary Fat Pad Tissue

	NW Control	NW Control + Sulindac	NW Control + Omega-3	DIO	DIO + Sulindac	DIO + Omega-3
Amphiregulin	2722 ± 1214[a]	2222 ± 1586[a]	1404 ± 1475[a]	7622 ± 2889[b]	2893 ± 2193[a]	2748 ± 1434[a]
bFGF	12885 ± 6824[a]	12012 ± 6511[a]	15387 ± 6233[a]	26487 ± 5736[b]	13302 ± 4710[a]	10650 ± 2636[b]
CTLA-4	423.4 ± 420.6[a]	969.7 ± 529.9[a]	716 ± 342[a]	8846 ± 4505[b]	2128 ± 852.4[a]	2516 ± 1443[a]
SDF-1	13845 ± 5118[a]	15896 ± 11915[a,b]	34623 ± 30836[a,b]	51252 ± 36596[b]	16644 ± 6480[a,b]	14862 ± 7903[a]
DKK-1	6452 ± 3384[a]	4435 ± 2078[a]	5264 ± 3169[a]	17518 ± 9293[b]	7112 ± 1779[a]	5116 ± 3295[a]
EGF	9885 ± 5046[a]	20425 ± 12573[a]	16400 ± 2079[a]	153643 ± 62137[b]	15409 ± 5247[a]	17413 ± 3899[a]
Fas Ligand	6315 ± 2922[a]	4155 ± 1957[a]	7620 ± 2768[a]	20015 ± 9072[b]	6615 ± 4579[a]	7816 ± 1512[a]
GCSF	11555 ± 5480[a]	10717 ± 6930[a]	14014 ± 8510[a]	28002 ± 4227[b]	8368 ± 2709[a]	7550 ± 2451[a]
GM-CSF	15926 ± 4657[a]	17997 ± 15180[a]	26839 ± 15527[a,b]	42281 ± 9051[a]	16387 ± 4516[a]	16277 ± 4426[a]
HGF	6864 ± 3525[a]	3574 ± 3728[a]	5839 ± 3268[a]	24373 ± 9920[b]	7511 ± 2774[a]	8769 ± 3361[a]
HGF R	6167 ± 1088[a]	5245 ± 3141[a]	6774 ± 3311[a]	18108 ± 8708[b]	7410 ± 3535[a]	7666 ± 2545[a]
ICAM-1	98801 ± 32115[a]	95376 ± 36186[a]	126863 ± 25656[a,b]	160182 ± 37439[b]	106253 ± 32385[a]	116220 ± 30030[a]
IGF-2	35713 ± 11449[a]	31352 ± 5672[a]	54389 ± 11017[b]	86954 ± 6937[c]	44700 ± 12770[a]	41328 ± 6442[a]
IL-1α	15738 ± 7396[a]	13698 ± 8994[a]	18505 ± 5089[a]	35799 ± 9504[b]	17942 ± 6894[a]	18660 ± 6644[a]
IL-1β	2931 ± 1415[a]	2978 ± 708.4[a]	3914 ± 2215[a]	10265 ± 2872[b]	4718 ± 2177[a]	5075 ± 3133[a]
IL-10	6598 ± 3268	6737 ± 2526	7092 ± 3094	12804 ± 6085	6846 ± 1178	7670 ± 3369
IL-13	7713 ± 2032[a]	7644 ± 3125[a]	9501 ± 4418[a]	20507 ± 3999[b]	10122 ± 3169[a]	10825 ± 2777[a]
IL-17A	3699 ± 1591[a]	2419 ± 1144[a]	3392 ± 1456[a]	13481 ± 5548[b]	4338 ± 1137[a]	3903 ± 1786[a]
IL-2	8138 ± 1741[a]	5443 ± 3374[a]	7772 ± 3116[a]	20299 ± 6820[b]	8633 ± 3070[a]	9039 ± 2841[a]
IL-2RA	4678 ± 2401[a]	3892 ± 2968[a]	5379 ± 2850[a]	20485 ± 11490[b]	5443 ± 1239[a]	5450 ± 2080[a]
IL-3	19688 ± 6230[a]	19255 ± 12221[a]	18898 ± 10644[a]	39078 ± 9912[b]	20130 ± 6696[a,b]	23144 ± 15045[a,b]
IL-4	35524 ±	34342 ±	46583 ±	73100 ±	37402 ±	55579 ±

	15513[a]	23325[a]	12073[a,b]	12816[b]	18522[a]	22683[a,b]
IL-5	5943 ± 1682[a]	5386 ± 5217[a]	8635 ± 3251[a]	21804 ± 6466[b]	6157 ± 2786[a]	8773 ± 2762[a]
IL-6	4134 ± 2494[a]	3160 ± 2891[a]	4224 ± 3477[a]	21712 ± 9440[b]	5660 ± 3632[a]	7373 ± 2231[a]
IL-9	6044 ± 2354[a]	9408 ± 5162[a,b]	11399 ± 7779[a,b]	20695 ± 16624[b]	12090 ± 3205[a,b]	14492 ± 3019[a,b]
KC	9524 ± 2473[a]	7388 ± 2423[a]	8914 ± 2221[a]	26285 ± 5439[b]	9980 ± 3419[a]	11059 ± 2713[a]
Leptin	5418 ± 3209[a]	3261 ± 2491[a]	4992 ± 1430[a]	28225 ± 8902[b]	6236 ± 2360[a]	10502 ± 3880[a]
Leptin R	11709 ± 2562[a]	16916 ± 5626[a]	16612 ± 6010[a]	31388 ± 10023[b]	16990 ± 3698[a]	18306 ± 5929[a]
LIX	181341 ± 104023[a]	231418 ± 38180[a]	254116 ± 43798[a]	251215 ± 101043[a]	255434 ± 150578[a]	255319 ± 39832[a]
M-CSF	22947 ± 5347[a]	28362 ± 10587[a]	28281 ± 6372[a]	49583 ± 4393[b]	29652 ± 5748[a]	37673 ± 15436[a,b]
MCP-1	47771 ± 10737[a]	49632 ± 19694[a]	59069 ± 15067[a]	115272 ± 14204[b]	61399 ± 8643[a]	64711 ± 16096[a]
MDC	1940 ± 1776[a]	1314 ± 768[a]	213 ± 642[a]	12093 ± 4382[b]	2327 ± 439[a]	3088 ± 777[a]
MMP-2	8204 ± 5422[a]	7858 ± 4521[a]	10055 ± 4250[a]	28233 ± 16289[b]	10676 ± 4162[a]	11252 ± 5626[a]
MMP-3	43469 ± 12866[a]	41908 ± 22351[a]	42475 ± 14190[a]	88358 ± 23027[b]	44543 ± 12682[a]	54281 ± 13397[a]
Pro MMP-9	17451 ± 4888[a]	14833 ± 2921[a]	16673 ± 7337[a]	51057 ± 31889[b]	15419 ± 3374[a]	19645 ± 7025[a]
RANTES	12338 ± 1995[a]	11447 ± 5128[a]	14506 ± 3411[a]	33485 ± 6579[b]	14870 ± 5816[a]	14645 ± 14645[a]
SCF	3768 ± 1748[a]	3696 ± 2197[a]	3370 ± 1672[a]	18115 ± 3744[b]	5116 ± 3445[a]	4506 ± 1851[a]
Shh N	13628 ± 2516[a]	11340 ± 5583[a]	14744 ± 4374[a]	42221 ± 16837[b]	15385 ± 5833[a]	19066 ± 6583[a]
TNF R1	37552 ± 10725[a]	35557 ± 16391[a]	37176 ± 16410[a]	97790 ± 29100[b]	37780 ± 4503[a]	47125 ± 11256[a]
TNF-α	6321 ± 2199[a]	5771 ± 2234[a]	6850 ± 2242[a]	36981 ± 21997[b]	7206 ± 2266[a]	9520 ± 3721[a]
TREM-1	5952 ± 1613[a]	5817 ± 2146[a]	6892 ± 3478[a]	18922 ± 6550[b]	6148 ± 1856[a]	8268 ± 2554[a]
VCAM-1	176771 ± 119840[a]	236798 ± 40653[a]	253938 ± 35510[a]	233392 ± 75724[a]	286735 ± 45180[a]	254157 ± 40714[a]
VEGF	2186 ± 454[a]	1769 ± 744[a]	1427 ± 822[a]	14223 ± 2980[b]	2346 ± 1874[a]	3033 ± 2370[a]
VEGF R1	3184 ± 1360[a]	2903 ± 1917[a]	2894 ± 798[a]	19574 ± 3402[b]	3207 ± 2671[a]	5379 ± 2496[a]
VEGF R2	10282 ± 5142[a]	8471 ± 3878[a]	10670 ± 4691[a]	30204 ± 12874[b]	12137 ± 4676[a]	16737 ± 5328[a]

***values reported in mean pixel density**

Sulindac more effectively blunts obesity-associated alterations in tumor metabolism compared to Omega-3 supplementation in DIO mice

Obese mice supplemented with Sulindac demonstrated modest divergence of inflammatory and metabolism related genes in the tumor tissue. DIO+Sulindac mice had an intermediate expression of COX-2 but a significant decrease in HIF-1α (indicative of hypoxia) and Emr1 (indicative of macrophage infiltration). DIO+Sulindac mice, compared to DIO+Omega-3 mice, had decreased expression of glycolytic genes hexokinase 2 (HK2) and pyruvate kinase isozymes M2 (PKM2) compared to DIO mice. DIO+Sulindac mice had decreased expression of diglyceride acyltransferase 1 (DGAT1) (involved in triglyceride synthesis) but increased expression of PPARγ (promotes adipogenesis and also corresponds to improved prognosis) relative to DIO mice. Furthermore, DIO mice expressed increased CD36 mRNA, involved in fatty acid uptake, while CD36 expression was normalized to NW Control levels in DIO+Sulindac mice. DIO+Omega-3 mice had an intermediate level of expression, not significantly different from NW Control or DIO (Figure 3.7).

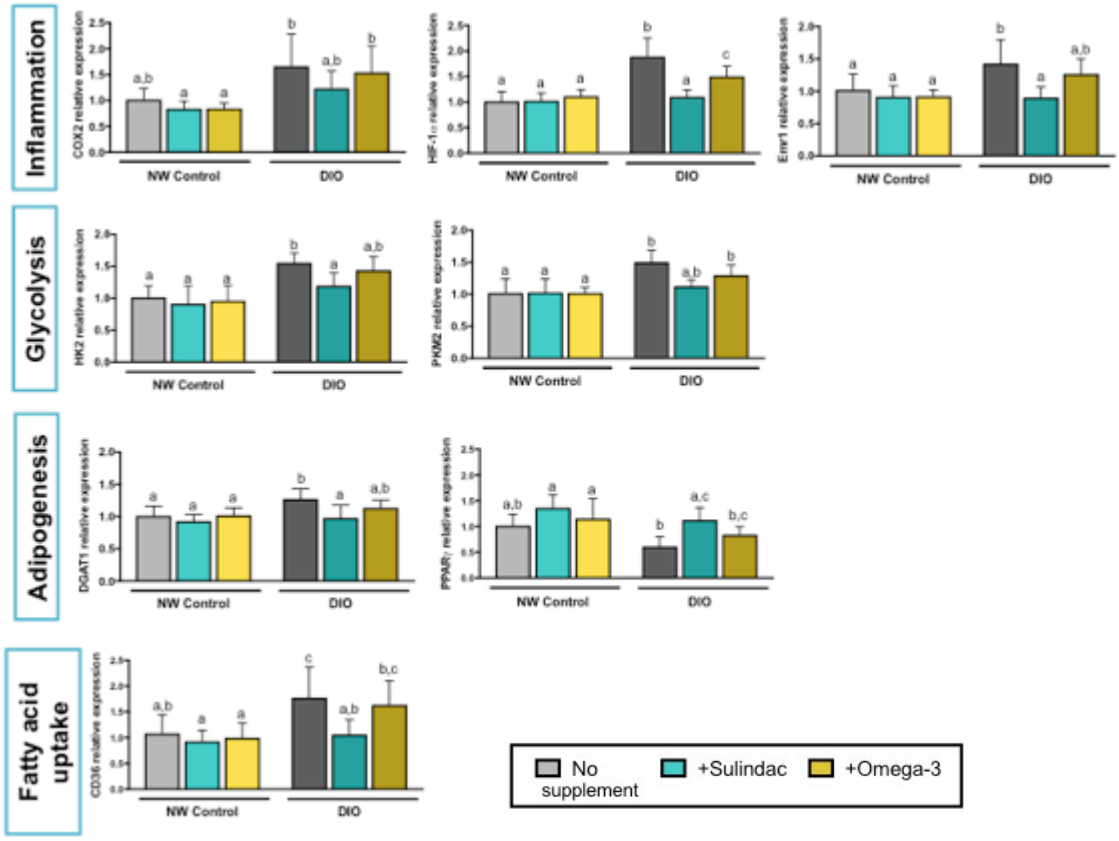

Figure 3.8. Sulindac more effectively blunts obesity-associated alterations in tumor metabolism compared to Omega-3 supplementation in DIO mice. DIO+Sulindac mice possessed gene expression more similar to NW Control mice for (A) Inflammation: COX-2, HIF-1α, and Emr1; (B) Glycolysis: HK2, PKM2; (C) Adipogenesis: DGAT1, PPARγ; (D) Fatty acid uptake: CD36.

Sulindac reduces E0771 cell viability *in vitro* independent of PGE_2

To follow up on our findings that DIO and DIO+Omega-3 mice generally possessed increased levels of eicanoids (the most abundant, PGE_2) and distinct gene expression of metabolism related genes in the tumor, we treated cells with PGE_2 and/or Sulindac to characterize direct effects on tumor cells *in vitro*. E0771 cells treated with PGE_2 did not display enhanced viability. Treating cells with a high dose (250 ng/mL) of Sulindac resulted in reduced proliferation. Co-treatment with PGE_2 did not impact these effects (Figure 3.9A). Treatment of E0771 cells with Sulindac alone resulted in reduced

cell viability after three days (relative to vehicle) with a high dose 500 μM, however a lower dose of 50 μM recovered to viability levels comparable to cells treated with vehicle after six days (Figure 3.9B).

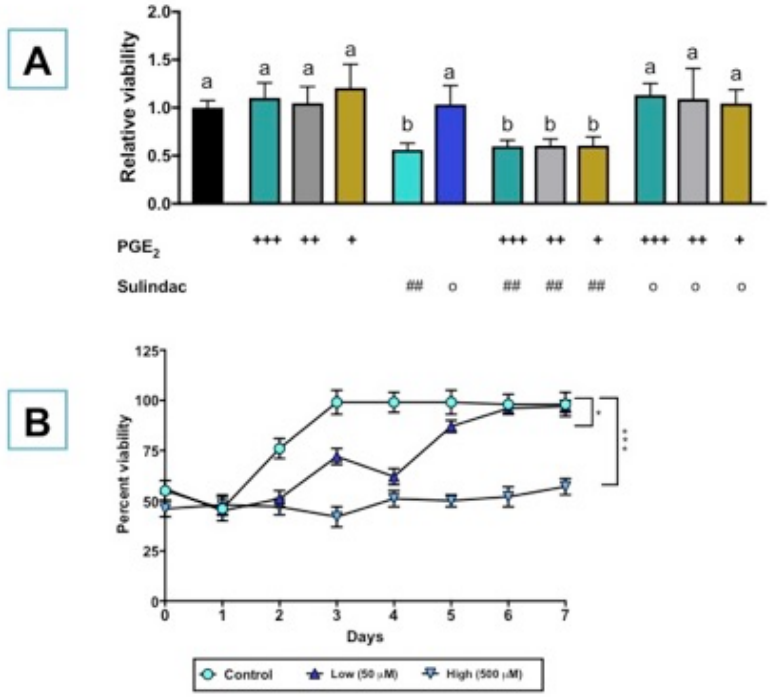

Figure 3.9. Sulindac reduces E0771 cell viability *in vitro* independent of PGE_2. (A) E0771 cells were treated with PGE_2 and/or Sulindac. Legend: PGE_2 (250 ng/mL): +++, PGE_2 (50 ng/mL): ++, PGE_2 (5 ng/mL) +, Sulindac 500 μM: ##, Sulindac 50 μM o (B) E0771 cells were treated with Sulindac and cell viability was measured over seven days. Differences in significance denoted by different letters (a,b) or by asterics, * $P < 0.05$; ** $P < 0.01$; *** $P < 0.0001$.

E. Discussion

Sulindac supplementation in DIO but not Control mice significantly decreased interim tumor volume and tumor latency in association with significant reductions in tumor-infiltrating adipocyte area and tumor concentration of COX-2 pro-inflammatory metabolites. Sulindac supplementation in DIO mice also significantly reduced mammary adipocyte size, CLS density and gene and protein expression of pro-inflammatory

mediators in the mammary tissue, suggesting an inhibition of adipose tissue dysregulation. Omega-3 supplementation in DIO mice produced an intermediate reduction in tumor volume without impacting mammary adipocyte area and tumor levels of $PGF_{2\alpha}$, PGD_2 and 13 PGE_2. In all biological outcomes measured, we saw minimal effects of anti-inflammatory supplementation among NW Control mice. This suggests that obesity-associated adipose tissue inflammation and associated metabolic dysfunction is responsible for the pro-tumor effects of obesity in our mouse model of BLBC and that Sulindac, more so than Omega-3, was able to block obesity's effects. DIO+Sulindac mice maintained a normal adipocyte size, and this likely played a role in their resistance to obesity-induced perturbations in inflammatory and metabolic signaling in the mammary fat pad. However, Sulindac supplementation did not modulate body weight or body fat percentage in the DIO mice, suggesting that Sulindac indeed offsets some of the pro-tumorigeneic effects of obesity rather than impacting obesity directly.

Adipocytes have the ability to donate fuel and nutrient sources to neighboring tumor cells, providing growth signals and promoting evasion from apoptotic and check point signals through substantial supply of cytokines. Comparison of gene expression patterns in tumor and mammary tissues support a cooperation between the two in DIO mice, with increased expression of genes encoding for lipases in the mammary fat pad and an upregulation in the fatty acid transport protein CD36 in the tumor. DIO+Sulindac mice displayed significantly reduced expression of lipolysis mediators in the mammary tissue compared to DIO, whereas DIO+Omega-3 did not. Furthermore, genes that were

altered in the tumors of DIO mice that would enable an adaptive utilization of a variety of fuel sources exhibited similar levels in DIO+Omega-3, but not DIO+Sulindac mice.

These findings strongly implicate the increase levels of PGE_2 in obesity as a mediator of adipose tissue dysfunction. We treated E0771 cells with PGE_2 and failed to find a direct effect on tumor cell viability. These results suggest that the tumor-promoting effects of PGE_2 may be dependent on an interplay between factors in the microenvironment, such as reprogramming the expression of immune cells, which subsequently affects tumor growth and survival. Alternatively, treatment of E0771 cells with Sulindac decreased cell viability, which supports an anti-cancer effect of Sulindac independent of PGE_2. The overall results of this work demonstrate that targeting obesity-associated inflammation can break the obesity-cancer link, in part through preventing adipose tissue dysfunction.

CHAPTER IV. OBESITY-ASSOCIATED ALTERATIONS IN INFLAMMATION, EPIGENETICS AND MAMMARY TUMOR GROWTH PERSIST IN FORMERLY OBESE MICE

A. Chapter Précis

Using a murine model of basal-like breast cancer, we tested the hypothesis that chronic obesity, an established breast cancer risk and progression factor in women, induces mammary gland epigenetic reprogramming and increases mammary tumor growth. Moreover, we assessed whether the obesity-induced epigenetic and protumor effects are reversed by weight normalization. Ovariectomized female C57BL/6 mice were fed a control diet or diet-induced obesity (DIO) regimen for 17 weeks, resulting in a normal weight or obese phenotype, respectively. Mice on the DIO regimen were then randomized to continue the DIO diet or were switched to the control diet, resulting in formerly obese (FOb) mice with weights comparable to control mice**.** At week 24, all mice were orthotopically injected with MMTV-Wnt-1 mouse mammary tumor cells. Mean tumor volume, serum IL-6 levels, expression of pro-inflammatory genes in the mammary fat pad, and mammary DNA methylation profiles were similar in DIO and FOb mice, and higher than in controls. Many of the genes found to have obesity-associated hypermethylation in mice were also found to be hypermethylated in the normal breast tissue of obese versus non-obese human subjects, and nearly all of these concordant genes remained hypermethylated after significant weight loss in the FOb mice. Our findings suggest that weight normalization may not be sufficient to reverse the effects of

chronic obesity on epigenetic reprogramming and inflammatory signals in the microenvironment that are associated with breast cancer progression.

B. Introduction

Obesity is highly prevalent in the United States and many other parts of the world and is an established risk and progression factor for several intrinsic subtypes of breast cancer, including basal-like breast cancer (BLBC), in postmenopausal women [177]. Greater rates of metastatic breast cancer and increased mortality are seen in the obese breast cancer patient population, independent of disease stage at diagnosis [30,31]. These effects may be mediated in part by adipose tissue inflammation, as excess adipose tissue results in local as well as systemic effects. Obesity is typically accompanied by increased systemic levels of pro-inflammatory mediators, such as interleukin-6 (IL-6), tumor necrosis factor alpha (TNF-α), matrix metalloproteinase-9 (MMP-9) and interleukin-1 beta (IL-1β), and these can independently influence tumor growth. In addition, obesity enhances the secretion of monocyte chemoattractant protein-1 (MCP-1), which stimulates the recruitment of macrophages to adipose tissue, including the breast adipose. These tumor-associated macrophages likely contribute to tumor growth by increasing local and/or systemic inflammatory and angiogenic factors and generating reactive oxygen species [178,179].

In obese mice, calorie restriction reduces mammary tissue expression of several mediators of inflammation including TNF-α and IL-1β [180]. Less is known about the effects of obesity or weight loss interventions on the epigenome. There is mounting evidence that DNA methylation can be affected by energy balance. For example,

weight loss interventions (30% energy reduction) in obese male subjects have been shown to induce DNA methylation changes at the TNF-α promoter after only eight weeks of diet intervention [181]. In another study, severe weight loss after gastric bypass surgery in obese humans normalized methylation in the promoter regions of 11 out of 14 metabolic genes that had been dysregulated by obesity [46]. Expression of the EZH2 gene, which encodes the epigenetic regulator histone-lysine-N-methyltransferase, has been linked to breast cancer growth and metastasis [182]. It is also modulated in the offspring of obese mothers [183], suggesting that this enzyme may mediate some of the effects of energy balance on epigenetic regulation. Although DNA methylation patterns are energy responsive, the relationship between weight loss, aberrant DNA methylation, adipose tissue inflammation, and cancer progression are unknown.

Epidemiological and preclinical studies have clearly shown that the metabolic perturbations typically accompanying obesity promote breast cancer progression [184]. One study in particular illustrated how women who underwent bariatric surgery had a 5-fold reduction in incidence of breast cancer after 5 years of follow up from surgery compared to women who did not undergo a weight loss intervention- surgical or otherwise [47]. However, with the exception of bariatric surgery interventions, the impact of intentional obesity reversal prior to diagnosis has not been well-established. The epidemiologic data have been mixed regarding non-surgically induced weight loss, reflecting the difficulties in achieving and maintaining meaningful weight loss. Despite their limitations, animal model studies may be informative in addressing this question given their benefit of greater control of diet, physical activity and numerous other confounding variables. Sundaram et al. (2014) found that a high-fat diet promotes

mammary tumor progression in a transgenic mouse model of BLBC, and switching mice to a low-fat diet after a short-term high-fat diet exposure led to small but statistically significant weight loss and reversed many of the high-fat diet effects on tumor progression to that of control levels [185]. However, the transgenic mouse model used in this study were resistant to obesity induction, and tumors arose early in life, so the question of whether the mammary tumor-promoting effects of chronic obesity are reversed by weight loss was not addressed. We have previously found in a mouse model of chronic obesity, as well as in clinical studies of obese women, that a severe weight loss intervention may provide an anti-cancer benefit, but moderate weight loss had minimal effects on cancer-related biomarkers in mice and women and tumor growth in mice [72,186].

Given the uncertainty regarding the benefits of obesity reversal, we sought to determine the effects of weight loss on the host microenvironment and tumor progression in an orthotopic transplant model of murine BLBC in syngeneic mice. Here we demonstrate that tumor growth did not change with significant weight loss prior to orthotopic tumor transplant, despite the normalization of several obesity-related hormones. Moreover, we provide evidence that breast tumor growth after obesity reversal may be driven by epigenetic dysregulation in the microenvironment as well as sustained elevations in inflammatory signaling. These findings suggest that short-term weight loss may not reverse the tumor-promoting epigenetic reprogramming and increased inflammatory signaling that accompanies chronic obesity.

C. Materials and methods

Mice and diets

All animal protocols were approved by the University of Texas at Austin Institutional Animal Care and Use Committee (IACUC) and carried out in compliance with all guidelines and regulations. Six-week-old female ovariectomized C57BL/6 mice were obtained from Charles River Laboratories, Inc. (Frederick, MD), individually housed on a 12-hour light/dark cycle, and consumed food and water *ad libitum*. Food intake was measured twice a week and body weights were measured weekly. Mice were randomized to continue on the control diet (n=17) or a 60% kcal from fat diet-induced obesity (DIO) diet regimen (n=34; D12492, Research Diets, Inc.). After 17 weeks on diet, the DIO mice were randomized to either continue on the DIO regimen (DIO, n=17) or switch to the control diet to induce gradual weight loss; this latter group is referred to as formerly obese (FOb, n=17). After 24 weeks on diet, 5 mice per group were fasted for 6-8 hours and then euthanized for pre-tumor tissue collection. The remaining mice (n=15/group) were orthotopically injected with $5x10^4$ syngeneic viable MMTV-Wnt-1 mammary tumor cells as previously described [16]. *In vivo* growth was measured twice/week with skinfold calipers, and *in vivo* tumor area was approximated using the formula πr^2. At study endpoint (week 36), mice were euthanized and mammary tumors, tumor-adjacent and tumor-distal mammary fat pad were excised and divided in portions to be formalin fixed or flash frozen in liquid nitrogen and stored at -80°C until further analysis. Mice were excluded if they had developed dermatitis during study (one DIO mouse and one FOb mouse). *Ex vivo* tumor volume was calculated

using the formula $4/3\pi \times R_1^2 \times R_{2,}$ (with R1 denoting the smaller radius of the ellipsoid) [187].

Quantitative magnetic resonance analysis

Body composition was measured on all mice at weeks 17 and 24 of diet treatments by quantitative magnetic resonance (qMR) (Echo Medical Systems, Houston, TX). Measurements included lean mass, fat mass and total water mass. Percent body fat was calculated by dividing fat mass by total body weight.

Serum hormone, cytokine and adipokine measurement

Serum was collected from mice fasted 6-8 hours, prior to tumor cell injection (week 24) by retro-orbital bleed. Serum hormones, adipokines, and cytokines, including leptin, adiponectin, insulin, and IL-6, were measured using mouse adipokine LINCOplex®Multiplex Assays (Millipore, Inc., Billerica, MA) and analyzed on a BioRad Bioplex 200 analysis system (Biorad, Inc., Hercules, CA). Insulin-like growth factor 1 (IGF-1) concentrations were measured using a Millipore Milliplex Rat/Mouse IGF-1 Single Plex assay (Millipore, Inc.).

Crown-like structure analysis

Four micron-thick sections were prepared from formalin-fixed, paraffin-embedded mammary fat pad tissue and stained with hematoxylin and eosin. The total number of CLS per section was quantified by a pathologist, blind to the sample group, and the

amount of adipose tissue present on each slide was determined using NIH Image J. Prevalence of CLS was quantified as CLS per cm^2 of adipose tissue.

Quantification of adipocyte infiltration in tumor tissue

Four micron-thick sections were prepared from formalin-fixed, paraffin-embedded tumor tissue and stained with hematoxylin and eosin. Tumors were chosen at random (4-5/group) and digitally imaged under 20X magnification. The total number of adipocytes per section (2-4 representative sections, each 830 μm x 580 μm) was quantified independently by 3 investigators who were blinded to experimental group.

Quantitative RT-PCR

Total RNA was extracted from the flash-frozen tumor-adjacent and tumor-distal mammary fat pad samples collected at end of study using TRI-Reagent (Sigma-Aldrich, St.Louis, MO) according to manufacturer's instructions. RNA concentration was spectrophotometrically determined using a nanodrop (Thermo Scientific, Logan, UT) and quality was confirmed using an Agilent 2100 Bioanalyzer (Santa Clara, CA). RNA was reverse transcribed with Multiscribe RT (Applied Biosystems, Carlsbad, CA). Resulting cDNA from tissue samples were assayed in triplicate for PCR using Taqman® Gene Expression Assays for IL-6, TNF-α, MMP-9, IL-1β, IGFBP6, CITED1, TFE3, JAK3, EZH2, SMYD3, and TSC22D3 (Applied Biosystems). PCR reactions were completed using a ViiA™7 Real time PCR system (Applied Biosciences). Gene expression data were normalized to the housekeeping gene β-actin and analyzed using the delta delta cycle threshold method [188].

Methylation analysis

DNA was extracted from the 9th mammary fat pad, distal to tumor, at end of study (n=3/group) using UltraPure™ Phenol:Chloroform:Isoamyl Alcohol per manufacturer's instructions (Life Technologies, Carlsbad, CA). Genome-wide methylation profiles for mammary fat pad from control, DIO and FOb mice were determined by RRBS (Reduced Representation Bisulfite Sequencing). Among the available methods for genome-wide analysis of the DNA methylation, we selected RRBS based in its compatibility and validation with mouse DNA, its capacity to investigate individual sites by bisulfite-sequencing, and the large number (above 400 thousand) of CpG sites that are evaluated in a single experiment. Library preparation and sequencing were completed at the UT MD Anderson Cancer Center's DNA Methylation Analysis Core and Science Park Next-Generation Sequencing Facility, according to published protocols [189,190]. Briefly, 1 μg of genomic DNA was digested with MspI, a methylation-insensitive enzyme that cleaves the DNA at CCGG sequences, followed by end-repair, A-tailing and size selection. Enrichment for CpG sites in CG-dense and CpG islands is achieved by selective collection and PCR amplification of MspI fragments with sizes between 40bp and 170bp.Sequence reads were mapped to the mouse genome (mm10) using Bismark bisulfite read mapper. The location of individual CpG sites in relationship to known genes was based on the mm10 RefSeq gene annotations and classified as promoter (CpG sites 1 kb upstream of the annotated transcription start site (TSS) and extending 500 base pairs downstream of TSS), exon, intron, or CpG island. CpG island coordinates were collected from the UCSC Genome Browser mm10 version, Genome

Reference Consortium GRCm38. Differential methylation was calculated by filtering samples based on read coverage ≥ 20, then performed at the single base level independent of the CpG site location. TSS of transcripts smaller than 300 bp were removed for the analysis. Methylkit R package was used to apply logistic regression and the likelihood ratio test. Observed p-values were adjusted with the success likelihood index method (SLIM).

Selection of samples from the normal breast study for methylation analysis

Selection criteria for the Normal Breast Study included having an invasive ductal carcinoma with a tissue specimen sampled ≥ 4 cm from tumor margins, undergoing reduction mammoplasty, or undergoing prophylactic surgery [191]. There were 150 participants with invasive breast cancer had tissue collected that was > 4 cm from the tumor. Participants were randomly selected from each BMI group: 30 from the high BMI (>30), 20 from the normal BMI (25-30), and 22 from the low BMI (<25) group. All prophylactics and reduction participants were also included. In all, 96 participants were selected. All tissue specimens were snap frozen. A 50 mg sample was taken from the participants' tissue specimens and used for methylation assessment. The University of North Carolina at Chapel Hill Institutional Review Board approved this study.

DNA extraction from human breast samples

DNA was isolated using the DNeasy Blood and Tissue kit from Qiagen (Venlo, Netherlands) following the manufacturer's protocol. Sodium bisulfite modification of the DNA was conducted using EZ DNA Methylation Gold Kit (Zymo Research, Orange,

CA), and 500 ng of DNA was used for the HumanMethylation450 BeadChip platform. The samples were processed for DNA methylation analysis by the University of North Carolina at Chapel Hill's Mammalian Genotyping Core.

Concordance between mouse and human genes methylated in response to energy balance modulation

We compared our mouse methylation dataset with a dataset obtained from the University of North Carolina Normal Breast Study utilizing non-tumorous breast tissue, subject to methylation array and stratified by BMI. A methylation difference was calculated for each significant methylation change (obese vs. non-obese) with a positive coefficient signifying increasing methylation with increased adiposity. Intraspecies concordance was assayed only for genes with significant differences within species. Welch's t-test was used for the pairwise comparisons between obese and non-obese humans using R version 3.1.2 (http://www.r-project.org). Comparisons between both species was done by one-way analysis of variance (ANOVA) using GraphPad Prism V6 with Bonferroni correction for multiple comparisons.

Statistical Analysis

Values are presented as mean ± standard deviation (s.d.). One-way ANOVA using Tukey's multiple comparisons correction was used to assess the effects of diet treatment on body weight and fat percentage, mean tumor size, serum hormone and cytokine concentrations, and mammary fat pad gene expression. Student's t-test was used to compare differences in CLS between experimental groups and control. For all

tests, GraphPad Prism software was used (GraphPad Software Inc., La Jolla, CA), and $P \leq 0.05$ was considered statistically significant.

D. Results

Body weight and body composition of control, DIO, and FOb mice

Mice were fed a low-fat control or a diet-induced obesity (DIO) regimen for 17 weeks, at which time percent body fat, assessed by quantitative resonance analysis, was higher in DIO mice (59.7 ± 1.8%) compared to control mice (39.5 ± 4.0%) ($P < 0.001$; Fig. 4.1A). DIO mice also had a higher mean body weight (51.5 ± 0.7 g) than control mice (33.1 ± 0.7 g) (Fig. 4.1B). After weight loss was initiated at week 17, FOb mice lost 27.6 ± 3.4% of their body weight (14.2 ± 1.7 g) ($P < 0.0001$) relative to their last weight taken while on the DIO diet. By week 24, the body fat percentage in FOb mice (45.1 ± 3.5%) did not significantly differ from mice maintained on the control diet

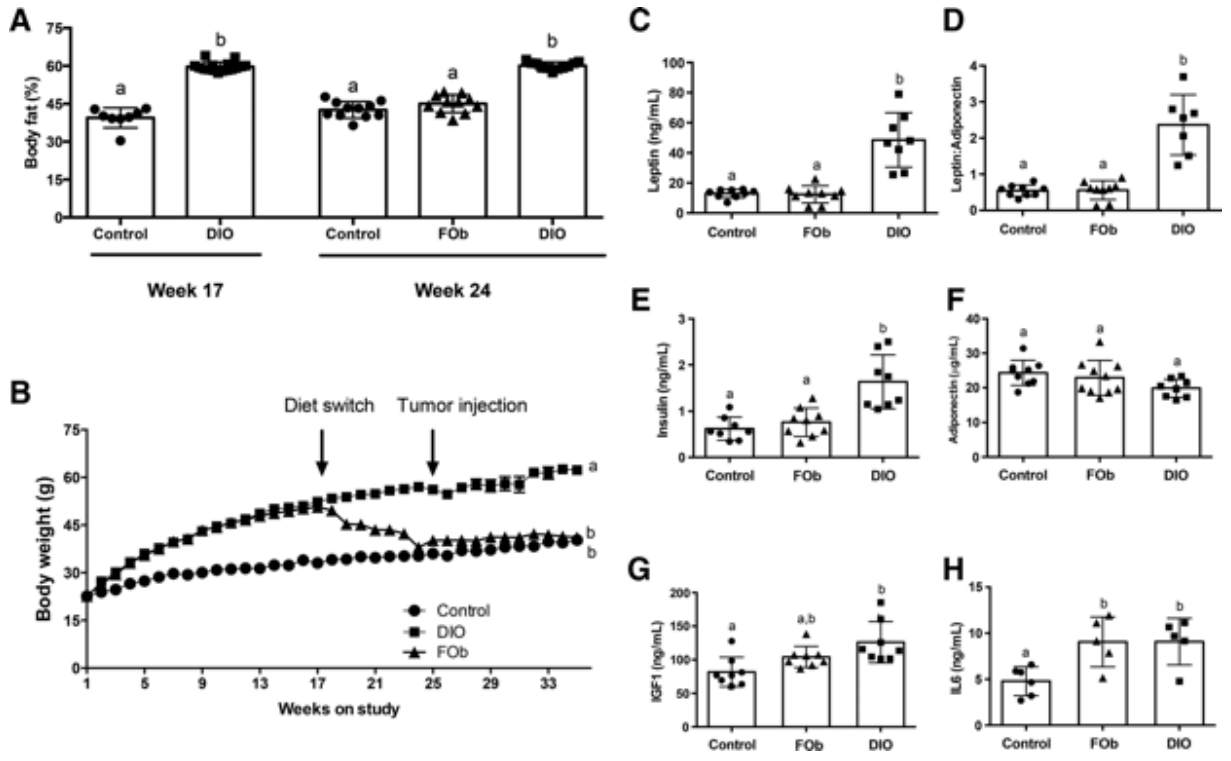

Figure 4.1. Body composition, body weight and serum metabolic hormones control, DIO and FOb mice (A) Percent body fat mass in control versus obese mice at week 17 on diet and in control, FOb, and obese mice at week 24. (B) Body weight in the three diet groups over the course of the study. Different letters indicate statistically significant differences between groups, $P < 0.05$. Serum levels of several hormones, growth factors, and adipokines were measured in mice from all three diet groups at week 24 of the study, including leptin (C), leptin:adiponectin ratio (D), insulin (E), adiponectin (F), IGF-1 (G), and IL-6 (H). Different letters indicate statistically significant differences between groups, $P < 0.05$.

throughout study (42.6 ± 3.3%), with DIO mice (60.1 ± 1.5%) having significantly greater body fat percentage than control and FOb mice ($P < 0.001$; Fig. 4.1A). FOb and control mice maintained significantly lower body weights than DIO mice through the end of study ($P < 0.0001$, Fig. 4.1B).

Effect of weight loss on serum metabolic and inflammatory markers

Serum was collected from mice at week 24 by retro-orbital bleed, prior to tumor cell injection and when the body weights of the FOb mice were statistically equivalent to the control mice. The reduction in adiposity in the FOb mice was accompanied by lower serum leptin ($P < 0.0001$), leptin:adiponectin ratio ($P < 0.0001$), and insulin ($P < 0.0001$) relative to DIO mice (Fig. 4.1C-E), with concentrations statistically equivalent to those found in the control mice. IGF-1 levels were significantly higher in DIO mice relative to control ($P < 0.05$; Fig. 4.1G) but were intermediate in FOb mice and not statistically different from the levels seen in control or DIO mice. Furthermore, IL-6 levels did not differ between FOb and DIO mice and were significantly elevated in both groups compared to control mice ($P < 0.05$; Fig. 4.1H).

Weight loss in FOb mice reduced prevalence of crown-like structures (CLS)

The high-fat dietary regimen increased the prevalence of CLS (expressed as CLS / area of tissue in cm^2) in the mammary fat pad of DIO mice relative to control mice ($P < 0.003$; Fig. 4.2). This was analyzed in tissue harvested at the interim (week 24) time point. FOb mice had a significant reduction in CLS compared to DIO mice ($P < 0.03$); however, prevalence of CLS remained slightly elevated relative to control, though this difference was not statistically significant ($P = 0.4$).

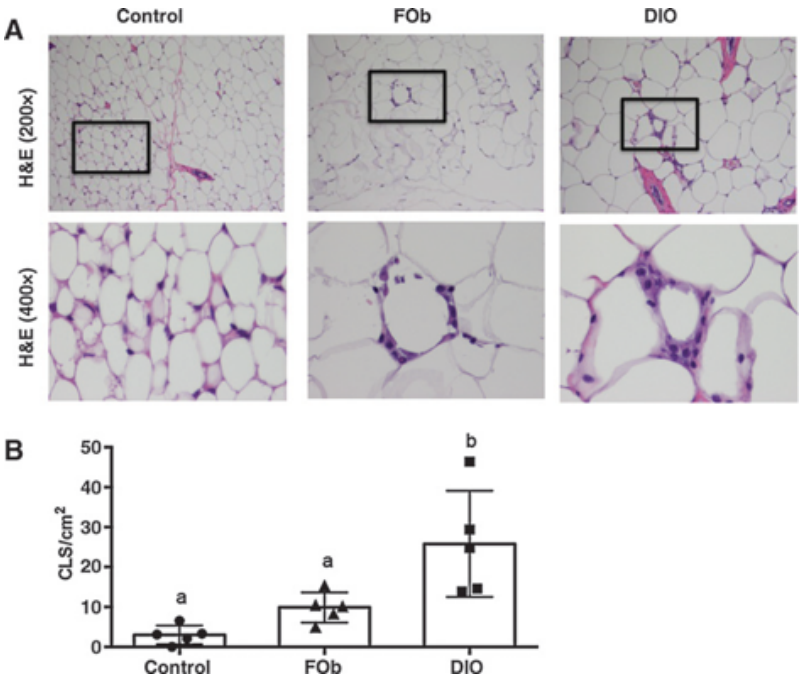

Figure 4.2. Weight loss in FOb mice reduced prevalence of CLS. Mouse mammary fat pad tissue at week 24 on diet was assessed for the prevalence of CLS (A) using hematoxylin and eosin (H&E) stained tissue sections, representative image shown. (B), CLS were quantified for each tissue sample as number of CLS per cm^2. Different letters indicate significant differences, $P < 0.05$.

Weight loss in FOb mice does not decrease basal-like mammary tumor burden

Ex vivo tumor volume from DIO and FOb mice were larger (1792.7± 1132.9 mm^3, 1563.4 ± 1673.3 mm^3, respectively) than tumors from the control mice (51.6 ± 139.8 mm^3) ($P < 0.05$; Fig. 4.3A). Furthermore, a shared attribute of tumors from both the DIO and FOb groups were the presence of adipose cells infiltrating the tumor in greater number compared to control (Fig. 4.3B). Tumors from DIO mice contained a significantly higher number of adipocytes than control tumors (168.4 ± 83.4 adipocytes / mm^2 and 34.6 ± 32.2 adipocytes / mm^2, respectively; $P < 0.05$). Tumors in FOb mice had an intermediate level of adipocyte infiltration (127.1 ± 83.6 adipocytes/mm^2) that did not significantly differ from either control ($P = 0.19$) or DIO ($P = 0.66$). Collectively, these

findings suggest that significant weight loss does not completely reverse the effects of obesity on BLBC growth and adipocyte-infiltration.

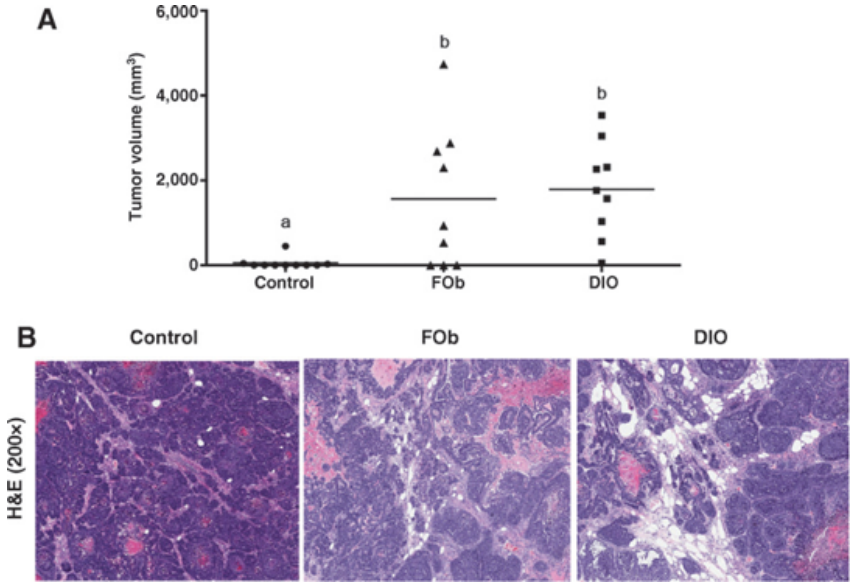

Figure 4.3. Weight loss in FOb mice does not decrease basal-like mammary tumor burden. (A) Ex-vivo tumor volume at the end of the study. (B) Differing levels of adipocyte infiltration into the tumor tissue of mice from the three diet groups. Different letters indicate significant differences, $P < 0.05$.

Pro-inflammatory cytokine gene expression is elevated in mammary fat pad from FOb mice

RT-PCR analysis was performed on tumor-distal mammary fat pad (n=4-5 mice). Relative to control, FOb mice had significantly elevated IL-6 expression ($P < 0.001$, Fig. 4.4A), with DIO mice having non-significantly elevated levels relative to control. TNF-α expression was significantly elevated in DIO ($P < 0.04$) and FOb ($P < 0.03$; Fig 4.4B) versus control mice. MMP-9 expression was greater in FOb mice ($P < 0.05$; Figure 4.4C) with DIO mice experiencing an intermediate increase compared to control. IL1-β expression was significantly higher in FOb and DIO mice ($P < 0.01$; Fig. 4.4D) compared to control.

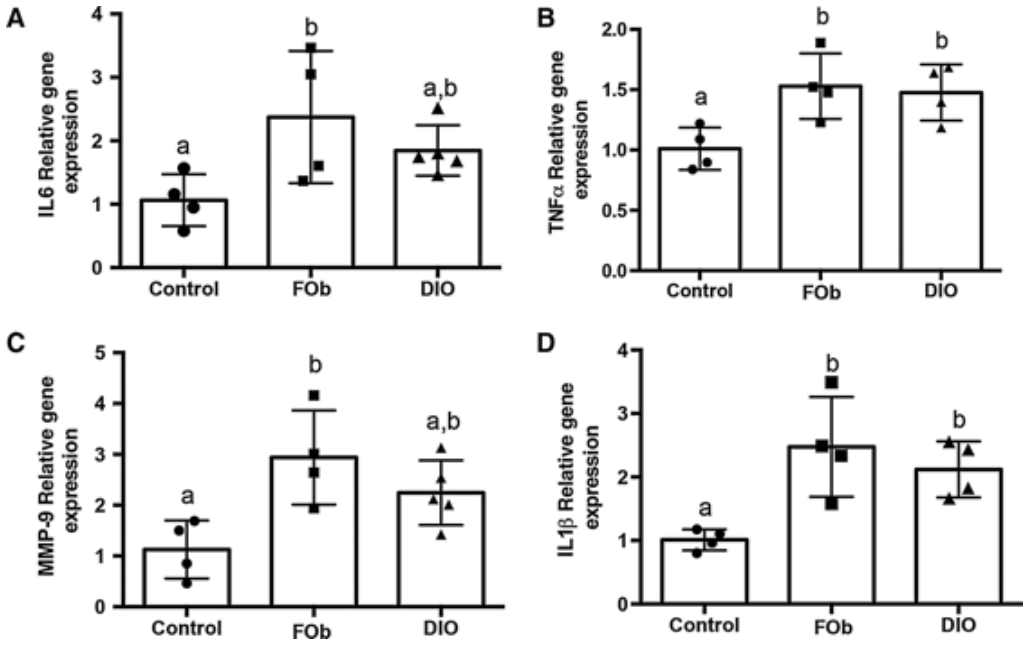

Figure 4.4. Pro-inflammatory cytokine gene expression is elevated in mammary fat pad from FOb mice. (A) mRNA expression of pro-inflammatory genes was measured in the tumor-distal mammary fat pad of mice sacrificed at the end of the study, including (A) IL-6 (B)TNF-α; (C) MMP-9 (D); and IL-1β. Different letters indicate significant differences, $P < 0.05$.

Weight loss fails to normalize obesity-induced hypermethylation patterns and histone methyltransferase enzymes EZH2 and SMYD3 in mammary fat pad

To determine whether the sustained elevation in tumor growth observed in FOb mice may be mediated in part by epigenetic reprogramming in the microenvironment, we assessed the global DNA methylation pattern of the tumor-distal mammary fat pad at end of study. DIO mice had 39 genes significantly hypermethylated compared to control. Of these 39 differentially methylated genes, FOb mice generally possessed intermediate levels of methylation relative to control and DIO mice, suggesting that weight reduction back to control levels was insufficient to completely reverse the epigenetic reprogramming that occurs with chronic obesity (Fig. 4.5A). FOb mice had 11 genes significantly hypermethylated compared to control. While the methylation levels

of these genes were also elevated in DIO mice, they were not significantly different from control.

Hypermethylated genes in DIO and FOb mice relative to control were entered into Qiagen's Ingenuity® Pathway Analysis (IPA) to delineate pathological signaling pathways. Gene expression was confirmed on a select number of genes (Fig. 4.5B-H). IPA Biofunction analysis connected the genes from our methylation analysis to a disease or biological function. Cancer was the primary disease with 23 genes hypermethylated in DIO (22 of the genes) or DIO and FOb (1 gene) implicated in cancer, specifically neoplasia of epithelial tissue (Table 4.1). Another biofunction with 17 genes associated with it was cellular growth and proliferation. Four genes in our data set were identified as playing a role in cell-mediated immune response. Significant overlap of differentially methylated genes in DIO or FOb mice with each biofunction was determined by Fisher's exact test.

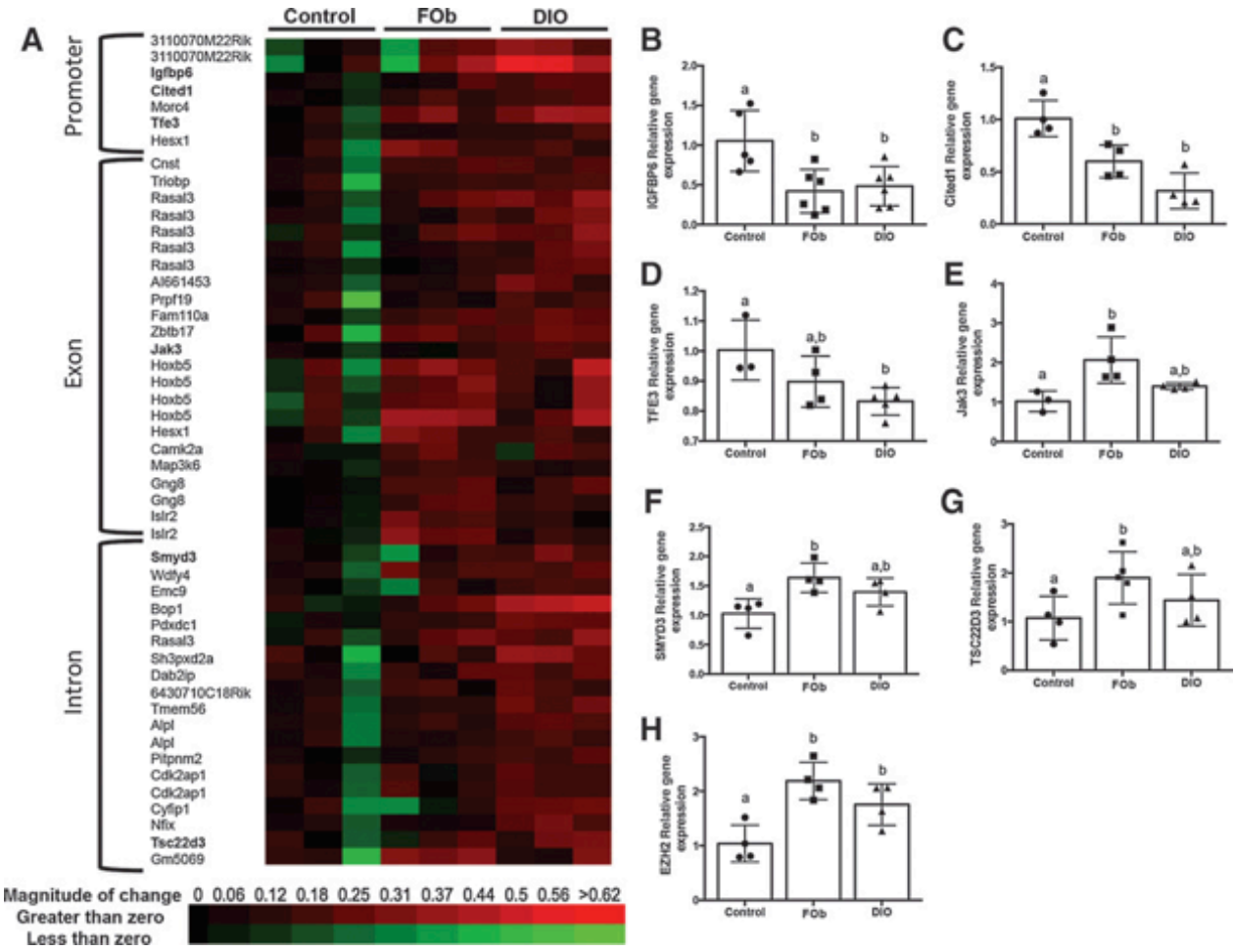

Figure 4.5. Weight loss fails to normalize obesity-induced hypermethylation patterns and histone methyltransferase enzymes EZH2 and SMYD3 in mammary fat pad. (A) Heatmap representation of gene methylation values expressed as % methylated DNA. Corresponding gene expression of (B) IGFBP6, (C) CITED1, (D) TFE3, (E) JAK3, (F) SMYD3, and (G) TSC22D3 in mammary fat pad. Additional expression shown for implicated (H) EZH2. Different letters indicate significant differences, $P < 0.05$.

Table 4.1. IPA biofunction analysis

Disease or Biofunction Annotation	p-value	Molecules	# of Molecules
Cancer			
Neoplasia of epithelial tissue	2.67E-02	ALPL, AP1S2, BOP1, CYFIP1, DAB2IP, EMC9, ETS1, EXTL3, IGFBP6, JAK3, MAML3, MORC4, MSC, PDXDC1, PEX2, PITPNM2, PRPF19, RASAL3, SMYD3, TFE3, TRIOBP, WDFY4, ZBTB17	23
Growth of tumor	4.86E-02	CYFIP1, DAB2IP, LYL1, ZBTB17	4
Cell Growth and Proliferation			
Proliferation of Cells	1.20E-04	BOP1, CDK2AP1, CITED1, DAB2IP, ETS1, EXTL3, IGFBP6, JAK3, LYL1, MAML3, NFIC, PEX2, PRPF19, SMYD3, TFE3, ZBTB17, ZNF503	17
Cell-mediated Immune Response, Cellular Development			
Differentiation of T lymphocytes	3.74E-03	ETS1, JAK3, LYL1, ZBTB17	4
Differentiation of helper T lymphocytes	3.67E-02	ETS1, JAK3	2
Cell Death and Survival			
Apoptosis	2.56E-02	CDK2AP1, CITED1, DAB2IP, ETS1, IGFBP6, JAK3, LYL1, NFIC, PRPF19, ZBTB17	10
Cell-To-Cell Signaling and Interactions, Inflammatory Response			
Innate immune response of tumor cell lines	1.60E-02	SMYD3	1

P-values calculated by Fisher's exact test.
Significant disease or biofunction annotated implicated by IPA software.

We moved forward with genes that appeared in the IPA Biofunction of cancer with a function of neoplasia of epithelial tissue (IGFBP6, SMYD3, and JAK3) and transcription factor TSC22D3 and investigated their role as regulators in inflammatory signaling, with particular interest in the relationship between each gene and IL-6. As stated previously, IL-6 serum (Fig. 4.1H) and tumor-distal mammary fat pad mRNA levels (Fig. 4.4A) were elevated in DIO and FOb mice relative to controls. Of note, inhibitors of IL-6 including TSC22D3 (intron) and JAK3 (exon) were hypermethylated. EZH2 was also predicted by the IPA analysis to be regulated by these genes, and expression of EZH2 in tumor-distal mammary fat pad of endpoint animals was significantly higher in DIO ($P < 0.05$) and FOb ($P < 0.005$) mice compared to control mice (Fig. 4.5H). The gene for another

methyltransferase enzyme, SET and MYND domain-containing protein 3 (SMYD3), was also identified as differentially methylated in our analysis, and its expression in tumor-distal mammary fat pad was significantly elevated in FOb mice ($P < 0.02$), with DIO mice having non-significantly elevated levels.

Hypermethylation concordance in mammary tissue from non-obese and obese humans and mice

After we identified a panel of genes that were significantly hypermethylated in the mammary fat pad of DIO mice compared to controls, we assessed the methylation status of this gene panel in a methylation data set from normal human breast tissue involving subjects stratified by body mass index (BMI). Thirteen genes were identified with concordant hypermethylation (% methylation difference with the same directionality) in DNA from normal mammary tissue at the same genomic feature (i.e. intron vs. exon) in obese vs. non-obese women and mice (Table 4.2). However, as some significant methylation changes mapped to the same gene, of the 13 concordant genes, 6 had additional discordant methylation sites. We also identified an additional 3 genes with only discordant methylation between species. We then compared methylation (as % methylated DNA) for CpG's related to the same gene in the same genomic feature (i.e. intron or exon) between women and mice. Non-obese women and control fed mice had levels of DNA methylation that were statistically equivalent for 4 of the 13 concordant genes identified. Of the 13 hypermethylated genes in obese women and DIO mice, 6 genes reached statistical equivalence (CDK2AP1, CYFIP1, MAF, MAML3, SH3PXD2A, SMYD3). Of those 4 were statistically equivalent in obese women,

DIO mice, and FOb mice. Seven genes were significantly different between obese humans and DIO mice due to varying degrees of hypermethylation.

Table 4.2. DNA methylation comparisons between obese and non-obese women and DIO, FOb and control mice

Gene	Chr. Human	Chr. Mouse	Genomic Location	Methylation % Increase in Obesity (Human)	Methylation % Increase in Obesity (Obese Mouse)	Methylation % Increase in Obesity (FOb Mouse)	Human Non-Obese vs. Mouse Control	Human Obese vs. Mouse Obese	Human Obese vs. Mouse FOb
ALPL	chr1:21838665	chr4:137770933	Intron	**4.25**	35.45	17.92	*P* <0.0001	*P* <0.0001	*P* <0.0001
		chr4:137770959	Intron		29.90	14.60	*P* <0.0001	*P* <0.0001	*P* <0.0001
	chr1:21868624	chr4:137770933	Intron	**5.47**	35.450	17.92	*P* <0.004	*P* <0.0001	*P* <0.0001
		chr4:137770959	Intron		29.90	14.60	*P* <0.001	*P* <0.001	*P* <0.001
CDK2AP1	chr12:123750864	chr5:124349413	Intron	**5.54**	29.03	13.97	ns	ns	ns
		chr5:124349431	Intron		28.96	19.28	ns	ns	ns
CYFIP1	chr15:22921184	chr7:55891934	Intron	**3.24**	25.64	-3.38	*P* <0.0001	ns	*P* <0.001
ETS1	chr11:128457459	chr9:32787134	Downstream	**5.42**	29.64	-5.86	ns	p<0.001	ns
EXTL3	chr8:28560486	chr14:65111008	Intron	**5.10**	33.38	18.68	*P* <0.01	*P* <0.001	*P* <0.001
FAM110A	chr20:825415	chr2:151970815	Exon	**1.49**	25.06	19.17	*P* <0.001	*P* <0.001	*P* <0.001
MAF	chr16:79638744	chr8:115536869	Downstream	**8.65**	16.85	29.12	ns	ns	ns
		chr8:115536892	Downstream		12.77	28.26	*P* <0.03	ns	ns
MAML3	chr4:140834011	chr3:52171869	Intron	**9.06**	28.02	24.40	ns	ns	ns
	chr4:140877994		Intron	**7.72**			ns	*P* <0.0001	*P* <0.0003
	chr4:140907113		Intron	**4.49**			*P* <0.0001	ns	ns
	chr4:141013584		Intron	**3.21**			*P* <0.0001	*P* <0.0001	*P* <0.0001
PITPNM2	chr12:123579358	chr5:124185502	Intron	**3.83**	24.23	12.61	*P* <0.003	*P* <0.001	*P* <0.001
PRPF19	chr11:60670992	chr19:10905776	Exon	**2.04**	21.03	44.79	*P* <0.0001	*P* <0.0001	*P* <0.003
RASAL3	chr19:15568360	chr17:32392415	Exon	**0.90**	24.58	14.17	*P* <0.05	*P* <0.0001	*P* <0.0001
		chr17:32392416	Exon		25.96	10.81	*P* <0.0001	*P* <0.0001	*P* <0.0001
		chr17:32392421	Exon		23.31	14.72	*P* <0.005	*P* <0.0001	*P* <0.0001
		chr17:32392422	Exon		24.82	8.99	*P* <0.005	*P* <0.0001	*P* <0.0001
		chr17:32392435	Exon		27.60	6.75	*P* <0.005	*P* <0.0001	*P* <0.0001
SH3PXD2A	chr10:105421249	chr19:47302650	Intron	**5.87**	32.67	8.68	*P* <0.0001	ns	*P* <0.002
	chr10:105451802		Intron	**4.10**			*P* <0.05	*P* <0.0001	ns
SMYD3	chr1:245951603	chr1:179443579	Intron	**3.58**	31.84	2.44	*P* <0.0001	ns	*P* <0.0001

NOTE: Differences in methylation calculated by taking the average DNA methylation for obese and subtracting the average DNA methylation for non-obese (women) or control (mice). Statistical significance calculated by one-way ANOVA. Abbreviations: chr, chromosome; ns, not significant.

E. Discussion

In our orthotopic tumor transplant model of BLBC in C57BL/6 mice, we found that DIO, relative to control diet, elevated: a) body fat percentage; b) serum leptin, leptin:adiponectin ratio, insulin, IGF-1, and IL-6; c) prevalence of CLS in mammary fat pad; d) mammary tumor growth; and e) genome-wide mammary gland hypermethylation. Significant weight loss initiated after 17 weeks on DIO diet resulted in a normalization of percent body fat and serum leptin, leptin:adiponectin, insulin levels, and prevalence of CLS in mammary fat pad in the FOb mice. Serum IGF-1 decreased to levels intermediate to DIO and control levels. Despite these beneficial metabolic changes and weight normalization, FOb mice had a final tumor volume nearly identical to DIO mice. Additionally, we observed that obesity reversal in the FOb mice failed to normalize serum IL-6 and mammary fat pad inflammatory gene expression as well as aberrant methylation in the mammary gland, and these may contribute to the persistence of the pro-cancer effects of obesity even after weight is normalized. We have identified several genes with concordant obesity-related hypermethylation in humans and mice, and the DNA methylation levels of many of these genes were unchanged after significant weight loss in the FOb mice, providing further support that obesity-associated epigenetic reprogramming may not be easily reversed with weight normalization alone.

To our knowledge, this is the first study to: i) characterize the effects of obesity reversal on mammary gland microenvironment (including DNA methylation) and tumor growth; ii) identify genes with concordant and discordant obesity-related methylation

patterns in normal mammary tissue from mice and humans. We and others have previously found that a severe weight loss intervention, or inhibiting the mTOR signaling pathway in obese mice using genetic or pharmacologic approaches [188,192,193], decreases murine mammary tumor progression. Severe weight loss in humans, such as that achieved by bariatric surgery, has also shown the ability to significantly decrease inflammatory signaling [194], DNA hypermethylation [46], and cancer risk [47,195]. However, the weight loss that was achieved in our udy via an *ad libitum* low-fat diet, which models many human weight loss plans, failed to reduce inflammatory signaling and elevated methylation levels in the FOb mice.

Inflammation is implicated in many of the deleterious effects of obesity [196,197]. In the present study, weight loss in FOb mice normalized metabolic regulators that are elevated in obesity such as serum leptin:adiponectin, insulin, and adipose tissue CLS. However, several measures of inflammation persisted after weight loss, including serum IL-6 and gene expression of inflammatory cytokines in the mammary tissue. Thus, we are able to distinguish the pro-cancer effects of obesity-related metabolic perturbations from obesity-related inflammation, which persists after weight loss.

We also found evidence suggesting that obesity-induced aberrant hypermethylation contributes to the maintenance of a pro-inflammatory, pro-growth microenvironment in the mammary fat pad of mice, and this is not normalized by significant weight loss. Abnormal expression of EZH2 plays a role in cancer growth and metastasis in a variety of cancers, including breast [198]. A high-density tissue microarray analysis of breast tumors from 280 patients revealed that EZH2 levels were increased in patients with invasive breast carcinoma relative to patients with no lesions

or atypical hyperplasia [199]. Additionally, EZH2 increases expression of SMYD3, a histone H3 lysine-4 specific methyltransferase, which plays a key role in the proliferation and migration of several cancers. Cell culture studies have shown that silencing of SMYD3 by siRNA inhibits growth of breast cancer cells [200]. We demonstrated here that both EZH2 and SMYD3 expression remained elevated in the mammary fat pad tissue of FOb mice, similar to the DIO group, indicating that these epigenetic regulators may be involved in mediating the mammary tumor-promoting effects of obesity. Study limitations include the lack of a time course, since it is plausible that FOb mice could have had decreased tumor growth if challenged after a longer period of weight normalization. Additionally, as serum IL-6, mammary fat pad inflammatory gene expression, and mammary fat pad methylation all remained elevated in FOb mice compared to control, we are unable to delineate the individual contribution of each factor to the increased tumor burden. As expected, many but not all methylation changes investigated resulted in a corresponding change in gene expression. This is likely influenced by distance between the site of methylation change and promoter region, influence of chromatin features, or multiple systemic levels of regulation at play [201,202].

The results of our study raise important questions concerning the relationship between obesity and the progression of more aggressive breast cancers such as the basal type. Numerous studies have shown that obesity is associated with increased risk of mortality from breast cancer [203]. As weight loss did not suppress tumor progression in mice that had at one time been obese, further research is needed to investigate a potential critical window regarding the timing and magnitude of weight loss to achieve

an anti-tumor effect. Future studies should also explore weight loss in combination with adjuvant therapy, such as prophylactic NSAID use to combat inflammation. The hypermethylation observed in DIO and FOb mice may also provide a new druggable target for breaking the obesity-breast cancer link.

In summary, we found that MMTV-Wnt-1 mammary tumor growth was similar in DIO and FOb mice, with both groups exhibiting larger tumors than control mice. DNA methylation in the distal-tumor mammary fat pad at study endpoint was also significantly elevated in DIO mice relative to control, with FOb mice possessing intermediate DNA methylation levels. This is particularly surprising considering that at the time of tumor cell injection, FOb mice did not differ from control mice in terms of body weight, body composition, and serum metabolic markers of obesity, with the exception of serum IL-6. Taken together, our findings suggest a relationship between chronic obesity, the epigenome, inflammation and mammary cancer. Consequently, a combination of weight loss and epigenetic or anti-inflammatory interventions may be required to effectively break the obesity-breast cancer link.

CHAPTER V. SURGICAL, BUT NOT DIET-INDUCED WEIGHT LOSS, REVERSES THE PRO-TUMORIGENIC EFFECTS OF OBESITY IN A MOUSE MODEL OF BASAL-LIKE BREAST CANCER

A. Chapter Précis

Obesity is associated with increased incidence of basal-like breast cancer (BLBC), an aggressive and often deadly breast cancer subtype. To date, no studies on the effect of weight loss on BLBC risk in chronically obese women have been reported. The limited epidemiological data on weight loss and risk of other cancers suggests only interventions such as bariatric surgery that result in significant sustained weight loss produce a consistent anti-cancer benefit. We therefore compared the effects of surgically-induced weight loss via sleeve gastrectomy (SG) versus diet-induced weight loss via a low-fat diet, in our mouse model of obesity and BLBC. Mice were fed a low-fat diet resulting in a normal weight control (NW Control) phenotype, or high-fat diet-induced obesity (DIO) regimen for 15 weeks to model chronic obesity. After 15 weeks on diet, DIO mice were then randomized to continue the same diet (DIO) or receive a surgical or diet weight loss intervention, resulting in formerly obese (FOB)-Surg and FOB-Diet groups, respectively. FOB-Surg mice were subject to sleeve gastrectomy (~70% excision of the stomach), and NW Control, DIO, and FOB-Diet mice received a sham procedure. Eight weeks after surgical procedures and diet switches, when the average body weight for NW Control, FOB-Surg, and FOB-Diet mice did not statistically differ, all mice on study were orthotopically injected with E0771 mammary tumor cells,

which model BLBC. At the end of study, *ex vivo* tumor volume in FOB-Surg mice was significantly lower than DIO mice, whereas the average tumor volume of FOB-Diet mice did not statistically differ from DIO mice. In addition, FOB-Surg mice had levels of serum tumor necrosis factor-alpha (TNF-α), insulin, and adipocyte size that were significantly lower than FOB-Diet and DIO mice, but did not differ from NW Control mice. Genome wide analysis of gene expression (RNA Seq) and DNA methylation (RRBS) revealed that weight loss via sleeve gastrectomy restored metabolic flexibility (the ability to respond to nutrient signals appropriately) to a greater extent than in FOB-Diet mice. Our results demonstrate that surgical weight loss imparted a plurality of metabolic advantages, functional genomic changes, and successful reversal of obesity-associated mammary tumor burden that were not similarly achieved by dietary weight loss.

B. Introduction

The global prevalence of obesity, an established risk and prognostic factor for several chronic diseases including many cancers, remains very high [1,2]. Currently, an estimated 37.9% of the US adult population is obese, defined by a body mass index (BMI) $\geq$ 30 kg/m^2, while only 27.6% of U.S. adults are at a healthy weight, defined as having a BMI 18.6-24.9 kg/m^2 [1,2]. The overall risk of breast cancer is 18% higher in women with Class I obesity (BMI = 30-34.9 kg/m^2), 32% higher in women with Class II obesity (BMI = 35-39.9 kg/m^2), and 62% higher in women who are severely obese (BMI $\geq$ 40) [5]. Furthermore, obese women experience poorer breast cancer outcomes by virtue of their breast cancer subtype (with luminal A and basal-like breast cancers most strongly associated with obesity), increased tumor grade at clinical presentation,

accelerated disease recurrence, and diminished response to certain therapies [115]. Therefore, research is urgently needed to identify mechanistic targets and intervention strategies for reducing the burden of obesity on breast cancer.

Adipose tissue is a dynamic energy reservoir, able to sense and respond to systemic signals. In obesity, adipocytes expand to pathogenic size to accommodate triglyceride storage needs, resulting in hypertrophic adipocytes and adipose tissue dysregulation [48,123]. The secretome of hypertrophied adipocytes, particularly in visceral white adipose tissue, contributes to an obesity-associated state of low-grade inflammation and influx of immune cells into adipose tissue [204-207]. Moreover, adipocytes in the obese state no longer contribute to energy homeostasis and instead promote lipotoxicity with a steady efflux of free fatty acids (FFAs) into circulation, due to the inability of insulin to inhibit lipolysis [123,208]. Ultimately, the chronic exposure of breast epithelial cells to increased local and systemic pro-inflammatory cytokines, adipokines, and FFA's from hypertrophied adipocytes and recruited immune cells enhances breast cancer development and progression in obese individuals [209,210].

The World Health Organization's International Agency for Research on Cancer Working Group on Body Fatness and Cancer recently identified a major gap in the literature regarding the impact and underlying mechanisms of intentional weight loss in the context of chronic obesity on cancer [211]. Their summary report stated that, with the exception of studies of bariatric surgery-induced weight loss, epidemiological and clinical studies have been sparse and inconsistent regarding whether intentional weight loss can reverse the pro-inflammatory and procancer effects of obesity. The high

recidivism rate following dietary weight loss interventions no doubt contributes to this important knowledge gap about the reversibility of the obesity-cancer link [41,42].

Preclinical studies addressing the anticancer effects of weight loss in obese mice were deemed by the IARC group as sparse and inconsistent. We previously reported that obesity-associated alterations in inflammation, DNA methylation, and mammary tumor growth persist in formerly obese mice [212]. These findings suggest that weight normalization may not be sufficient to reverse the effects of chronic obesity on epigenetic reprogramming and inflammatory signals in the microenvironment that are associated with breast cancer progression. Although DNA methylation patterns are energy responsive, the relationship between weight loss, aberrant DNA methylation, and cancer progression is unclear, again with the possible exception of bariatric surgery. In humans bariatric surgery is more adept at reversing obesity-associated changes in DNA methylation compared to weight loss by diet alone [212,213]. To our knowledge there are no reports of preclinical studies of bariatric surgery in a murine model of breast cancer. We therefore employed our mouse model of obesity and basal-like breast cancer to test the hypothesis that surgery-induced weight loss (via sleeve gastrectomy) is more effective than diet-induced weight loss at reversing obesity-associated DNA methylation changes, metabolic perturbations and increased basal-like mammary tumor growth.

C. Materials and methods

In vivo studies

All animal study protocols were approved and coordinated in compliance with guidelines issued by the University of North Carolina at Chapel Hill Institutional Care and Use Committee (IACUC). Ninety four female 6-8 week old C57BL/6 mice (a well characterized energy balance-responsive mouse model) were purchased from Charles River Laboratories International, Inc. (Wilmington, MA). Upon arrival, mice were housed two per cage on a 12-hour light/dark cycle and offered food and water *ad libitum*. A diet of standard chow was administered to all mice for a one week acclimation period. Next, mice were randomized to two groups, receiving either a control (CON; 10% kcal from fat) diet (n=22; Product # D12450J; Research Diets, Inc.) or a diet-induced obesity (DIO; 60% kcal from fat) regimen (n=72; Product # D12492; Research Diets, Inc.) to generate a normal-weight (NW) control or obese phenotype, respectively. Body weight and food intake were measured weekly. After 15 weeks on diet, with the weights of NW CON and DIO mice significantly different from each other ($P < 0.001$), obese mice were then randomized to continue the same diet (DIO) or receive a surgical or diet weight loss intervention, resulting in formerly obese (FOB)-Surg and FOB-Diet groups, respectively. FOB-Surg mice were subject to sleeve gastrectomy (~80% excision of the stomach), and NW Control, DIO, and FOB-Diet mice received a sham procedure. Three days post-operation, both FOB-Surg and FOB-Diet began the same low-fat control diet as the NW Control group. Eight weeks after surgery when body weights of mice were relatively stabile, all mice were orthotopically injected with 3.5×10^4 E0771 mammary tumor cells into the 4th mammary fat pad (Figure 5.1A), a model of basal-like breast

cancer originally isolated from a spontaneous medullary breast adenocarcinoma in a C57BL/6 mouse [214]. In vivo tumor growth was measured two times per week with skinfold calipers and in vivo tumor area was determined using the formula πr^2. Four weeks following orthotopic injection, tumors in 50% of DIO mice (the fastest growing group) reached the requisite size defined by the IACUC protocol; therefore, all mice on study were sacrificed. Mammary tumors, tumor-adjacent and tumor-distal mammary fat pad were excised and sectioned to either be formalin fixed or flash frozen in liquid nitrogen and stored at -80°C until further analysis. *Ex vivo* tumor volume was calculated using the formula 1/6π x D1 x D2 x D3 (where D is equal to *ex vivo* diameter of the tumor). End of study blood was collected by cardiac puncture, allowed to clot at room temperature for 30 minutes and centrifuged for 10 minutes at 1,000 x g to isolate serum, and stored at -80°C.

Sleeve gastrectomy and sham procedures

Sleeve gastrectomy and sham procedures were performed by trained animal surgeons according to a validated protocol [215]. Briefly, vertical sleeve gastrectomy (SG) involved excision of ~80% of the lateral stomach. The sham procedure, performed on NW Control, DIO, and FOB-Diet mice to control for the physiological insult of surgery, was executed by first isolating the stomach and then applying manual pressure with forceps for five seconds. The excision and pressure were applied along a line continuous with the esophagus and pylorus. All surgeries occurred within a four day window, and mice within all study groups were randomized to the day of operation. Pre-operation fasting, exposure to isofluorane and administration of analgesics were

consistent across all groups. Additionally, all mice received a three-day liquid diet (Osmolite OneCal) before being reintroduced to solid food. Antibiotics were given to all mice three days post-op. All mice were weighed daily and food intake was quantified for one week post-op.

Quantitative magnetic resonance analysis

Quantitative magnetic resonance imaging (qMRI) (Echo Medical Systems, Houston, TX) was used to measure the body composition for all groups (n=6-9 mice/group) at the end of study. Lean body mass, fat body mass, and free water were quantified. Body fat percentage was calculated by dividing the fat body mass by the body weight measured with a digital scale.

Serum hormone, adipokine, and cytokine measurement

One week prior to tumor injection, serum was collected from mice fasted 4-6 hours by submandibular bleed. Serum hormones, cytokines, and adipokines including insulin, leptin, adiponectin, IL-6, TNF-α, and resistin, were measured using Milliplex Mouse Metabolic Hormone Magnetic bead Panel (MMHMAG-44K), Bio-Plex Pro^{TM} Mouse Adiponectin Assay, and Mouse Cytokine Panel A 6- Plex, respectively (Bio-Rad Laboratories; Hercules, California). Insulin-like growth factor 1 (IGF- 1) concentrations were measured using R&D Systems IGF-1 Bead-Based Single-plex Luminex assay (Minneapolis, MN).

Mammary fat pad adipocyte size and crown-like structure analysis

Hematoxylin and eosin (H&E) staining on 4-micron thick sections from formalin-fixed, paraffin embedded distal mammary fat pad tissue was processed, scanned and imaged using Aperio CS2 Digital Pathology Scanner (Leica Biosystems, Wetzlar, Germany) at 40X magnification. Representative snapshots (n=9-11 mice/group; 3 snapshots were sample) were randomly selected from whole tissue images zoomed in at 8.8X (300 μM) utilizing ImageScope Viewing Software Version 12.0 (Leica Biosystems). Mammary fat pad average adipocytes size and number of adipocytes were quantified using ImageJ Version 1.51e (National Institute of Health, Bethesda, Maryland). An adipocyte tool macro (MRI Adipocyte Tools.txt) was downloaded from (http://dev.mri.cnrs.fr/projects/imagej-macros/wiki/Adipocytes_Tool) and imported into ImageJ. Furthermore, the number of crown-like structures (CLS) [216] was quantified from whole tissue H&E stained distal mammary fat pad sections (n=10-15 mice/group). Briefly, the number of CLS were counted in a blinded fashion, and CLS density measures were achieved by dividing the number of CLS by the total slide area eligible for analysis using ImageScope Viewing Software Version 12.0 (Leica Biosystems).

DNA methylation analysis

Genome-wide methylation profiles for the distal mammary fat pad were determined by reduced representation bisulfite sequencing (RBBS). DNA was extracted from a random sample (n=4 mice/group) of distal mammary tissues using TRI Reagent (Sigma-Aldrich) according to the manufacturer's instructions. Library preparation and sequencing were performed at the University of North Carolina at Chapel Hill High-

Throughput Sequencing Facility. Alignment and differential methylation analysis were conducted as previously described [212].

RNA-Seq analysis

Total RNA was extracted from the flash-frozen tumor-adjacent and tumor-distal mammary fat pad samples collected at the end of the study using TRI Reagent (Sigma-Aldrich) according to the manufacturer's instructions. RNA libraries were prepared using the Illumina TruSeq Stranded Total RNA Sample Preparation kit according to manufactures instructions. The libraries were sequenced using a 2x76 bases paired end protocol on the Illumina HiSeq 2000 instrument. The reads were mapped to mouse genome (mm10) by TopHat (version 2.0.7). The number of fragments in each known gene from RefSeq database (UCSC Genome Browser 2013) was enumerated using HTSeq-count from HTSeq package (version 0.5.3p9). Differential expression was performed using DESeq2.

Pathway analysis

WebGestalt (www.webgestalt.org) [217] over representation enrichment analysis (ORA) of KEGG pathways and gene ontology biological process curated gene sets was performed for selected pairwise comparisons of RNA-Seq and RRBS data.

Statistical analysis

All values are represented as mean ± standard deviation (s.d.). One-way analysis of variance (ANOVA) using Tukey’s post hoc multiple comparisons correction

was used to assess the effects of diet and weight loss on body weight and fat percentage, tumor volume, serum hormone and cytokine concentrations, and mammary fat pad adipocyte size and CLS density. Results were analyzed using GraphPad Prism software (Graphpad Software Inc., La Jolla, CA) and $P \leq 0.05$ was considered statistically significant.

D. Results

Weight loss interventions by surgery (FOB-Surg) or diet alone (FOB-Diet) are equally effective at reducing body weight and fat mass

Mice were fed a low fat control or a diet-induced obesity regimen for 15 weeks in order to establish a normal weight control or obese phenotype, respectively. DIO mice had significantly higher body weight at the time of sleeve gastrectomy or sham procedure relative to control mice ($P < 0.0001$). Eight weeks following the operations and diet switch, body weight between FOB-Surg and FOB-Diet mice was not significantly different (Figure 5.1A), and neither group was significantly different from NW Control mice, however all were significantly different from DIO mice prior to tumor cell injection ($P < 0.0001$ for all comparisons, NW Control vs. DIO, FOB-Surg vs. DIO, FOB-Diet vs. DIO). At end of study, body fat percentage (Figure 5.1B) was not statistically different among NW Control, FOB-Surg and FOB-Diet mice, and all groups were significantly lower than DIO mice ($P < 0.0001$ for all comparisons, NW Control vs. DIO, FOB-Surg vs. DIO, FOB-Diet vs. DIO), indicating successful and equivalent reversal of the obese phenotype in both weight loss groups.

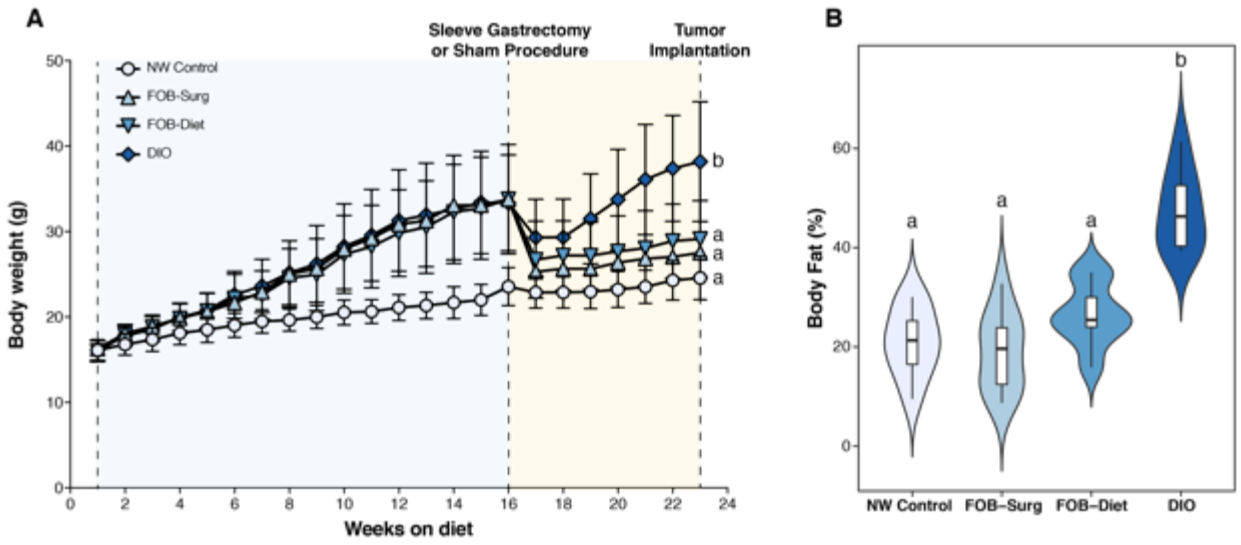

Figure 5.1 Weight loss interventions by surgery (FOB-Surg) or diet alone (FOB-Diet) are equally effective at reducing body weight and fat mass. Surgical and dietary weight loss generate comparable reductions in body weight and body fat percentage. (A) Body weight of mice throughout the course of study. (B) Combined violin and box plots of body fat percentage at end of study. Differences in significance denoted by different letters (a,b) $P < 0.05$.

Surgical weight loss reduces obesity-associated serum growth factors and pro-inflammatory mediators more effectively than diet-induced weight loss

Seven weeks after surgical procedures and diet switch when weights were stabilized, serum was collected from mice (n=10-12 mice/group) by submandibular bleed for multiplex metabolite analyses. For all metabolites measured except adiponectin, levels in NW Control mice were significantly lower than DIO mice. Insulin levels in FOB-Surg mice were significantly different from both FOB-Diet and DIO mice and not significantly different from NW Control mice; insulin levels in FOB-Diet exhibited intermediate reductions from DIO levels but were not significantly different. For Insulin-like growth factor-1 (IGF-1) and resistin, FOB-Surg mice displayed significantly lower levels than DIO mice, whereas FOB-Diet mice displayed intermediate, non-significant reductions from DIO levels. For measures of leptin, leptin to adiponectin ratio,

interleukin-6 (IL-6), and monocyte chemoattractant protein-1 (MCP-1), both FOB-Surg and FOB-Diet mice displayed significantly lower levels relative to DIO mice. Lastly, FOB-Surg mice exhibited significantly lower levels of tumor necrosis factor alpha (TNF-α) than both FOB-Diet and DIO mice; levels of TNF-α in FOB-Diet mice were not statistically different from only DIO mice (Table 5.1).

Table 5.1 Surgical weight loss in mice more effectively reduces circulating growth factors and pro-inflammatory mediators in serum

	NW Control	FOB-Surg	FOB-Diet	DIO
Hormones				
Insulin (ng/mL)	0.74 ± 0.25^{a,b}	0.56 ± 0.22^{a}	1.04 ± 0.35^{b,c}	1.35 ± 0.49^{c}
IGF-1 (ng/mL)	42.2 ± 13.8^{a}	39.0 ± 15.9^{a}	1.4 ± 18.6^{a,b}	76.7 ± 29.6^{b}
Leptin (ng/mL)	2.41 ± 0.89^{a}	2.16 ± 1.20^{a}	4.77 ± 4.21^{a}	11.5 ± 0.05^{b}
Adiponectin (μg/mL)	12.0 ± 2.99	11.1 ± 5.01	12.6 ± 2.91	9.68 ± 5.13
Leptin: Adiponectin	2.2E-06 ± 1.3E-06^{a}	2.3E-06 ± 1.3E-06^{a}	4.9E-06 ± 5.3E-06^{a}	3.5E-05 ± 1.3E-05^{b}
Resistin (ng/mL)	11840 ± 4143^{a}	6732 ± 2237^{a}	2528 ± 4717^{a,b}	20214 ± 10323^{b}
Cytokines				
TNF-α (pg/mL)	11.5 ± 7.31^{a}	18.8 ± 14.1^{a}	41.2 ± 14.1^{b}	56.9 ± 18.2^{b}
IL-6 (pg/mL)	30.6 ± 8.21^{a}	39.5 ± 17.5^{a}	50.8 ± 24.0^{a}	89.4 ± 20.6^{b}
MCP-1 (pg/mL)	99.8 ± 5.34^{a}	102.2 ± 22.4^{a}	136.8 ± 50.4^{a}	192.3 ± 51.9^{b}

Data presented as mean ± s.d. One-way ANOVA and Tukey's post hoc multiple comparisons were used to test statistical differences between study groups. Results from pairwise comparisons are presented as letters, where common letters indicate statistical equivalence and different letters indicate statistical difference according to $P < 0.05$.

Surgical weight loss, but not diet-induced weight loss, reverses adipocyte hypertrophy and crown-like structure density in mammary tissue

The size of adipocytes (measured by two-dimensional area) in the mammary fat pad were significantly larger in DIO mice compared with NW Control mice. Both surgical and dietary weight loss resulted in reduced adipocyte area, relative to DIO mice, with the most profound differences occurring at the 50^{th} and 90^{th} percentile of adipocyte area (Figure 5.2A). FOB-Surg mice exhibited a median adipocyte area significantly lower than FOB-Diet and DIO ($P < 0.05$, $P < 0.0001$, respectively), but not NW Control mice.

The median adipocyte area of FOB-Diet mice displayed significant reduction relative to DIO mice ($P < 0.001$), but remained significantly different from both NW Control ($P < 0.01$) (Figure 5.2B). Furthermore, density of crown-like structures in the mammary fat pad was remarkably decreased in FOB-Surg mice and was significantly lower than that of FOB-Diet ($P < 0.001$) and DIO mice ($P < 0.001$). Notably, crown-like structure density in FOB-Diet mice was not statistically different from DIO or NW Control mice (Figure 5.2C).

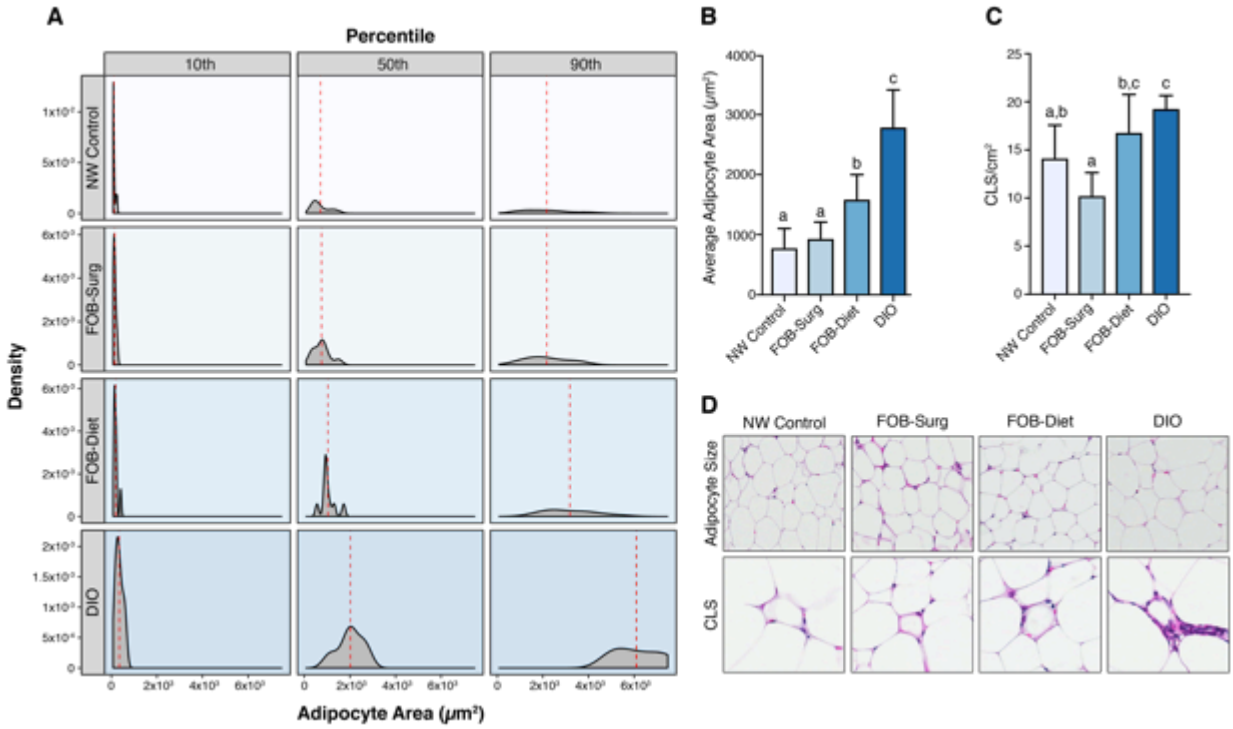

Figure 5.2 Surgical weight loss, but not diet-induced weight loss, reverses adipocyte hypertrophy and crown-like structure density in mammary tissue. Surgical weight loss results in more robust reductions in adipocyte hypertrophy and crown-like structure density in the mammary fat pad. (A) Panel displaying density functions for 10th, 50th, and 90th percentiles of adipocyte area across all groups; dashed red line indicates mean of distribution. (B) Average adipocyte area. (C) Crown-like structure density. (D) Representative images of H&E stained mammary fat pad sections depicting adipocyte size and CLS. Differences in significance denoted by different letters (a,b) $P < 0.05$.

Surgical weight loss, but not diet-induced weight loss, reverses the pro-tumorigenic effects of obesity

Ex vivo tumor volume of FOB-Surg mice was not statistically different from NW Control mice and significantly different than DIO mice. However, FOB-Diet mice had tumors that were not significantly different from DIO mice and significantly different than NW Control mice (Figure 5.3). Therefore, FOB-Surg mice, but not FOB-Diet mice, achieved reversal of obesity-associated mammary tumor burden.

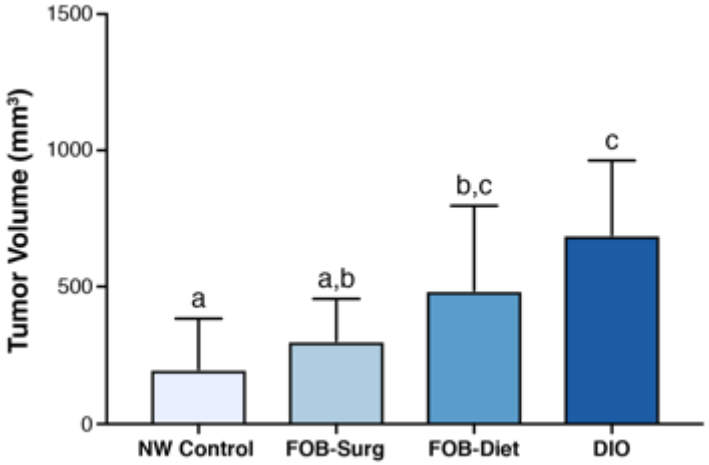

Figure 5.3. Surgical weight loss, but not diet-induced weight loss, reverses the pro-tumorigenic effects of obesity. *Ex vivo* tumor volume reveals unique cancer-protective effects of surgical versus dietary weight loss. Differences in significance denoted by different letters (a,b) $P < 0.05$.

Surgical weight loss reverses obesity-induced aberrant mammary DNA methylation more effectively than diet-induced weight loss

The complete RRBS dataset was filtered by pairwise comparisons between all study groups with $P < 0.0001$ and false discovery rate (FDR) < 0.0001 as filtering criteria for differential methylation. Gene lists were entered into WebGestalt for overrepresentation enrichment analysis (ORA) in curated KEGG pathways (Table 5.2). The genes harboring differential methylation between DIO and FOB-Surg mice were highly enriched for a variety of pathways implicated in mammary carcinogenesis and a tumorigenic microenvironment. Interestingly, there were markedly fewer genes displaying differential methylation according to the criteria above in DIO vs. FOB-Diet mice relative to DIO vs. FOB-Surg mice (2011 and 4258 genes, respectively), suggesting that DIO mice have a global DNA methylation profile more similar to FOB-Diet mice than FOB-Surg mice. There was considerable redundancy in pathways represented by differentially methylated genes between FOB-Diet vs FOB-Surg mice

and DIO vs FOB-Surg mice, further suggesting that DIO and FOB-Diet mice share a significant number of similar DNA methylation features that likely explain overlapping pathway enrichment relative to FOB-Surg mice.

Table 5.2 KEGG pathways enriched for differentially methylated genes

Pathway	*Observed Genes in Pathway*	*% of All Genes in Pathway*	*P-value*	*FDR*
Differentially methylated DIO vs FOB-Surg (n = 4258)				
Signaling pathways regulating pluripotency of stem cells*	47	33.6	1.3E-07	2.0E-05
Breast cancer*	47	32.4	4.4E-07	3.8E-05
Pathways in cancer*	99	25.3	5.0E-07	3.8E-05
Rap1 signaling pathway	56	26.5	3.8E-05	1.9E-03
Insulin secretion*	27	33.3	7.2E-05	2.6E-03
Ras signaling pathway	58	25.7	7.7E-05	2.6E-03
Wnt signaling pathway	41	28.1	1.1E-04	2.9E-03
Hippo signaling pathway*	42	27.3	1.8E-04	4.3E-03
Focal adhesion*	51	25.1	3.6E-04	6.7E-03
Differentially methylated DIO vs FOB-Diet (n = 2011)				
Insulin secretion*	18	22.2	5.4E-05	6.4E-03
Breast cancer*	26	17.9	7.1E-05	6.4E-03
Pathways in cancer*	53	13.5	8.5E-05	6.4E-03
Differentially methylated FOB-Surg vs FOB-Diet (n = 1107)				
Signaling pathways regulating pluripotency of stem cells*	20	14.3	6.3E-06	1.9E-03
Focal adhesion*	23	11.3	6.1E-05	5.2E-03
Hippo signaling pathway*	19	12.3	8.6E-05	5.2E-03
Breast cancer*	18	12.4	1.2E-04	6.1E-03
Basal cell carcinoma*	10	18.2	1.9E-04	7.9E-03

Respective gene sets were subjected to over representation enrichment analysis (ORA) for specific KEGG pathways as compared to the mouse genome by applying a hypergeometric test and threshold minimum of five genes represented in the pathway. Asterisk indicates redundant pathway among the comparisons. FDR: false discovery rate.

Surgical weight loss, but not diet-induced weight loss, alters mammary transcriptional profiles relative to DIO mice

RNA Sequencing data was filtered to create gene lists for all pairwise comparisons between groups; differential expression with group-specific directionality was achieved by selecting genes with $\log_2$ (fold change) > 0.58 (which is equivalent to fold change > 1.5) for each inter-group comparison. Gene lists were entered into WebGestalt for overrepresentation enrichment analysis (ORA) in curated KEGG pathways. Similar to the DNA methylation results, there was significant overlap between pathways upregulated in DIO vs. FOB-Surg mice and FOB-Diet vs FOB-Surg mice, pointing to critical gene clusters that display robust activation by obesity and persist despite weight loss by diet alone. Notably, ECM-receptor interaction, pathways in cancer and PI3K-Akt signaling were included in KEGG pathways upregulated in DIO vs. FOB-Surg, but not DIO vs. FOB-Diet (Figure 5.4A and 5.4B). Next, comparisons of the two weight loss groups to DIO mice reveals significant overlap in pathway characterization (Fatty acid metabolism, metabolic pathways, PPAR signaling, insulin resistance, etc.) reflecting upregulated genes in FOB-Surg (Figure 5.4C) and FOB-Diet (Figure 5.4E) mice vs. DIO mice. There were remarkably few upregulated genes in DIO vs. FOB-Diet mice relative to other comparisons (Figure 5.4D), indicative of latent obesity-associated gene expression patters in FOB-Diet but not FOB-Surg mice. The genes that were upregulated in FOB-Surg vs. FOB-Diet mice were enriched for pathways implicated in a spectrum of inflammatory processes (Figure 5.4F). Considering the potential inconsistencies between this pathway analysis and the serum metabolite data in Table 1 showing FOB-Surg mice having lower levels of inflammatory markers relative to FOB-Diet mice, gene-level analyses were pursued.

Interestingly, explorations of redundant pathways upregulated in both FOB-Diet and FOB-Surg mice revealed group-exclusive expression profiles of distinct molecular functions. For example, the “Cytokine-cytokine receptor interaction” KEGG pathway was shown to be enriched for genes upregulated in FOB-Diet vs. FOB-Surg mice and vice versa. In this pathway, Lep, the gene encoding the adipokine leptin, was upregulated in FOB-Diet vs.FOB-Surg mice, whereas Lepr, the gene encoding leptin receptor, was upregulated in FOB-Surg vs. FOB-Diet mice, suggesting resolution of leptin resistance, however both contribute to the same KEGG pathway.

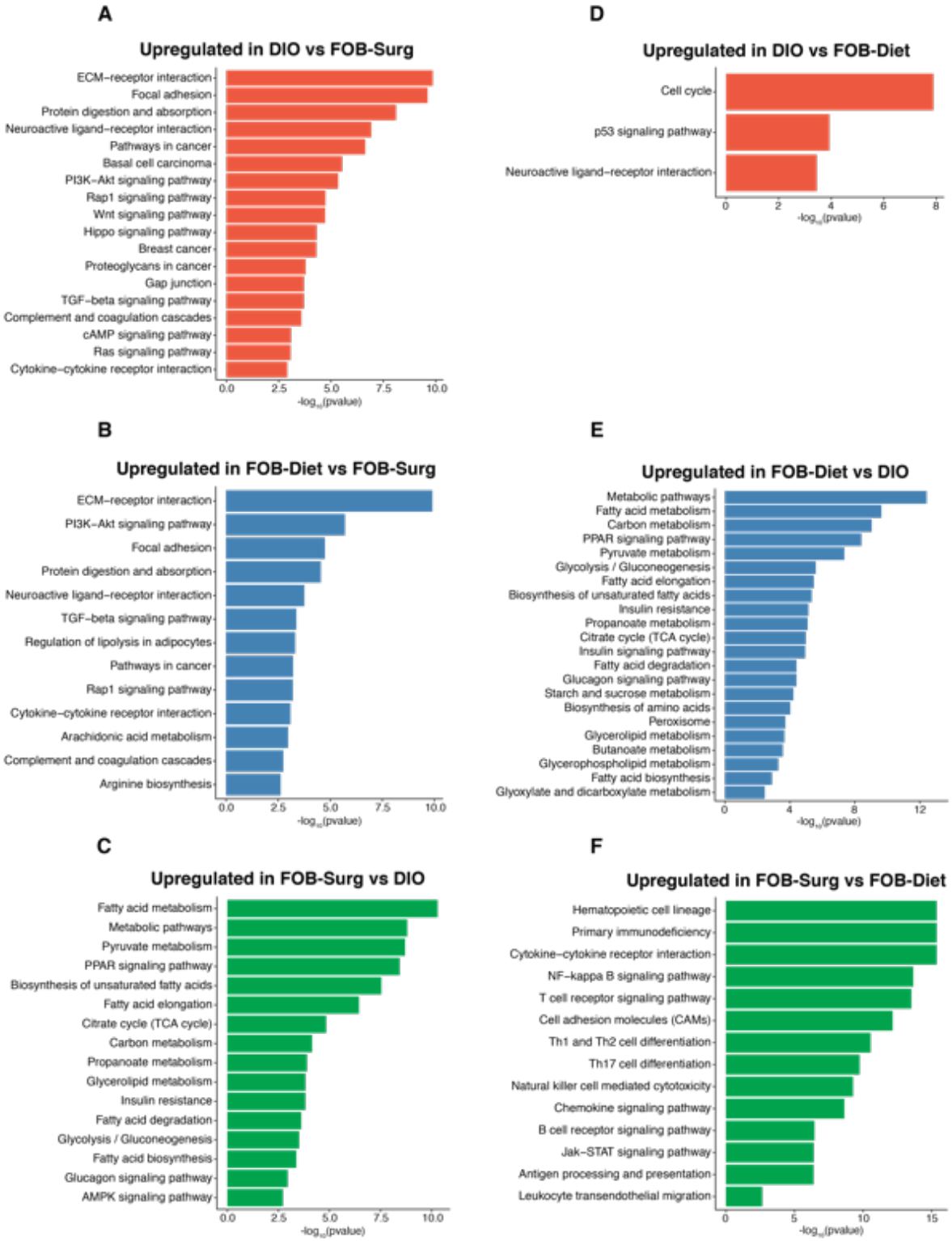

Figure 5.4. Pathway analysis of differentially expressed genes in the mammary fat pad. Pathways displayed for genes (A) upregulated in DIO vs FOB-Surg mice, (B) upregulated in FOB-Surg vs DIO mice, (C) upregulated in FOB-Diet vs FOB-Surg mice, (D) upregulated in DIO vs FOB-Diet mice, (E) upregulated in FOB-Surg vs FOB-Diet mice, and (F) upregulated in FOB-Diet vs. DIO mice.

Surgical weight loss and diet-induced weight loss differentially modulate the expression of genes involved in sphingolipid metabolism

The balance between sphingolipid metabolites influence mitogen-activated pathways and thus heavily influence the fate of a cell. Ceramide inhibits cell growth and induces apoptosis. In contract**,** sphingosine 1-phosphate (S1P) promotes proliferation and survival of inflammatory cells, in part through stimulating the extracellular signal-regulated kinase (ERK) pathway and counteracts the ceramide-induced activation of stress-activated protein kinase (SAPK/JNK) [218]. FOB-Surg mice had increased expression of genes encoding the enzymes that catalyze the recycling of S1P to sphingosin. Sphingosine 1-phosphate phosphatase 1 (SGPP1) and SGPP2 were increased in FOB-Surg mice compared to FOB-Diet with the later reaching statistical significance (Figure 5.5A). Furthermore, expression of Delta 4-Desaturase, Sphingolipid 1 (DEGS1) was similar between groups but DEGS2 was significantly increased in FOB-Surg compared to FOB-Diet, which would favor the accumulation of ceramide (Figure 5.5B). FOB-Surg and FOB-Diet mice generally displayed opposing expression of genes encoding enzymes that regulate the balance between ceramide and sphingomyelin. FOB-Surg displayed decreased expression of spingomyelin phosphodiesterase 1 (SMPD1) and SMPD3 relative to FOB-Diet, which would favor pro-apototic Ceramide over pro-survival Sphingomyelin. FOB-Surg mice also had increased expression of SMPD2 and spingomyelin synthase (SMS) which both promote the conversion of sphingomyelin to ceramide (Figure 5.5C). Sphingosine kinase (Sphk) types 1 and 2 are two isoforms with opposite roles in the regulation of ceramide biosynthesis, with Sphk1 generally deemed as pro-survival and Sphk2 generally pro-apoptotic [219]. The

expression of Sphk1 contrasts Sphk2 expression for essentially in the mice from all groups. FOB-Diet mice had significantly increased expression of Sphk1 and a reduced expression of Sphk2, which did not reach statistical significance (Figure 5.5D).

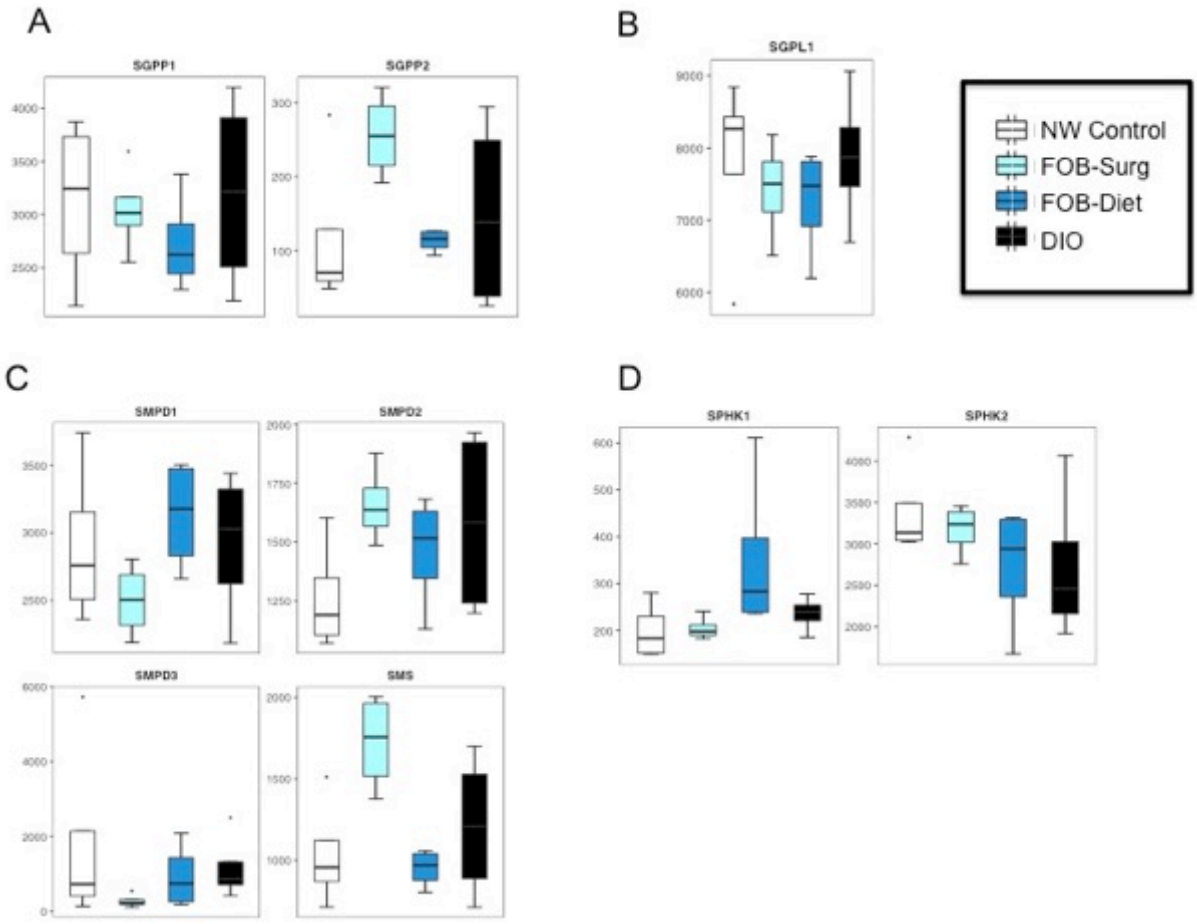

Figure 5.5. Surgical weight loss and diet-induced weight loss differentially modulate the expression of genes involved in sphingolipid metabolism. FOB-Surg and FOB-Diet mice displayed divergent expression of genes involved in (A) recycling of sphingosine 1-phosphate to sphingosin; (B) Degredation of sphingosine 1-phosphate; (C) recycling of ceramide to sphingomyelin, and (D) Generation of spingosine 1-phosphate.

DNA methylation and gene expression profiles of genes altered after surgical weight loss displays partial concordance with human data sets

Genes exhibiting significant hyper- and hypomethylation in DIO vs NW Control, FOB-Surg, or FOB-Diet mice were selected by calculating the difference in average

percent methylation of the groups and attributing significance according to false discovery rate < 0.05 and $P < 0.05$. These differentially methylated features were compared to DNA methylation data obtained from mammary tissue cataloged in the Normal Breast Study showing concordant hyper- or hypomethylation in obese subjects. Displayed are results of concordance analysis (Table 5.3) showing robust alignment of genes implicated in a variety of pathways relevant to carcinogenesis and regulation of cell proliferation. Additionally, gene ontology (GO) and KEGG pathways regulated by differential gene expression were compared to a microarray gene expression study of white adipose tissue (WAT) of obese vs. lean subjects and subjects after vs. before undergoing bariatric surgery performed by Henegar et al. [220]. For concordance analysis, DIO vs. NW Control mice were used in comparison with obese vs. lean subjects. Our data exhibited bi-directional overlap energy-responsive pathways, with six out of eleven GO and five out of ten KEGG pathways showing mirrored regulation for comparisons between obese vs. lean subjects and DIO vs. NW Control mice. Furthermore, DIO vs. FOB-Surg mice were used in comparison with analysis of samples after vs. before bariatric surgery. Again, our data displayed distinct similarity with directional regulation of GO and KEGG pathways, with eight out of fourteen GO and five out of 12 KEGG pathways showing identical regulation.

Table 5.3 DNA methylation comparison between obese vs. nonobese women and DIO vs. NW Control, FOB-Surg and FOB-Diet mice

		Mouse Data								Human Data			
				DIO vs NW Control		DIO vs FOB-Surg		DIO vs FOB-Diet			Obese vs Nonobese		
		Chr Loc.	Reg.	Methyl Δ (%)	P-value	Methyl Δ(%)	P-value	Methyl Δ (%)	P-value	Probe ID	Reg.	ρ	P-value
Fgf family	*Fgf3*	chr7.144 838338	P	-10.8	3E-04	-6.5	3E-03	-0.9	7E-01	cg103 61167	B	-25.8	4.2E-03
	Fgfr1	chr8.25 519344	P	8.7	5E-03	8.9	2E-04	7.1	5E-02	cg108 23844	TSS	17.3	6.3E-04
Pathways in cancer	*Runx1*	chr16.92 695764	P	-13.5	2E-08	-28.5	3E-21	-4.0	3E-01	cg015 19261	5'UTR	-65.2	4.9E-04
	Itga2b	chr11.1 024685 91	I	-5.1	1E-03	-8.9	3E-07	-0.2	7E-01	cg223 81590	B	-78.3	8.4E-03
	Lama5	chr2.1802 14995	I	-10.2	2E-03	-9.3	2E-05	-0.8	1E-01	cg140 07090	B	-83.8	5.1E-06
	Ptger1	chr8.83 661250	E	-10.5	9E-03	-20.1	2E-06	-7.5	6E-02	cg006 12299	B	-40.0	1.7E-03
		chr8.83 668613	E	-12.3	5E-09	-5.6	4E-03	-1.7	6E-01	cg104 68702	5'UTR	-29.1	4.8E-03
	Rxra	chr2.27 691622	I	-12.9	5E-03	-16.4	8E-06	-7.3	9E-02	cg139 31640	B	-40.6	5.4E-04
		chr2.27 750764	I	-8.0	9E-03	-9.9	1E-04	-5.1	5E-02	cg142 36758	B	-38.7	1.4E-03
	Vegfa	chr17.45 915090		-12.6	1E-11	-12.0	1E-10	-3.6	1E-01	cg253 73579	3'UTR	-55.6	7.3E-03
Wnt signaling pathway	*Tcf7*	chr17.28 232857	P	-11.5	5E-03	-7.0	1E-02	-8.6	6E-01	cg156 11037	B	-61.5	1.4E-02
		chr11.52 286547	P	16.8	8E-04	11.2	2E-04	4.8	1E-01	cg206 82563	B	36.9	5.1E-05
	Wnt4	chr4.137 291750	I	-5.9	9E-03	-9.4	2E-06	-4.2	1E-01	cg035 19931	B	-20.7	2.1E-03
	Wnt5a	chr14.28 506637	I	-6.1	8E-03	-8.2	2E-03	-4.2	1E-01	cg088 52968	B	-35.0	9.2E-04
	Wnt3a	chr11.59 289014	I	-10.9	2E-03	-9.2	1E-04	-1.6	3E-01	cg161 70838	B	-85.5	5.1E-04

Abbreviations: Chr: Chromosome, Fgf: Fibroblast growth factor, Loc.:Location, Reg.:Region, P:Promoter, I:Intron, E:Exon, B:Body, TSS: transcription start site, *ρ:* correlation coefficient

E. Discussion

The results of our preclinical study using a mouse model of premenopausal basal-like breast cancer demonstrate that weight loss by bariatric surgery, but not weight loss by a low-fat diet regimen alone, is able to reverse obesity-driven transformations in metabolism, inflammation, DNA methylation, gene expression, and mammary tumor burden. Consistent with established trends in the literature, DIO mice, relative to NW Control mice, exhibited significantly higher levels of the following obesity-associated cancer promoting perturbations: serum hormones (insulin, IGF-1, leptin:adiponectin, resistin), circulating inflammatory markers (TNF-α, IL-6, MCP-1), body weight, body fat percentage, adipocyte size, and CLS density in the mammary fat pad. FOB-Surg mice, which achieved an obese phenotype by consuming a high fat diet for 15 weeks and underwent a vertical sleeve gastrectomy procedure followed by a switch to a low fat diet, displayed significant reductions in the obesity-associated cancer promoting perturbations from DIO mice and not significantly different from NW Control mice in all of these measures. FOB-Diet mice, which likewise achieved an obese phenotype and received a sham procedure followed by a switch to a low-fat diet to lose weight, displayed significant reductions from DIO mice in measures of body weight, body percentage, leptin:adiponectin, IL-6, and MCP-1, although mammary adipocyte size remained significantly higher than NW Control mice. FOB-Surg mice, but not FOB-Diet mice, exhibited average adipocyte size, CLS density, circulating TNF-α, and *ex vivo* mammary tumor volume was not significantly different from NW Control mice, while the same measures in FOB-Diet mice, (with the exception of adipocyte size, which was

intermediate), were not significantly different from DIO mice. Therefore, we conclude that surgical weight loss imparted a plurality of metabolic advantages and successful reversal of obesity-associated mammary tumor burden that were not similarly achieved by dietary weight loss.

In order to provide a comprehensive molecular comparison of surgical and dietary weight loss relevant to breast cancer risk and progression, we performed parallel mRNA sequencing and reduced representation bisulfite sequencing of the mammary fat pad to delineate functional changes in the transcriptome and epigenome. Intriguingly, there were many more genes with differentially methylated features in DIO vs. FOB-Surg mice (n=4258 genes) than DIO vs. FOB-Diet mice (n=2011 genes), suggesting that surgical weight loss was more effective at generating a DNA methylation profile distinct from DIO mice. Differentially methylated genes in DIO vs. FOB-Surg mice and FOB-Diet vs. FOB-Surg mice were enriched for similar canonical signaling pathways, pointing to DNA methylation as a potential mechanism by which obesity-driven cellular changes remain active in FOB-Diet mice but not FOB-Surg mice.

Next, differentially expressed genes were subjected to unbiased pathway analysis to highlight coherent gene clusters in the context of curated signaling pathways. Similar to trends observed in pathway analysis of differentially methylated genes, pathways upregulated in DIO vs. FOB-Surg mice and FOB-Diet vs. FOB-Surg mice exhibited substantial redundancy, suggesting that obesity-associated gene expression profiles in the mammary fat pad are responsible for characterizing differential gene expression between mice that underwent dietary vs. surgical weight loss. Genes and pathways that were upregulated by the weight loss interventions (that

is, upregulated genes and pathways in FOB-Diet vs. DIO mice and FOB-Surg vs. DIO mice) showed considerable similarity in their biological function. Namely, the majority of the pathways involved macronutrient metabolism and metabolic machinery of core anabolic and catabolic pathways, such as fatty acid metabolism, tricarboxylic acid (TCA) cycle, insulin signaling, pyruvate metabolism, and peroxisome proliferator-activated receptor (PPAR) signaling. These results provide robust evidence for the centrality of metabolic control in obesity-reversal interventions. Interestingly, genes upregulated in FOB-Surg vs. FOB-Diet mice are heavily enriched for pathways implicated in a variety of inflammatory processes, despite powerful anti-inflammatory effects of surgical weight loss substantiated by circulating cytokine levels and CLS density in the mammary fat pad. Analysis at the gene level implicates the inclusion of positive and negative regulators of inflammation for these results.

Additionally, FOB-Surg and FOB-Diet displayed differential expression of genes involved in sphingolipid metabolism, with opposing expression levels of the same gene. FOB-Surg mice expressed decreased SMPD3, whereas FOB-Diet mice expressed increased levels (similar to DIO). SMPD3 expression, but not SMPD1 or SMPD2, has correlated significantly with concentrations of ceramide and is also increased in obese humans and mice [221,222]. Sphingosine 1-phosphate is heavily implicated in the development of insulin resistance. Mouse models lacking functional sphingosine 1-phosphate receptor 2 (S1P2) are protected from adipose tissue dysfunction (adipocyte hypertrophy, influx of macrophages, and insulin resistance) while on a high-fat diet [223]. Sphingosine kinase(Sphk) types 1 and 2 are two isoforms that phosphorylate sphingosine to produce spingosine 1-phosphate (S1P), however their expression differs

throughout tissues in the body and in subcellular location [224]. The Sphk isoforms have opposing functions, as Sphk1 promotes survival and Sphk2 promotes apoptosis [219]. The expression of Sphk1 contrasts Sphk2 expression for essentially in the mice from all groups. In FOB-Surg mice, Sphk2 prevails over Sphk1 while the opposite occurs in FOB-Diet mice. This is particularly relevant as both TNF-α and IGF-1 can promote the expression of Sphk1 [225]. Sphk1 regulates HIF-1α and also promotes breast epithelial cell proliferation and malignant transformation of breast epithelial cells [226-228]. Thus, alterations in the absorption of lipids or increases in bile acids characteristic of bariatric surgery may mediate the anti-cancer effect of surgery through sphingolipid-dependent mechanisms.

The sequencing results of our animal study demonstrate considerable similarity with similar molecular investigations in humans. The results of our RRBS studies were compared to DNA methylation in normal breast tissue from the Normal Breast Study. This study generated correlation coefficients between methylation levels and obesity, and accordingly each methylation probe can be observed for up- or downregulation in obesity. Concordance analysis between these two datasets revealed a number of gene features that exhibit concordant reduction or enrichment of CpG methylation in obese vs. non-obese women in comparisons to DIO vs. NW Control mice, DIO vs. FOB-Surg mice, and failure to reverse these trends in FOB-Diet mice. The resulting genes are therefore critical targets under epigenetic control that in part mediate the differential outcomes between the two weight loss groups.

This is the first study to compare the effects of surgical vs. dietary weight loss on mammary tumor burden in a preclinical mouse model of basal-like breast cancer.

Leveraging the power of next-generation sequencing platforms, RNA-Seq revealed upregulation of macronutrient metabolic machinery as a consistent transcriptomic phenomenon between both weight loss groups. However, we observed divergent effects of certain molecular processes implicated in the innate immune and inflammatory response and sphingolipid metaolism in FOB-Surg mice compared to FOB-Diet, which likely contribute to the exclusive cancer-protective effects observed in FOB-Surg mice.

CHAPTER VI. SUMMARY AND CONCLUDING REMARKS

A. Introduction

Epidemiological data demonstrates that obesity increases the risk of ER-positive and ER-negative breast cancer in postmenopausal women and also increases the risk of ER-negative breast cancer in premenopausal women. In pre- and postmenopausal women, obesity is associated with increased stage at diagnosis, risk of metastasis and mortality from their disease [30,229,230]. Approximately 85,000 new cancer cases per year are attributed to obesity in the United States [4]. Furthermore, its estimated that 20% of all cancer deaths in women are attributable to BMI ≥ 25 kg/m^2, which underlines the deficiency for effective strategies to prevent and treat cancer in obese individuals [5].

The cancer promoting effects of obesity are a major public health concern, and the current gap in knowledge on the anticancer effects of weight loss on breast cancer contributes to this concern. Few studies are able to effectively study the potential anticancer effects of diet-induced weight loss due to low success rates of weight loss interventions and even lower maintenance of weight due to recidivism. Recent studies report that 17.3% of US adults who have ever been overweight or obese were able to lose 10% of their body weight and maintain weight loss for at least one year [231]. However, only 4.4% of US adults are able to lose 20% of their body weight and maintain

weight loss for at least one year [232]. The physiological responses to weight loss is dynamic and yields metabolic, epigenetic, and immune responses. Verhoef et al. found that a 10% weight loss in humans resulted in a 16% decrease in adipocyte size in association with increased fatty acid transport expression of FABP4 [233]. However, survival mechanisms associated with weight loss, including adaptive thermogenesis and physiological responses in adipocyte metabolism, may mitigate some of the health benefits of weight loss. In the same study, Verhoef et al. also found that after 10% weight loss, markers for mitochondrial beta-oxidation (HADHsc) and lipolysis (ATGL) were increased at the 10-month follow up [233]. The precise regulation of lipolytic catabolism of fat stores is required to prevent free fatty acid efflux, lipotoxicity, and resultant insulin resistance [234].

Additionally, other studies have shown that resulting adaptive thermogenesis after weight loss potentially predisposes individuals to regain weight several years after weight loss [235,236]. Studies investigating the content of adipose tissue macrophage during and after weight loss have produced vague results. Kosteli et. al demonstrated that lipolysis in negative energy balance recruits macrophages to white adipose tissue, while Kovacikova et al. showed that weight loss decrease the total prevalence of macrophages, but did not selectively modify pro- or anti-inflammatory macrophage subpopulation [237,238]. Furthermore, suppressed thermogenesis in skeletal muscle is a constituent of a thrifty phenotype and is associated with insulin insulin resistance and abdominal obesity [239]. Therefore, while weight loss has great potential in decreasing cancer risk, molecular mechanisms at play to perpetuate weight cycling require careful attention as they have the ability to confer an advantageous tumor microenvironment.

B. Obesity-associated adipose tissue remodeling underlies inflammation and is mediated in part by epigenetic perturbations

The primary mechanistic drivers underlying the obesity-breast cancer link are the metabolic and inflammatory perturbations often accompanying obesity, notably insulin resistance, increased local and systemic cytokines, and a decreased adipogenic capacity. The obese state is thus associated with profound expansion of the adipose tissue, which occurs by adipocyte hyperplasia (increase in adipocyte number) predominating over hypertrophy (increase in adipocyte size). Adipocyte hypertrophy, and the associated fatty acid spill over, is strongly implicated in insulin resistance and other obesity-associated metabolic alterations [48,123].

Similar to the adaptive metabolic changes in response to nutritional status observed *in utero*, epigenetic programming continues throughout the adult life to produce a metabolism-related phenotype in adults. Fraga et al. found that that monozygotic twins accumulated discordant DNA methylation and histone acetylation in life, diverging from a nearly indistinguishable epigenome in early life [240]. Additionally, a multitude of studies have reported changings in DNA methylation in response to environmental contaminants, aging, and obesity [241-246]. Several metabolic perturbations in obesity are mediated by epigenetic modifications, which confer adaptation to the immediate environment. However, without further stimuli, these aberrant epigenetic changes are preserved and can prime obese adults for metabolic inflexibility (i.e. a limited adipogenic potential) if epigenetic mechanisms impede an appropriate response to nutrient signals [76,247]. The number of adipocytes is generally constant in lean and obese adults, unaffected by weight gain or weight loss, indicative

of rigid control of adipogenesis. Accordingly, the integration of pro-adipogenic hormonal cascades and activated transcription factors requires epigenetic mechanisms to coordinate the complex process of adipogenesis. Notably, CCCTC-binding factor (CTCF) is required for adipocyte differentiation executing DNA methylation remodeling of adipose tissue with TET methylcytosine dioxygenase (TET) enzymes [248]. The expression of genes encoding epigenetic machinery, including lysine methyltransferases was significantly decreased in mice with obese mothers. Furthermore, only a subset of epigenetic machinery genes were restored in mice whose mothers lost weight prior to conception, while many remained altered [249].

In preadipocytes, activated PPARγ binds to enhancer regions in target genes to induce transcription, however this action is dependent upon an active chromatin state as evidenced by low DNA methylation levels [250]. However, in preadipocytes the DNA methylation levels of the leptin, adiponectin, and other pro-adipogenic genes at the promoter region are high and rely on demethylation during adipogenesis for transcriptional competence [251]. Therefore, in addition to adipogenic targets, PPARγ also activates histone lysine methyltransferases to complete chromatin modification permitting a transcriptionally activate state [252].

The promoters of the genes encoding adiponectin, GLUT4, glycerol-3-phosphate dehydrogenase (GPD1), and leptin are enriched in dimethylated histone H3 Lys (H3-K4). In early-phase adipogenesis, transcription of adiponectin occurs in concert with histone modifications (promoter H3 hyperacetylation and H3-K4 trimethylation) [253]. Findings from Musri et al. support the notion that H3-K4 dimethylation is a distinguishing

feature of adipogenic genes expressed later during the differentiation process in committed preadipcoytes [253].

Therefore, fixed methylation of adipogenic genes, or inadequate expression of genes constituting ‘epigenetic machinery’ to accomplish demethylation of genes could have deleterious consequences. Furthermore, pathogenic increases in DNMT3A expression could result in gene hypermethylation [254,255]. DNA methylation can promote or impede adipogenesis, dependent upon the gene and location. The epigenome of adipocytes from obese individuals implicates aberrant DNA methylation of pro-adipogenic genes (PPARγ) and genes that confer an insulin sensitive phenotype (IRS1, Lipe, GLUT4) in obesity-associated impaired adipogenesis [256-259].

Kamei et al. showed that mRNA expression of DNA methyltransferase (Dnmt)-3a, an enzyme tht catalyzes the transfer of methyl groups to DNA, is increased in the adipose tissue of wild-type mice on a high-fat diet relative to wild-type mice on a chow diet. Interestingly, DNMT3A mRNA expression was also increased in the mature adipocyte fraction and stromal vascular fraction isolated from obese db/db mice (relative to wild-type littermates) and in 3T3-L1 adipocytes cocultured with RAW264 macrophages [260]. Furthermore, transgenic mice overexpressing DNMT3A in adipose tissue experienced increased MCP-1 and TNF-α expression after exposure to a high-fat diet, relative to wild-type mice on a high-fat diet [260].

Leptin and TNF-α are two genes that possess energy-responsive methylation patterns and also contribute importantly to metabolic flexibility. In adipocytes, leptin suppresses insulin-stimulated glucose metabolism and inhibits lipid synthesis. Leptin also stimulates nitric oxide production, which inhibits glycerol synthesis, thus reducing

the opportunity for adipocytes to re-esterify fatty acids [261]. Zhou et al. utilized a model of adenovirus-induced hyperleptinemia in rats, which resulted in dedifferentiation of adipocytes, in association with the loss of adipocyte markers and loss of lipogenic enzymes [262]. Multiple pre-clinical studies have demonstrated that high-fat diet results in leptin promoter hypermethylation [263,264]. In vitro, treating preadipcoytes with 5-azacytidine, an inhibitor of DNA methyltransferase, increased leptin expression as cells matured into adipocytes [265]. Without 5-azacytidine treatment, lipid accumulation in maturing adipocytes stimulated leptin expression but not insulin stimulation [265]. In vitro work has shown that leptin increases the net efflux of free fatty acids from adipocytes by as much as 30% [266].

C. Summary of mechanisms linking adipose tissue remodeling and obesity with breast cancer growth

The adipocyte hypertrophy-insulin resistance-aberrant lipolysis axis that occurs in obesity has profound effects on the composition of cells in the environment. Adipocyte size positively correlates with macrophage infiltration in the adipose tissue [80]. Free fatty acid efflux and a disturbed secretome, results in a pro-inflammatory milieu enhancing cross-talk between macrophages, adipocytes, and other immune cells in the adipose tissue.

PGE_2 is a bioactive lipid that regulates of vascularity and proliferation in the microenvironment and is a mitogen for tumor cells [267]. Obesity is associated with extracellular matrix remodeling, resulting in an increase in adipose tissue fibrosis [98]. Thus, in the obese mammary stroma, fibroblasts and preadipocytes are rich sources of

PGE_2 which drive cancer growth [100]. However, Hu et al. used a combination of in vivo and in vitro techniques to show that adipocytes undergoing lipolysis produce PGE_2, which can further promote macrophage migration [94].

As the size of hypertrophic adipocytes exceeds the capacity of the body to supply the tissue with adequate oxygen, adipocyte hypertrophy promotes adipose tissue hypoxia, oxidative stress and mitochondrial dysfunction [77]. The bioenergetics in remodeled adipose tissue contributes to a microenvironment that provides the necessary substrate to support the rapid growth of proliferating tumor cells.

D. Molecular targets identified with anti-inflammatory and surgical weight loss interventions to break the obesity-cancer link

The preclinical studies described in the previous chapters provided mechanistic insight informing strategies to break the obesity-cancer link. Metabolism in the mammary microenvironment dictates lipids and other nutrients available to the tumor. The ability of adipocytes to respond to insulin appropriately is largely affected by adipocyte size and requires a maintenance of adipogenesis (i.e. expansion of adipose tissue by hyperplasia) to prevent adipocyte hypertrophy. The metabolism and mitochondrial function of adipocytes varies in relation to size with increasing metabolic dysfunction, lipolysis, and insulin resistance increasing with pathogenic adipocyte size [268]. Our results suggest that the consequence of adipocyte hypertrophy is enhanced interactions between adipocytes and pro-inflammatory macrophages. Maintaining metabolically healthy adipocyte size is associated with decreases in chemoattractant signals, macrophage influx, and COX-2/PGE_2 activity in the mammary fat pad.

Macrophage infiltration, increased accumulation of ectopic lipids and increases in COX-2/PGE_2 activity have been identified as distinguishing and advantageous factors which promote tumor growth in obese mice and are associated with disturbances in the tumor microenvironment.

We found that resveratrol supplementation in obese mice significantly decreased mammary tumor growth in a claudin-low model of breast cancer. Mice on a diet-induced obesity regimen supplemented with resveratrol (DIO + resveratrol) were protected from adipocyte hypertrophy and the associated shift in pro-inflammatory cytokines (including TNF-α and IL-6) produced by hypertrophied adipocytes. DIO + resveratrol mice, relative to DIO mice, had lower gene expression of cytokines associated with recruitment of macrophages, as well as lower COX-2 expression. Prevention of the aberrant decrease in gene expression of adipogenesis-related genes observed in DIO mice may also contribute importantly to the protective effects of resveratrol against tumor growth in DIO + resveratrol mice. The culmination of changes in the microenvironment ultimately changed the adipose secretome and limited lipids and other nutrients available to the tumor, which blunted mammary tumor growth and also resulted in a decrease influx of tumor-associated macrophages.

We expanding our findings with resveratrol by specifically targeting obesity-associated inflammation and supplemented diet-induced obese (DIO) mice with a nonsteroidal anti-inflammatory Sulindac or omega-3 fatty acids. Our findings demonstrate that Sulindac was a more effective anti-inflammatory supplement than Omega-3. Sulindac supplementation in DIO but not Control mice significantly decreased basal-like mammary tumor volume and tumor latency in association with inhibition of

adipose tissue dysregulation. Sulindac supplementation in DIO mice significantly reduced mammary CLS density, adipocyte area, and COX-2 pro-inflammatory metabolites in the tumor. These effects were in association with significantly decreased mammary tumor volume compared to DIO mice without supplementation. Omega-3 supplementation in DIO mice produced an intermediate reduction in basal-like tumor growth without impacting mammary adipocyte area and tumor levels of $PGF_{2\alpha}$, PGD_2 and 13 PGE_2.

Next we assessed whether the pro-tumorigenic effects of obesity are reversed by weight normalization. Surprisingly, we found that basal-like tumor volume, serum IL-6 levels, expression of pro-inflammatory genes in the mammary fat pad, and mammary DNA methylation profiles were similar in DIO and formerly obese (FOb) mice, and higher than in controls. These results suggested that the epigenetic dysregulation in the microenvironment in association with sustained elevations in inflammatory signaling may have greater influence on mammary tumor growth than adiposity and serum growth hormones such as insulin and IGF-1, as adiposity and metabolic hormones were lowered to levels observed in control mice.

Considering the substantial evidence demonstrating that weight loss via bariatric surgery reduces cancer risk, we established a surgical sleeve gastrectomy (SG) protocol in our mouse model of obesity. We found that the modality of weight loss, either surgical (FOB-Surg) or diet alone (FOB-Diet) differentially modified basal-like mammary tumor growth and markers of inflammation. Specifically, FOB-Surg mice had levels of serum tumor necrosis factor-alpha (TNF-α), insulin, and mammary adipocyte size that were not significantly different from NW Control mice and significantly different

from FOB-Diet and DIO mice. Genome wide analysis of gene expression (RNA Seq) and DNA methylation (RRBS) revealed that weight loss via sleeve gastrectomy restored metabolic flexibility (the ability to respond to nutrient signals appropriately) to a greater extent than in FOB-Diet mice. Alterations in genes regulating sphingolipid metabolism in the mammary of FOB-Surg mice also implicate bioactive lipids in the differences in tumor growth.

E. Concluding remarks and future directs

The cancer promoting effects of obesity are a major public health concern, with an established relationship between obesity and increased risk of estrogen receptor-positive breast cancer in postmenopausal women and increased risk of triple-negative breast cancer in premenopausal women. Triple-negative breast cancer is a subtype with poor prognosis, at least in part due to lack of established targeted therapies [16,17]. However, obesity is associated with increased mortality in hormone receptor-positive and negative subtypes [17]. A meta-analysis found that each 5 kg/m^2 increment of BMI before diagnosis resulted in a 18% increase in breast cancer mortality [32]. Clearly, more effective prevention and treatment strategies are urgently needed to reduce the burden of obesity on breast cancer.

The World Health Organization's International Agency for Research on Cancer Working Group on Body Fatness and Cancer recently identified a major gap in the literature regarding the impact and underlying mechanisms of intentional weight loss in the context of chronic obesity on cancer [211]. Their summary report stated that, with

the exception of studies of bariatric surgery-induced weight loss, epidemiological and clinical studies have been sparse and inconsistent regarding whether intentional weight loss can reverse the pro-inflammatory and procancer effects of obesity. The high recidivism rate following dietary weight loss interventions no doubt contributes to this important knowledge gap about the reversibility of the obesity-cancer link [41,42].

The current gap in the literature on the anticancer effects of weight loss hinders our ability to identify anticancer mechanisms that occur in weight loss that could be targeted in a population that is obese. The objective of my dissertation work was to 1) work towards establishing the relationship between weight loss and cancer and 2) identify mechanistic targets in weight loss that could be modulated in an obese population to break the obesity-cancer link. We found in our preclinical studies that weight loss achieved by switching from a DIO regimen to a low-fat diet did not have an anticancer benefit, in association with sustained inflammatory and epigenetic signals. However, weight loss by surgery did provide an anticancer effect in association with restored metabolic flexibility, mediated in part, by alterations in DNA methylation.

Given that weight loss by diet failed to reduce basal-like mammary tumor growth due to sustained inflammatory signaling, we targeted obesity-associated inflammation. We found that adipose tissue dysfunction largely mediates obesity-associated inflammation. Anti-inflammatory interventions, which modulate the ratio of PGE_2 and PPARγ, such as COX-2 inhibitors or PPARγ agonists, ameliorate adipose tissue dysfunction. Preventing the loss of PPARγ function, which has been documented in obesity, alleviates the limited adipogenic potential and reduces adipocyte hypertrophy [122,123]. Overcoming impaired preadipocyte differentiation yields reprieve of the pro-

inflammatory contributions from the macrophage-like phenotype preadipocytes. Additionally, with inhibition release of PPARγ, adipogenesis enriches the number of small adipocytes, which possess a phenotype capable of responding to insulin and storing lipid. COX-2 inhibition via non-steroidal anti-inflammatory drugs (NSAIDs) [119] and some anti-diabetic drugs such as thiazolidinediones (TZD), favorably modulate the ratio of PPARγ to COX-2. A higher ratio of PPARγ to COX-2 is associated with decreased macrophage infiltration and adipocyte insulin sensitivity [120]. The anti-inflammatory and anti-diabetic effect of NSAIDs and TZDs involves decreasing NF-κB activation, which then alleviates the inhibition of preadipocyte differentiation or adipocyte maturation. Furthermore, PPARγ activation allows for adipocyte turnover, including replacing large mature adipocytes with newly differentiated small adipocytes, promoting insulin sensitivity in adipocytes [121].

Targeting the epigenetic mechanisms that exacerbate metabolic disease is an attractive intervention to break the obesity-cancer link. DNA methylation is a key epigenetic contributor to insulin resistance by regulating adipogenesis. An alternative strategy to restore insulin sensitivity would be to modify the epigenome of mesenchymal stem cells and preadipocytes to increase the adipogenic potential. Ensuring inhibition of Wnt signaling (via methylation of chromatin modifications) to allow for adipogenesis could also improve insulin sensitivity [269]. Alternatively, specifically manipulating the methylation of genes that confer an insulin sensitive phenotype (IRS1, Lipe, GLUT4) could improve insulin sensitivity and mitochondrial function [256-259].

Our findings are in agreement with a large body of literature demonstrating that bariatric surgery results in a dramatic metabolic reprogramming, mediated in part by

epigenetic mechanisms [46]. Advances in CpG bisulfite sequencing have enabled the identification of obesity-associated gene methylation, which can be confirmed by a multitude of studies. Furthermore, recent studies have reported global DNA methylation profiling of adipose tissue before and after weight loss to identify aberrant methylation that can be targeted in individuals without surgery [270]. Furthermore, changing the behavior of the adipose tissue to favor adipocyte beiging is possible by targeted modification of PRDM16 or RXR methylation, which is possible with CRISPR/Cas9 technology [271,272].

The work described in this dissertation has enhanced our understanding of the mechanisms by which obesity promotes breast cancer progression. This improved knowledge on the relationship between adipose tissue dysfunction, inflammation, and breast cancer growth will inform the development of future studies in the Hursting laboratory. Additionally, providing critical insight on the concordance between mouse and human DNA methylation in mammary tissue validates our preclinical work. We have identified the critical mechanisms underlying the protective effects of anti-inflammatory supplementation or bariatric surgery as preventing adipocyte hypertrophy and macrophage infiltration, decreasing expression of pro-inflammatory mediators, and normalizing DNA methylation in the mammary tissue. These results could inform the development of mechanism-based strategies to more precisely intervene to prevent obesity-related cancers.

REFERENCES

1. Health, United States, 2015: With Special Feature on Racial and Ethnic Health Disparities. Hyattsville, MD 2016.

2. Fryar CD OC. Prevalence of Underweight Among Adults Aged 20 Years and Over: United States, 2007-2008. National Center for Health Statistics; 2010.

3. Moore JX CN, Akinyemiju T. Metabolic Syndrome Prevalence by Race/Ethnicity and Sex in the United States, National Health and Nutrition Examination Survey, 1988-2012. Prev Chronic Dis 2017;14:160287.

4. Basen-Engquist K, Chang M. Obesity and cancer risk: recent review and evidence. Curr Oncol Rep 2011;13(1):71-76.

5. Calle EE, Rodriguez C, Walker-Thurmond K, Thun MJ. Overweight, obesity, and mortality from cancer in a prospectively studied cohort of U.S. adults. N Engl J Med 2003;348(17):1625-1638.

6. Hu X, Stern HM, Ge L et al. Genetic alterations and oncogenic pathways associated with breast cancer subtypes. Mol Cancer Res 2009;7(4):511-522.

7. Cejalvo JM, Martinez de Duenas E, Galvan P et al. Intrinsic Subtypes and Gene Expression Profiles in Primary and Metastatic Breast Cancer. Cancer Res 2017;77(9):2213-2221.

8. Parker JS, Mullins M, Cheang MC et al. Supervised risk predictor of breast cancer based on intrinsic subtypes. J Clin Oncol 2009;27(8):1160-1167.

9. Hammond ME, Hayes DF, Dowsett M et al. American Society of Clinical Oncology/College Of American Pathologists guideline recommendations for immunohistochemical testing of estrogen and progesterone receptors in breast cancer. J Clin Oncol 2010;28(16):2784-2795.

10. Dai X, Li T, Bai Z et al. Breast cancer intrinsic subtype classification, clinical use and future trends. Am J Cancer Res 2015;5(10):2929-2943.

11. Perou CM. Molecular stratification of triple-negative breast cancers. Oncologist 2010;15 Suppl 5:39-48.

12. Cornen S, Guille A, Adelaide J et al. Candidate luminal B breast cancer genes identified by genome, gene expression and DNA methylation profiling. PLoS One 2014;9(1):e81843.

13. Hu Z, Fan C, Oh DS et al. The molecular portraits of breast tumors are conserved across microarray platforms. BMC Genomics 2006;7:96.

14. Cancer Genome Atlas N. Comprehensive molecular portraits of human breast tumours. Nature 2012;490(7418):61-70.

15. Gong Y, Liu YR, Ji P, Hu X, Shao ZM. Impact of molecular subtypes on metastatic breast cancer patients: a SEER population-based study. Sci Rep 2017;7:45411.

16. Dunlap SM, Chiao LJ, Nogueira L et al. Dietary energy balance modulates epithelial-to-mesenchymal transition and tumor progression in murine claudin-low and basal-like mammary tumor models. Cancer Prev Res (Phila) 2012;5(7):930-942.

17. Niraula S, Ocana A, Ennis M, Goodwin PJ. Body size and breast cancer prognosis in relation to hormone receptor and menopausal status: a meta-analysis. Breast Cancer Res Treat 2012;134(2):769-781.

18. Herschkowitz JI, Simin K, Weigman VJ et al. Identification of conserved gene expression features between murine mammary carcinoma models and human breast tumors. Genome Biol 2007;8(5):R76.

19. Perou CM. Molecular stratification of triple-negative breast cancers. Oncologist 2011;16 Suppl 1:61-70.

20. Dias K, Dvorkin-Gheva A, Hallett RM et al. Claudin-Low Breast Cancer; Clinical & Pathological Characteristics. PLoS One 2017;12(1):e0168669.

21. Gauthier ML, Berman HK, Miller C et al. Abrogated response to cellular stress identifies DCIS associated with subsequent tumor events and defines basal-like breast tumors. Cancer Cell 2007;12(5):479-491.

22. Hu Z, Fan C, Livasy C et al. A compact VEGF signature associated with distant metastases and poor outcomes. BMC Med 2009;7:9.

23. Wang J, Yang DL, Chen ZZ, Gou BF. Associations of body mass index with cancer incidence among populations, genders, and menopausal status: A systematic review and meta-analysis. Cancer Epidemiol 2016;42:1-8.

24. Chen L, Cook LS, Tang MT et al. Body mass index and risk of luminal, HER2-overexpressing, and triple negative breast cancer. Breast Cancer Res Treat 2016;157(3):545-554.

25. Phipps AI, Chlebowski RT, Prentice R et al. Body size, physical activity, and risk of triple-negative and estrogen receptor-positive breast cancer. Cancer Epidemiol Biomarkers Prev 2011;20(3):454-463.

26. Lara-Medina F, Perez-Sanchez V, Saavedra-Perez D et al. Triple-negative breast cancer in Hispanic patients: high prevalence, poor prognosis, and association with menopausal status, body mass index, and parity. Cancer 2011;117(16):3658-3669.

27. Colditz GA, Rosner B. Cumulative risk of breast cancer to age 70 years according to risk factor status: data from the Nurses' Health Study. Am J Epidemiol 2000;152(10):950-964.

28. Lahmann PH, Schulz M, Hoffmann K et al. Long-term weight change and breast cancer risk: the European prospective investigation into cancer and nutrition (EPIC). Br J Cancer 2005;93(5):582-589.

29. Reeves KW, Faulkner K, Modugno F et al. Body mass index and mortality among older breast cancer survivors in the Study of Osteoporotic Fractures. Cancer Epidemiol Biomarkers Prev 2007;16(7):1468-1473.

30. Calle EE, Kaaks R. Overweight, obesity and cancer: epidemiological evidence and proposed mechanisms. Nat Rev Cancer 2004;4(8):579-591.

31. Reeves GK, Pirie K, Beral V et al. Cancer incidence and mortality in relation to body mass index in the Million Women Study: cohort study. BMJ 2007;335(7630):1134.

32. Chan DS, Vieira AR, Aune D et al. Body mass index and survival in women with breast cancer-systematic literature review and meta-analysis of 82 follow-up studies. Ann Oncol 2014;25(10):1901-1914.

33. Cakar B, Muslu U, Erdogan AP et al. The Role of Body Mass Index in Triple Negative Breast Cancer. Oncol Res Treat 2015;38(10):518-522.

34. Ademuyiwa FO, Groman A, O'Connor T, Ambrosone C, Watroba N, Edge SB. Impact of body mass index on clinical outcomes in triple-negative breast cancer. Cancer 2011;117(18):4132-4140.

35. Bowers LW, Brenner AJ, Hursting SD, Tekmal RR, deGraffenried LA. Obesity-associated systemic interleukin-6 promotes pre-adipocyte aromatase expression via increased breast cancer cell prostaglandin E2 production. Breast Cancer Res Treat 2015;149(1):49-57.

36. Simpson ER, Brown KA. Obesity and breast cancer: role of inflammation and aromatase. J Mol Endocrinol 2013;51(3):T51-59.

37. Han X, Stevens J, Truesdale KP et al. Body mass index at early adulthood, subsequent weight change and cancer incidence and mortality. Int J Cancer 2014;135(12):2900-2909.

38. Robinson E, Hunger JM, Daly M. Perceived weight status and risk of weight gain across life in US and UK adults. Int J Obes (Lond) 2015;39(12):1721-1726.

39. Brown T, Avenell A, Edmunds LD et al. Systematic review of long-term lifestyle interventions to prevent weight gain and morbidity in adults. Obes Rev 2009;10(6):627-638.

40. McGuire MT, Wing RR, Hill JO. The prevalence of weight loss maintenance among American adults. Int J Obes Relat Metab Disord 1999;23(12):1314-1319.

41. Hadziabdic MO, Mucalo I, Hrabac P, Matic T, Rahelic D, Bozikov V. Factors predictive of drop-out and weight loss success in weight management of obese patients. J Hum Nutr Diet 2015;28 Suppl 2:24-32.

42. Mason C, Foster-Schubert KE, Imayama I et al. Dietary weight loss and exercise effects on insulin resistance in postmenopausal women. Am J Prev Med 2011;41(4):366-375.

43. Harvie M, Howell A, Vierkant RA et al. Association of gain and loss of weight before and after menopause with risk of postmenopausal breast cancer in the Iowa women's health study. Cancer Epidemiol Biomarkers Prev 2005;14(3):656-661.

44. Sjostrom CD, Lissner L, Wedel H, Sjostrom L. Reduction in incidence of diabetes, hypertension and lipid disturbances after intentional weight loss induced by bariatric surgery: the SOS Intervention Study. Obes Res 1999;7(5):477-484.

45. Kirchner H, Nylen C, Laber S et al. Altered promoter methylation of PDK4, IL1 B, IL6, and TNF after Roux-en Y gastric bypass. Surg Obes Relat Dis 2014;10(4):671-678.

46. Barres R, Kirchner H, Rasmussen M et al. Weight loss after gastric bypass surgery in human obesity remodels promoter methylation. Cell Rep 2013;3(4):1020-1027.

47. Christou NV, Lieberman M, Sampalis F, Sampalis JS. Bariatric surgery reduces cancer risk in morbidly obese patients. Surg Obes Relat Dis 2008;4(6):691-695.

48. Drolet R, Richard C, Sniderman AD et al. Hypertrophy and hyperplasia of abdominal adipose tissues in women. Int J Obes (Lond) 2008;32(2):283-291.

49. Henninger AM, Eliasson B, Jenndahl LE, Hammarstedt A. Adipocyte hypertrophy, inflammation and fibrosis characterize subcutaneous adipose tissue of healthy, non-obese subjects predisposed to type 2 diabetes. PLoS One 2014;9(8):e105262.

50. Arner E, Westermark PO, Spalding KL et al. Adipocyte turnover: relevance to human adipose tissue morphology. Diabetes 2010;59(1):105-109.

51. Weyer C, Foley JE, Bogardus C, Tataranni PA, Pratley RE. Enlarged subcutaneous abdominal adipocyte size, but not obesity itself, predicts type II diabetes independent of insulin resistance. Diabetologia 2000;43(12):1498-1506.

52. Pasarica M, Rood J, Ravussin E, Schwarz JM, Smith SR, Redman LM. Reduced oxygenation in human obese adipose tissue is associated with impaired insulin suppression of lipolysis. J Clin Endocrinol Metab 2010;95(8):4052-4055.

53. Balogun KA, Cheema SK. Dietary Omega-3 Fatty Acids Prevented Adipocyte Hypertrophy by Downregulating DGAT-2 and FABP-4 in a Sex-Dependent Fashion. Lipids 2016;51(1):25-38.

54. Jimenez-Gomez Y, Mattison JA, Pearson KJ et al. Resveratrol improves adipose insulin signaling and reduces the inflammatory response in adipose tissue of rhesus monkeys on high-fat, high-sugar diet. Cell Metab 2013;18(4):533-545.

55. Vuguin P, Linder B, Rosenfeld RG, Saenger P, DiMartino-Nardi J. The roles of insulin sensitivity, insulin-like growth factor I (IGF-I), and IGF-binding protein-1 and -3 in the hyperandrogenism of African-American and Caribbean Hispanic girls with premature adrenarche. J Clin Endocrinol Metab 1999;84(6):2037-2042.

56. Berryman DE, Glad CA, List EO, Johannsson G. The GH/IGF-1 axis in obesity: pathophysiology and therapeutic considerations. Nat Rev Endocrinol 2013;9(6):346-356.

57. Wullschleger S, Loewith R, Hall MN. TOR signaling in growth and metabolism. Cell 2006;124(3):471-484.

58. Laplante M, Sabatini DM. mTOR signaling in growth control and disease. Cell 2012;149(2):274-293.

59. Zoncu R, Efeyan A, Sabatini DM. mTOR: from growth signal integration to cancer, diabetes and ageing. Nat Rev Mol Cell Biol 2011;12(1):21-35.

60. Magdalon J, Chimin P, Belchior T et al. Constitutive adipocyte mTORC1 activation enhances mitochondrial activity and reduces visceral adiposity in mice. Biochim Biophys Acta 2016;1861(5):430-438.

61. Paschoal VA, Amano MT, Belchior T et al. mTORC1 inhibition with rapamycin exacerbates adipose tissue inflammation in obese mice and dissociates macrophage phenotype from function. Immunobiology 2017;222(2):261-271.

62. Mercalli A, Calavita I, Dugnani E et al. Rapamycin unbalances the polarization of human macrophages to M1. Immunology 2013;140(2):179-190.

63. Nielsen S, Guo Z, Johnson CM, Hensrud DD, Jensen MD. Splanchnic lipolysis in human obesity. J Clin Invest 2004;113(11):1582-1588.

64. Wueest S, Item F, Boyle CN et al. Interleukin-6 contributes to early fasting-induced free fatty acid mobilization in mice. Am J Physiol Regul Integr Comp Physiol 2014;306(11):R861-867.

65. Nicklas BJ, Rogus EM, Colman EG, Goldberg AP. Visceral adiposity, increased adipocyte lipolysis, and metabolic dysfunction in obese postmenopausal women. Am J Physiol 1996;270(1 Pt 1):E72-78.

66. Schinner S, Scherbaum WA, Bornstein SR, Barthel A. Molecular mechanisms of insulin resistance. Diabet Med 2005;22(6):674-682.

67. White MF. IRS proteins and the common path to diabetes. Am J Physiol Endocrinol Metab 2002;283(3):E413-422.

68. Mlinar B, Marc J, Janez A, Pfeifer M. Molecular mechanisms of insulin resistance and associated diseases. Clin Chim Acta 2007;375(1-2):20-35.

69. Living with Diabetes: Center for Disease Control and Prevention (CDC).

70. Boyle P, Boniol M, Koechlin A et al. Diabetes and breast cancer risk: a meta-analysis. Br J Cancer 2012;107(9):1608-1617.

71. Shi R, Yu H, McLarty J, Glass J. IGF-I and breast cancer: a meta-analysis. Int J Cancer 2004;111(3):418-423.

72. Nogueira LM, Lavigne JA, Chandramouli GV, Lui H, Barrett JC, Hursting SD. Dose-dependent effects of calorie restriction on gene expression, metabolism, and tumor progression are partially mediated by insulin-like growth factor-1. Cancer Med 2012;1(2):275-288.

73. Kwon H, Pessin JE. Adipokines mediate inflammation and insulin resistance. Front Endocrinol (Lausanne) 2013;4:71.

74. Bijland S, Mancini SJ, Salt IP. Role of AMP-activated protein kinase in adipose tissue metabolism and inflammation. Clin Sci (Lond) 2013;124(8):491-507.

75. Hursting SD, Berger NA. Energy balance, host-related factors, and cancer progression. J Clin Oncol 2010;28(26):4058-4065.

76. Gustafson B, Gogg S, Hedjazifar S, Jenndahl L, Hammarstedt A, Smith U. Inflammation and impaired adipogenesis in hypertrophic obesity in man. Am J Physiol Endocrinol Metab 2009;297(5):E999-E1003.

77. Netzer N, Gatterer H, Faulhaber M, Burtscher M, Pramsohler S, Pesta D. Hypoxia, Oxidative Stress and Fat. Biomolecules 2015;5(2):1143-1150.

78. Jo J, Gavrilova O, Pack S et al. Hypertrophy and/or Hyperplasia: Dynamics of Adipose Tissue Growth. PLoS Comput Biol 2009;5(3):e1000324.

79. Skurk T, Alberti-Huber C, Herder C, Hauner H. Relationship between adipocyte size and adipokine expression and secretion. J Clin Endocrinol Metab 2007;92(3):1023-1033.

80. Jung UJ, Choi MS. Obesity and its metabolic complications: the role of adipokines and the relationship between obesity, inflammation, insulin resistance, dyslipidemia and nonalcoholic fatty liver disease. Int J Mol Sci 2014;15(4):6184-6223.

81. Yang J, Eliasson B, Smith U, Cushman SW, Sherman AS. The size of large adipose cells is a predictor of insulin resistance in first-degree relatives of type 2 diabetic patients. Obesity (Silver Spring) 2012;20(5):932-938.

82. Isakson P, Hammarstedt A, Gustafson B, Smith U. Impaired preadipocyte differentiation in human abdominal obesity: role of Wnt, tumor necrosis factor-alpha, and inflammation. Diabetes 2009;58(7):1550-1557.

83. Wueest S, Rapold RA, Rytka JM, Schoenle EJ, Konrad D. Basal lipolysis, not the degree of insulin resistance, differentiates large from small isolated adipocytes in high-fat fed mice. Diabetologia 2009;52(3):541-546.

84. Goossens GH, Bizzarri A, Venteclef N et al. Increased adipose tissue oxygen tension in obese compared with lean men is accompanied by insulin resistance, impaired adipose tissue capillarization, and inflammation. Circulation 2011;124(1):67-76.

85. Goossens GH, Blaak EE. Adipose tissue dysfunction and impaired metabolic health in human obesity: a matter of oxygen? Front Endocrinol (Lausanne) 2015;6:55.

86. Gartung A, Zhao J, Chen S et al. Characterization of Eicosanoids Produced by Adipocyte Lipolysis: IMPLICATION OF CYCLOOXYGENASE-2 IN ADIPOSE INFLAMMATION. J Biol Chem 2016;291(31):16001-16010.

87. Fujimori K. Prostaglandins as PPARgamma Modulators in Adipogenesis. PPAR Res 2012;2012:527607.

88. Gaidhu MP, Anthony NM, Patel P, Hawke TJ, Ceddia RB. Dysregulation of lipolysis and lipid metabolism in visceral and subcutaneous adipocytes by high-fat diet: role of ATGL, HSL, and AMPK. Am J Physiol Cell Physiol 2010;298(4):C961-971.

89. Wolf G. Adipose-specific phospholipase as regulator of adiposity. Nutr Rev 2009;67(9):551-554.

90. Ryden M, Jocken J, van Harmelen V et al. Comparative studies of the role of hormone-sensitive lipase and adipose triglyceride lipase in human fat cell lipolysis. Am J Physiol Endocrinol Metab 2007;292(6):E1847-1855.

91. Chatzipanteli K, Rudolph S, Axelrod L. Coordinate control of lipolysis by prostaglandin E2 and prostacyclin in rat adipose tissue. Diabetes 1992;41(8):927-935.

92. Hsieh PS, Lu KC, Chiang CF, Chen CH. Suppressive effect of COX2 inhibitor on the progression of adipose inflammation in high-fat-induced obese rats. Eur J Clin Invest 2010;40(2):164-171.

93. Adi N, Perriotte-Olson C, Desouza CV, Ramalingam R, Saraswathi V. Hematopoietic cyclooxygenase-2 deficiency increases adipose tissue inflammation and adiposity in obesity. Obesity (Silver Spring) 2015;23(10):2037-2045.

94. Hu X, Cifarelli V, Sun S, Kuda O, Abumrad NA, Su X. Major role of adipocyte prostaglandin E2 in lipolysis-induced macrophage recruitment. J Lipid Res 2016;57(4):663-673.

95. Ristimaki A, Sivula A, Lundin J et al. Prognostic significance of elevated cyclooxygenase-2 expression in breast cancer. Cancer Res 2002;62(3):632-635.

96. Howe LR, Subbaramaiah K, Brown AM, Dannenberg AJ. Cyclooxygenase-2: a target for the prevention and treatment of breast cancer. Endocr Relat Cancer 2001;8(2):97-114.

97. Wang X, Docanto MM, Sasano H et al. Prostaglandin E2 inhibits p53 in human breast adipose stromal cells: a novel mechanism for the regulation of aromatase in obesity and breast cancer. Cancer Res 2015;75(4):645-655.

98. Park J, Euhus DM, Scherer PE. Paracrine and endocrine effects of adipose tissue on cancer development and progression. Endocr Rev 2011;32(4):550-570.

99. Matsumoto T, Kano K, Kondo D et al. Mature adipocyte-derived dedifferentiated fat cells exhibit multilineage potential. J Cell Physiol 2008;215(1):210-222.

100. Schrey MP, Patel KV. Prostaglandin E2 production and metabolism in human breast cancer cells and breast fibroblasts. Regulation by inflammatory mediators. Br J Cancer 1995;72(6):1412-1419.

101. Greenhough A, Smartt HJ, Moore AE et al. The COX-2/PGE2 pathway: key roles in the hallmarks of cancer and adaptation to the tumour microenvironment. Carcinogenesis 2009;30(3):377-386.

102. Iyengar NM, Gucalp A, Dannenberg AJ, Hudis CA. Obesity and Cancer Mechanisms: Tumor Microenvironment and Inflammation. J Clin Oncol 2016;34(35):4270-4276.

103. Simpson ER, Brown KA. Minireview: Obesity and breast cancer: a tale of inflammation and dysregulated metabolism. Mol Endocrinol 2013;27(5):715-725.

104. Monaco ME. Fatty acid metabolism in breast cancer subtypes. Oncotarget 2017;8(17):29487-29500.

105. Cairns RA, Harris I, McCracken S, Mak TW. Cancer cell metabolism. Cold Spring Harb Symp Quant Biol 2011;76:299-311.

106. Anastasiou D. Tumour microenvironment factors shaping the cancer metabolism landscape. Br J Cancer 2017;116(3):277-286.

107. Kominsky DJ, Keely S, MacManus CF et al. An endogenously anti-inflammatory role for methylation in mucosal inflammation identified through metabolite profiling. J Immunol 2011;186(11):6505-6514.

108. Kiga K, Mimuro H, Suzuki M et al. Epigenetic silencing of miR-210 increases the proliferation of gastric epithelium during chronic Helicobacter pylori infection. Nat Commun 2014;5:4497.

109. Niwa T, Tsukamoto T, Toyoda T et al. Inflammatory processes triggered by Helicobacter pylori infection cause aberrant DNA methylation in gastric epithelial cells. Cancer Res 2010;70(4):1430-1440.

110. Lu T, Stark GR. NF-kappaB: Regulation by Methylation. Cancer Res 2015;75(18):3692-3695.

111. Cao B, Yang Y, Pan Y et al. Epigenetic silencing of CXCL14 induced colorectal cancer migration and invasion. Discov Med 2013;16(88):137-147.

112. Amodio N, Bellizzi D, Leotta M et al. miR-29b induces SOCS-1 expression by promoter demethylation and negatively regulates migration of multiple myeloma and endothelial cells. Cell Cycle 2013;12(23):3650-3662.

113. Iliopoulos D, Hirsch HA, Struhl K. An epigenetic switch involving NF-kappaB, Lin28, Let-7 MicroRNA, and IL6 links inflammation to cell transformation. Cell 2009;139(4):693-706.

114. Flegal KM, Kruszon-Moran D, Carroll MD, Fryar CD, Ogden CL. Trends in Obesity Among Adults in the United States, 2005 to 2014. JAMA 2016;315(21):2284-2291.

115. Jiralerspong S, Goodwin PJ. Obesity and Breast Cancer Prognosis: Evidence, Challenges, and Opportunities. J Clin Oncol 2016;34(35):4203-4216.

116. Yang XR, Chang-Claude J, Goode EL et al. Associations of breast cancer risk factors with tumor subtypes: a pooled analysis from the Breast Cancer Association Consortium studies. J Natl Cancer Inst 2011;103(3):250-263.

117. Litton JK, Gonzalez-Angulo AM, Warneke CL et al. Relationship between obesity and pathologic response to neoadjuvant chemotherapy among women with operable breast cancer. J Clin Oncol 2008;26(25):4072-4077.

118. Lashinger LM, Rossi EL, Hursting SD. Obesity and resistance to cancer chemotherapy: interacting roles of inflammation and metabolic dysregulation. Clin Pharmacol Ther 2014;96(4):458-463.

119. An Y, Liu K, Zhou Y, Liu B. Salicylate inhibits macrophage-secreted factors induced adipocyte inflammation and changes of adipokines in 3T3-L1 adipocytes. Inflammation 2009;32(5):296-303.

120. Shehzad A, Ha T, Subhan F, Lee YS. New mechanisms and the anti-inflammatory role of curcumin in obesity and obesity-related metabolic diseases. Eur J Nutr 2011;50(3):151-161.

121. Okuno A, Tamemoto H, Tobe K et al. Troglitazone increases the number of small adipocytes without the change of white adipose tissue mass in obese Zucker rats. J Clin Invest 1998;101(6):1354-1361.

122. Toubal A, Clement K, Fan R et al. SMRT-GPS2 corepressor pathway dysregulation coincides with obesity-linked adipocyte inflammation. J Clin Invest 2013;123(1):362-379.

123. Kusminski CM, Bickel PE, Scherer PE. Targeting adipose tissue in the treatment of obesity-associated diabetes. Nat Rev Drug Discov 2016;15(9):639-660.

124. Delmas D, Lancon A, Colin D, Jannin B, Latruffe N. Resveratrol as a chemopreventive agent: a promising molecule for fighting cancer. Curr Drug Targets 2006;7(4):423-442.

125. Lee HJ, Lim Y, Yang SJ. Involvement of resveratrol in crosstalk between adipokine adiponectin and hepatokine fetuin-A in vivo and in vitro. J Nutr Biochem 2015;26(11):1254-1260.

126. Ulrich S, Loitsch SM, Rau O et al. Peroxisome proliferator-activated receptor gamma as a molecular target of resveratrol-induced modulation of polyamine metabolism. Cancer Res 2006;66(14):7348-7354.

127. Ge H, Zhang JF, Guo BS et al. Resveratrol inhibits macrophage expression of EMMPRIN by activating PPARgamma. Vascul Pharmacol 2007;46(2):114-121.

128. Vanamala J, Reddivari L, Radhakrishnan S, Tarver C. Resveratrol suppresses IGF-1 induced human colon cancer cell proliferation and elevates apoptosis via suppression of IGF-1R/Wnt and activation of p53 signaling pathways. BMC Cancer 2010;10:238.

129. Yi CO, Jeon BT, Shin HJ et al. Resveratrol activates AMPK and suppresses LPS-induced NF-kappaB-dependent COX-2 activation in RAW 264.7 macrophage cells. Anat Cell Biol 2011;44(3):194-203.

130. Timmers S, Konings E, Bilet L et al. Calorie restriction-like effects of 30 days of resveratrol supplementation on energy metabolism and metabolic profile in obese humans. Cell Metab 2011;14(5):612-622.

131. Zagotta I, Dimova EY, Debatin KM, Wabitsch M, Kietzmann T, Fischer-Posovszky P. Obesity and inflammation: reduced cytokine expression due to resveratrol in a human in vitro model of inflamed adipose tissue. Front Pharmacol 2015;6:79.

132. Subbaramaiah K, Chung WJ, Michaluart P et al. Resveratrol inhibits cyclooxygenase-2 transcription and activity in phorbol ester-treated human mammary epithelial cells. J Biol Chem 1998;273(34):21875-21882.

133. Kundu JK, Shin YK, Kim SH, Surh YJ. Resveratrol inhibits phorbol ester-induced expression of COX-2 and activation of NF-kappaB in mouse skin by blocking IkappaB kinase activity. Carcinogenesis 2006;27(7):1465-1474.

134. Ford NA, Rossi EL, Barnett K et al. Omega-3-Acid Ethyl Esters Block the Protumorigenic Effects of Obesity in Mouse Models of Postmenopausal Basal-

like and Claudin-Low Breast Cancer. Cancer Prev Res (Phila) 2015;8(9):796-806.

135. Bowers LW, Maximo IX, Brenner AJ et al. NSAID use reduces breast cancer recurrence in overweight and obese women: role of prostaglandin-aromatase interactions. Cancer Res 2014;74(16):4446-4457.

136. Zeytin HE, Patel AC, Rogers CJ et al. Combination of a poxvirus-based vaccine with a cyclooxygenase-2 inhibitor (celecoxib) elicits antitumor immunity and long-term survival in CEA.Tg/MIN mice. Cancer Res 2004;64(10):3668-3678.

137. Lashinger LM, Malone LM, Brown GW et al. Rapamycin partially mimics the anticancer effects of calorie restriction in a murine model of pancreatic cancer. Cancer Prev Res (Phila) 2011;4(7):1041-1051.

138. Yee LD, Lester JL, Cole RM et al. Omega-3 fatty acid supplements in women at high risk of breast cancer have dose-dependent effects on breast adipose tissue fatty acid composition. Am J Clin Nutr 2010;91(5):1185-1194.

139. Yang P, Chan D, Felix E et al. Determination of endogenous tissue inflammation profiles by LC/MS/MS: COX- and LOX-derived bioactive lipids. Prostaglandins Leukot Essent Fatty Acids 2006;75(6):385-395.

140. Charan J, Kantharia ND. How to calculate sample size in animal studies? J Pharmacol Pharmacother 2013;4(4):303-306.

141. Ries CH, Cannarile MA, Hoves S et al. Targeting tumor-associated macrophages with anti-CSF-1R antibody reveals a strategy for cancer therapy. Cancer Cell 2014;25(6):846-859.

142. Katara GK, Kulshrestha A, Jaiswal MK, Pamarthy S, Gilman-Sachs A, Beaman KD. Inhibition of vacuolar ATPase subunit in tumor cells delays tumor growth by decreasing the essential macrophage population in the tumor microenvironment. Oncogene 2016;35(8):1058-1065.

143. Baur JA, Pearson KJ, Price NL et al. Resveratrol improves health and survival of mice on a high-calorie diet. Nature 2006;444(7117):337-342.

144. Zhang L, Dai F, Sheng PL, Chen ZQ, Xu QP, Guo YQ. Resveratrol analogue 3,4,4'-trihydroxy-trans-stilbene induces apoptosis and autophagy in human non-small-cell lung cancer cells in vitro. Acta Pharmacol Sin 2015;36(10):1256-1265.

145. Gu S, Chen C, Jiang X, Zhang Z. Resveratrol synergistically triggers apoptotic cell death with arsenic trioxide via oxidative stress in human lung adenocarcinoma A549 cells. Biol Trace Elem Res 2015;163(1-2):112-123.

146. Cho J, Rho O, Junco J et al. Effect of Combined Treatment with Ursolic Acid and Resveratrol on Skin Tumor Promotion by 12-O-Tetradecanoylphorbol-13-Acetate. Cancer Prev Res (Phila) 2015;8(9):817-825.

147. Tan L, Wang W, He G et al. Resveratrol inhibits ovarian tumor growth in an in vivo mouse model. Cancer 2016;122(5):722-729.

148. Demoulin B, Hermant M, Castrogiovanni C, Staudt C, Dumont P. Resveratrol induces DNA damage in colon cancer cells by poisoning topoisomerase II and activates the ATM kinase to trigger p53-dependent apoptosis. Toxicol In Vitro 2015;29(5):1156-1165.

149. Narayanan NK, Nargi D, Randolph C, Narayanan BA. Liposome encapsulation of curcumin and resveratrol in combination reduces prostate cancer incidence in PTEN knockout mice. Int J Cancer 2009;125(1):1-8.

150. Kang W, Hong HJ, Guan J et al. Resveratrol improves insulin signaling in a tissue-specific manner under insulin-resistant conditions only: in vitro and in vivo experiments in rodents. Metabolism 2012;61(3):424-433.

151. Carreras A, Zhang SX, Peris E et al. Effect of resveratrol on visceral white adipose tissue inflammation and insulin sensitivity in a mouse model of sleep apnea. Int J Obes (Lond) 2015;39(3):418-423.

152. Yusuf N, Nasti TH, Meleth S, Elmets CA. Resveratrol enhances cell-mediated immune response to DMBA through TLR4 and prevents DMBA induced cutaneous carcinogenesis. Mol Carcinog 2009;48(8):713-723.

153. Cawthorn WP, Heyd F, Hegyi K, Sethi JK. Tumour necrosis factor-alpha inhibits adipogenesis via a beta-catenin/TCF4(TCF7L2)-dependent pathway. Cell Death Differ 2007;14(7):1361-1373.

154. Qi C, Pekala PH. Tumor necrosis factor-alpha-induced insulin resistance in adipocytes. Proc Soc Exp Biol Med 2000;223(2):128-135.

155. Kang L, Heng W, Yuan A, Baolin L, Fang H. Resveratrol modulates adipokine expression and improves insulin sensitivity in adipocytes: Relative to inhibition of inflammatory responses. Biochimie 2010;92(7):789-796.

156. Ye J, Gimble JM. Regulation of stem cell differentiation in adipose tissue by chronic inflammation. Clin Exp Pharmacol Physiol 2011;38(12):872-878.

157. Hu P, Zhao L, Chen J. Physiologically achievable doses of resveratrol enhance 3T3-L1 adipocyte differentiation. Eur J Nutr 2015;54(4):569-579.

158. Engelman JA, Berg AH, Lewis RY, Lisanti MP, Scherer PE. Tumor necrosis factor alpha-mediated insulin resistance, but not dedifferentiation, is abrogated by MEK1/2 inhibitors in 3T3-L1 adipocytes. Mol Endocrinol 2000;14(10):1557-1569.

159. Colitti M, Stefanon B. Different anti-adipogenic effects of bio-compounds on primary visceral pre-adipocytes and adipocytes. EXCLI J 2016;15:362-377.

160. Floyd ZE, Wang ZQ, Kilroy G, Cefalu WT. Modulation of peroxisome proliferator-activated receptor gamma stability and transcriptional activity in adipocytes by resveratrol. Metabolism 2008;57(7 Suppl 1):S32-38.

161. Fu Y, Chang H, Peng X et al. Resveratrol inhibits breast cancer stem-like cells and induces autophagy via suppressing Wnt/beta-catenin signaling pathway. PLoS One 2014;9(7):e102535.

162. Agarwal B, Baur JA. Resveratrol and life extension. Ann N Y Acad Sci 2011;1215:138-143.

163. Konings E, Timmers S, Boekschoten MV et al. The effects of 30 days resveratrol supplementation on adipose tissue morphology and gene expression patterns in obese men. Int J Obes (Lond) 2014;38(3):470-473.

164. Mallon PW, Sedwell R, Rogers G et al. Effect of rosiglitazone on peroxisome proliferator-activated receptor gamma gene expression in human adipose tissue is limited by antiretroviral drug-induced mitochondrial dysfunction. J Infect Dis 2008;198(12):1794-1803.

165. Zou T, Chen D, Yang Q et al. Resveratrol supplementation of high-fat diet-fed pregnant mice promotes brown and beige adipocyte development and prevents obesity in male offspring. J Physiol 2017;595(5):1547-1562.

166. Arias N, Pico C, Teresa Macarulla M et al. A combination of resveratrol and quercetin induces browning in white adipose tissue of rats fed an obesogenic diet. Obesity (Silver Spring) 2017;25(1):111-121.

167. Price NL, Gomes AP, Ling AJ et al. SIRT1 is required for AMPK activation and the beneficial effects of resveratrol on mitochondrial function. Cell Metab 2012;15(5):675-690.

168. Lafontan M, Langin D. Lipolysis and lipid mobilization in human adipose tissue. Prog Lipid Res 2009;48(5):275-297.

169. Khatib SA, Rossi EL, Bowers LW, Hursting SD. Reducing the burden of obesity-associated cancers with anti-inflammatory long-chain omega-3 polyunsaturated fatty acids. Prostaglandins Other Lipid Mediat 2016;125:100-107.

170. Michaud A, Pelletier M, Noel S, Bouchard C, Tchernof A. Markers of macrophage infiltration and measures of lipolysis in human abdominal adipose tissues. Obesity (Silver Spring) 2013;21(11):2342-2349.

171. Kaidi A, Qualtrough D, Williams AC, Paraskeva C. Direct transcriptional up-regulation of cyclooxygenase-2 by hypoxia-inducible factor (HIF)-1 promotes colorectal tumor cell survival and enhances HIF-1 transcriptional activity during hypoxia. Cancer Res 2006;66(13):6683-6691.

172. Zhou L, Li K, Luo Y et al. Novel prognostic markers for patients with triple-negative breast cancer. Hum Pathol 2013;44(10):2180-2187.

173. Loveridge CJ, MacDonald AD, Thoms HC, Dunlop MG, Stark LA. The proapoptotic effects of sulindac, sulindac sulfone and indomethacin are mediated by nucleolar translocation of the RelA(p65) subunit of NF-kappaB. Oncogene 2008;27(18):2648-2655.

174. Yamamoto Y, Yin MJ, Lin KM, Gaynor RB. Sulindac inhibits activation of the NF-kappaB pathway. J Biol Chem 1999;274(38):27307-27314.

175. Yin T, Wang G, Ye T, Wang Y. Sulindac, a non-steroidal anti-inflammatory drug, mediates breast cancer inhibition as an immune modulator. Sci Rep 2016;6:19534.

176. Lopez-Vicario C, Alcaraz-Quiles J, Garcia-Alonso V et al. Inhibition of soluble epoxide hydrolase modulates inflammation and autophagy in obese adipose tissue and liver: role for omega-3 epoxides. Proc Natl Acad Sci U S A 2015;112(2):536-541.

177. Whiteman MK, Hillis SD, Curtis KM, McDonald JA, Wingo PA, Marchbanks PA. Body mass and mortality after breast cancer diagnosis. Cancer Epidemiol Biomarkers Prev 2005;14(8):2009-2014.

178. Sinicrope FA, Dannenberg AJ. Obesity and breast cancer prognosis: weight of the evidence. J Clin Oncol 2011;29(1):4-7.

179. Lashinger LM, Ford NA, Hursting SD. Interacting inflammatory and growth factor signals underlie the obesity-cancer link. J Nutr 2014;144(2):109-113.

180. Bhardwaj P, Du B, Zhou XK et al. Caloric restriction reverses obesity-induced mammary gland inflammation in mice. Cancer Prev Res (Phila) 2013;6(4):282-289.

181. Milagro FI, Campion J, Cordero P et al. A dual epigenomic approach for the search of obesity biomarkers: DNA methylation in relation to diet-induced weight loss. FASEB J 2011;25(4):1378-1389.

182. Yoo KH, Hennighausen L. EZH2 methyltransferase and H3K27 methylation in breast cancer. Int J Biol Sci 2012;8(1):59-65.

183. Borengasser SJ, Kang P, Faske J et al. High fat diet and in utero exposure to maternal obesity disrupts circadian rhythm and leads to metabolic programming of liver in rat offspring. PLoS One 2014;9(1):e84209.

184. Hursting SD, Digiovanni J, Dannenberg AJ et al. Obesity, energy balance, and cancer: new opportunities for prevention. Cancer Prev Res (Phila) 2012;5(11):1260-1272.

185. Sundaram S, Le TL, Essaid L et al. Weight Loss Reversed Obesity-Induced HGF/c-Met Pathway and Basal-Like Breast Cancer Progression. Front Oncol 2014;4:175.

186. Fabian CJ, Kimler BF, Donnelly JE et al. Favorable modulation of benign breast tissue and serum risk biomarkers is associated with > 10 % weight loss in postmenopausal women. Breast Cancer Res Treat 2013;142(1):119-132.

187. De Angel RE, Blando JM, Hogan MG et al. Stearoyl gemcitabine nanoparticles overcome obesity-induced cancer cell resistance to gemcitabine in a mouse postmenopausal breast cancer model. Cancer Biol Ther 2013;14(4):357-364.

188. Nogueira LM, Dunlap SM, Ford NA, Hursting SD. Calorie restriction and rapamycin inhibit MMTV-Wnt-1 mammary tumor growth in a mouse model of postmenopausal obesity. Endocr Relat Cancer 2012;19(1):57-68.

189. Gertz J, Varley KE, Reddy TE et al. Analysis of DNA methylation in a three-generation family reveals widespread genetic influence on epigenetic regulation. PLoS Genet 2011;7(8):e1002228.

190. Gu H, Smith ZD, Bock C, Boyle P, Gnirke A, Meissner A. Preparation of reduced representation bisulfite sequencing libraries for genome-scale DNA methylation profiling. Nat Protoc 2011;6(4):468-481.

191. Hair BY, Xu Z, Kirk EL et al. Body mass index associated with genome-wide methylation in breast tissue. Breast Cancer Res Treat 2015;151(2):453-463.

192. De Angel RE, Conti CJ, Wheatley KE et al. The enhancing effects of obesity on mammary tumor growth and Akt/mTOR pathway activation persist after weight loss and are reversed by RAD001. Mol Carcinog 2013;52(6):446-458.

193. Svirshchevskaya EV, Mariotti J, Wright MH et al. Rapamycin delays growth of Wnt-1 tumors in spite of suppression of host immunity. BMC Cancer 2008;8:176.

194. Furet JP, Kong LC, Tap J et al. Differential adaptation of human gut microbiota to bariatric surgery-induced weight loss: links with metabolic and low-grade inflammation markers. Diabetes 2010;59(12):3049-3057.

195. Sjostrom L, Narbro K, Sjostrom CD et al. Effects of bariatric surgery on mortality in Swedish obese subjects. N Engl J Med 2007;357(8):741-752.

196. Dandona P, Aljada A, Bandyopadhyay A. Inflammation: the link between insulin resistance, obesity and diabetes. Trends Immunol 2004;25(1):4-7.

197. Shoelson SE, Herrero L, Naaz A. Obesity, inflammation, and insulin resistance. Gastroenterology 2007;132(6):2169-2180.

198. Bachmann IM, Halvorsen OJ, Collett K et al. EZH2 expression is associated with high proliferation rate and aggressive tumor subgroups in cutaneous melanoma and cancers of the endometrium, prostate, and breast. J Clin Oncol 2006;24(2):268-273.

199. Kleer CG, Cao Q, Varambally S et al. EZH2 is a marker of aggressive breast cancer and promotes neoplastic transformation of breast epithelial cells. Proc Natl Acad Sci U S A 2003;100(20):11606-11611.

200. Hamamoto R, Silva FP, Tsuge M et al. Enhanced SMYD3 expression is essential for the growth of breast cancer cells. Cancer Sci 2006;97(2):113-118.

201. Wagner JR, Busche S, Ge B, Kwan T, Pastinen T, Blanchette M. The relationship between DNA methylation, genetic and expression inter-individual variation in untransformed human fibroblasts. Genome Biol 2014;15(2):R37.

202. Jones PA. Functions of DNA methylation: islands, start sites, gene bodies and beyond. Nat Rev Genet 2012;13(7):484-492.

203. Chen X, Lu W, Zheng W et al. Obesity and weight change in relation to breast cancer survival. Breast Cancer Res Treat 2010;122(3):823-833.

204. Chen J, Tian ZQ, Zhang WG et al. [Relationship between visceral adipose tissue and prevalence of metabolic syndrome MS in patients with MS, and hypertension and/or diabetes]. Zhonghua Yi Xue Za Zhi 2006;86(30):2110-2113.

205. Lekva T, Bollerslev J, Godang K et al. beta-cell dysfunction in women with previous gestational diabetes is associated with visceral adipose tissue distribution. Eur J Endocrinol 2015;173(1):63-70.

206. Gonzalez N, Moreno-Villegas Z, Gonzalez-Bris A, Egido J, Lorenzo O. Regulation of visceral and epicardial adipose tissue for preventing cardiovascular injuries associated to obesity and diabetes. Cardiovasc Diabetol 2017;16(1):44.

207. Rittig K, Hieronimus A, Thamer C et al. Reducing visceral adipose tissue mass is essential for improving endothelial function in type 2 diabetes prone individuals. Atherosclerosis 2010;212(2):575-579.

208. Morigny P, Houssier M, Mouisel E, Langin D. Adipocyte lipolysis and insulin resistance. Biochimie 2016;125:259-266.

209. Iyengar P, Combs TP, Shah SJ et al. Adipocyte-secreted factors synergistically promote mammary tumorigenesis through induction of anti-apoptotic transcriptional programs and proto-oncogene stabilization. Oncogene 2003;22(41):6408-6423.

210. Arner P. Human fat cell lipolysis: biochemistry, regulation and clinical role. Best Pract Res Clin Endocrinol Metab 2005;19(4):471-482.

211. Lauby-Secretan B, Scoccianti C, Loomis D et al. Body Fatness and Cancer--Viewpoint of the IARC Working Group. N Engl J Med 2016;375(8):794-798.

212. Rossi EL, de Angel RE, Bowers LW et al. Obesity-Associated Alterations in Inflammation, Epigenetics, and Mammary Tumor Growth Persist in Formerly Obese Mice. Cancer Prev Res (Phila) 2016;9(5):339-348.

213. Nicoletti CF, Nonino CB, de Oliveira BA et al. DNA Methylation and Hydroxymethylation Levels in Relation to Two Weight Loss Strategies: Energy-Restricted Diet or Bariatric Surgery. Obes Surg 2016;26(3):603-611.

214. Sugiura K, Stock CC. Studies in a tumor spectrum. II. The effect of 2,4,6-triethylenimino-s-triazine on the growth of a variety of mouse and rat tumors. Cancer 1952;5(5):979-991.

215. Wilson-Perez HE, Chambers AP, Ryan KK et al. Vertical sleeve gastrectomy is effective in two genetic mouse models of glucagon-like Peptide 1 receptor deficiency. Diabetes 2013;62(7):2380-2385.

216. Cinti S, Mitchell G, Barbatelli G et al. Adipocyte death defines macrophage localization and function in adipose tissue of obese mice and humans. J Lipid Res 2005;46(11):2347-2355.

217. Wang J, Duncan D, Shi Z, Zhang B. WEB-based GEne SeT AnaLysis Toolkit (WebGestalt): update 2013. Nucleic Acids Res 2013;41(Web Server issue):W77-83.

218. Cuvillier O, Pirianov G, Kleuser B et al. Suppression of ceramide-mediated programmed cell death by sphingosine-1-phosphate. Nature 1996;381(6585):800-803.

219. Maceyka M, Sankala H, Hait NC et al. SphK1 and SphK2, sphingosine kinase isoenzymes with opposing functions in sphingolipid metabolism. J Biol Chem 2005;280(44):37118-37129.

220. Henegar C, Tordjman J, Achard V et al. Adipose tissue transcriptomic signature highlights the pathological relevance of extracellular matrix in human obesity. Genome Biol 2008;9(1):R14.

221. Kolak M, Gertow J, Westerbacka J et al. Expression of ceramide-metabolising enzymes in subcutaneous and intra-abdominal human adipose tissue. Lipids Health Dis 2012;11:115.

222. Kolak M, Westerbacka J, Velagapudi VR et al. Adipose tissue inflammation and increased ceramide content characterize subjects with high liver fat content independent of obesity. Diabetes 2007;56(8):1960-1968.

223. Kitada Y, Kajita K, Taguchi K et al. Blockade of Sphingosine 1-Phosphate Receptor 2 Signaling Attenuates High-Fat Diet-Induced Adipocyte Hypertrophy and Systemic Glucose Intolerance in Mice. Endocrinology 2016;157(5):1839-1851.

224. Bryan L, Kordula T, Spiegel S, Milstien S. Regulation and functions of sphingosine kinases in the brain. Biochim Biophys Acta 2008;1781(9):459-466.

225. Granata R, Trovato L, Lupia E et al. Insulin-like growth factor binding protein-3 induces angiogenesis through IGF-I- and SphK1-dependent mechanisms. J Thromb Haemost 2007;5(4):835-845.

226. Xu CY, Liu SQ, Qin MB et al. SphK1 modulates cell migration and EMT-related marker expression by regulating the expression of p-FAK in colorectal cancer cells. Int J Mol Med 2017;39(5):1277-1284.

227. Zheng XD, Zhang Y, Qi XW et al. Role of Sphk1 in the malignant transformation of breast epithelial cells and breast cancer progression. Indian J Cancer 2014;51(4):524-529.

228. Bouquerel P, Gstalder C, Muller D et al. Essential role for SphK1/S1P signaling to regulate hypoxia-inducible factor 2alpha expression and activity in cancer. Oncogenesis 2016;5:e209.

229. Calle EE, Thun MJ. Obesity and cancer. Oncogene 2004;23(38):6365-6378.

230. Beasley JM, Newcomb PA, Trentham-Dietz A et al. Post-diagnosis dietary factors and survival after invasive breast cancer. Breast Cancer Res Treat 2011;128(1):229-236.

231. Kraschnewski JL, Boan J, Esposito J et al. Long-term weight loss maintenance in the United States. Int J Obes (Lond) 2010;34(11):1644-1654.

233. Verhoef SP, Camps SG, Bouwman FG, Mariman EC, Westerterp KR. Physiological response of adipocytes to weight loss and maintenance. PLoS One 2013;8(3):e58011.

234. Dulloo AG, Jacquet J, Seydoux J, Montani JP. The thrifty 'catch-up fat' phenotype: its impact on insulin sensitivity during growth trajectories to obesity and metabolic syndrome. Int J Obes (Lond) 2006;30 Suppl 4:S23-35.

235. Camps SG, Verhoef SP, Westerterp KR. Weight loss, weight maintenance, and adaptive thermogenesis. Am J Clin Nutr 2013;97(5):990-994.

236. Rosenbaum M, Hirsch J, Gallagher DA, Leibel RL. Long-term persistence of adaptive thermogenesis in subjects who have maintained a reduced body weight. Am J Clin Nutr 2008;88(4):906-912.

237. Kovacikova M, Sengenes C, Kovacova Z et al. Dietary intervention-induced weight loss decreases macrophage content in adipose tissue of obese women. Int J Obes (Lond) 2011;35(1):91-98.

238. Kosteli A, Sugaru E, Haemmerle G et al. Weight loss and lipolysis promote a dynamic immune response in murine adipose tissue. J Clin Invest 2010;120(10):3466-3479.

239. Dulloo AG. Regulation of fat storage via suppressed thermogenesis: a thrifty phenotype that predisposes individuals with catch-up growth to insulin resistance and obesity. Horm Res 2006;65 Suppl 3:90-97.

240. Fraga MF, Ballestar E, Paz MF et al. Epigenetic differences arise during the lifetime of monozygotic twins. Proc Natl Acad Sci U S A 2005;102(30):10604-10609.

241. Ma Y, Xia W, Wang DQ et al. Hepatic DNA methylation modifications in early development of rats resulting from perinatal BPA exposure contribute to insulin resistance in adulthood. Diabetologia 2013;56(9):2059-2067.

242. Kananen L, Marttila S, Nevalainen T et al. Aging-associated DNA methylation changes in middle-aged individuals: the Young Finns study. BMC Genomics 2016;17:103.

243. Weidner CI, Lin Q, Koch CM et al. Aging of blood can be tracked by DNA methylation changes at just three CpG sites. Genome Biol 2014;15(2):R24.

244. Wagner W, Fernandez-Rebollo E, Frobel J. DNA-methylation changes in replicative senescence and aging: two sides of the same coin? Epigenomics 2016;8(1):1-3.

245. Day SE, Coletta RL, Kim JY et al. Next-generation sequencing methylation profiling of subjects with obesity identifies novel gene changes. Clin Epigenetics 2016;8:77.

246. Youngson NA, Lecomte V, Maloney CA et al. Obesity-induced sperm DNA methylation changes at satellite repeats are reprogrammed in rat offspring. Asian J Androl 2016;18(6):930-936.

247. Nadler ST, Stoehr JP, Schueler KL, Tanimoto G, Yandell BS, Attie AD. The expression of adipogenic genes is decreased in obesity and diabetes mellitus. Proc Natl Acad Sci U S A 2000;97(21):11371-11376.

248. Dubois-Chevalier J, Staels B, Lefebvre P, Eeckhoute J. The ubiquitous transcription factor CTCF promotes lineage-specific epigenomic remodeling and establishment of transcriptional networks driving cell differentiation. Nucleus 2015;6(1):15-18.

249. Panchenko PE, Voisin S, Jouin M et al. Expression of epigenetic machinery genes is sensitive to maternal obesity and weight loss in relation to fetal growth in mice. Clin Epigenetics 2016;8:22.

250. Oger F, Dubois-Chevalier J, Gheeraert C et al. Peroxisome proliferator-activated receptor gamma regulates genes involved in insulin/insulin-like growth factor signaling and lipid metabolism during adipogenesis through functionally distinct enhancer classes. J Biol Chem 2014;289(2):708-722.

251. Melzner I, Scott V, Dorsch K et al. Leptin gene expression in human preadipocytes is switched on by maturation-induced demethylation of distinct CpGs in its proximal promoter. J Biol Chem 2002;277(47):45420-45427.

252. Okamura M, Inagaki T, Tanaka T, Sakai J. Role of histone methylation and demethylation in adipogenesis and obesity. Organogenesis 2010;6(1):24-32.

253. Musri MM, Corominola H, Casamitjana R, Gomis R, Parrizas M. Histone H3 lysine 4 dimethylation signals the transcriptional competence of the adiponectin promoter in preadipocytes. J Biol Chem 2006;281(25):17180-17188.

254. Parrillo L, Costa V, Raciti GA et al. Hoxa5 undergoes dynamic DNA methylation and transcriptional repression in the adipose tissue of mice exposed to high-fat diet. Int J Obes (Lond) 2016;40(6):929-937.

255. Szemes M, Dallosso AR, Melegh Z et al. Control of epigenetic states by WT1 via regulation of de novo DNA methyltransferase 3A. Hum Mol Genet 2013;22(1):74-83.

256. McLaughlin T, Lamendola C, Coghlan N et al. Subcutaneous adipose cell size and distribution: relationship to insulin resistance and body fat. Obesity (Silver Spring) 2014;22(3):673-680.

257. Crujeiras AB, Diaz-Lagares A, Moreno-Navarrete JM et al. Genome-wide DNA methylation pattern in visceral adipose tissue differentiates insulin-resistant from insulin-sensitive obese subjects. Transl Res 2016;178:13-24 e15.

258. Volkov P, Olsson AH, Gillberg L et al. A Genome-Wide mQTL Analysis in Human Adipose Tissue Identifies Genetic Variants Associated with DNA Methylation, Gene Expression and Metabolic Traits. PLoS One 2016;11(6):e0157776.

259. Drogan D, Boeing H, Janke J et al. Regional distribution of body fat in relation to DNA methylation within the LPL, ADIPOQ and PPARgamma promoters in subcutaneous adipose tissue. Nutr Diabetes 2015;5:e168.

260. Kamei Y, Suganami T, Ehara T et al. Increased expression of DNA methyltransferase 3a in obese adipose tissue: studies with transgenic mice. Obesity (Silver Spring) 2010;18(2):314-321.

261. Harris RB. Direct and indirect effects of leptin on adipocyte metabolism. Biochim Biophys Acta 2014;1842(3):414-423.

262. Zhou YT, Wang ZW, Higa M, Newgard CB, Unger RH. Reversing adipocyte differentiation: implications for treatment of obesity. Proc Natl Acad Sci U S A 1999;96(5):2391-2395.

263. Milagro FI, Campion J, Garcia-Diaz DF, Goyenechea E, Paternain L, Martinez JA. High fat diet-induced obesity modifies the methylation pattern of leptin promoter in rats. J Physiol Biochem 2009;65(1):1-9.

264. Zwamborn RA, Slieker RC, Mulder PC et al. Prolonged high-fat diet induces gradual and fat depot-specific DNA methylation changes in adult mice. Sci Rep 2017;7:43261.

265. Kuroda M, Tominaga A, Nakagawa K et al. DNA Methylation Suppresses Leptin Gene in 3T3-L1 Adipocytes. PLoS One 2016;11(8):e0160532.

266. William WN, Jr., Ceddia RB, Curi R. Leptin controls the fate of fatty acids in isolated rat white adipocytes. J Endocrinol 2002;175(3):735-744.

267. Finetti F, Solito R, Morbidelli L, Giachetti A, Ziche M, Donnini S. Prostaglandin E2 regulates angiogenesis via activation of fibroblast growth factor receptor-1. J Biol Chem 2008;283(4):2139-2146.

268. Choe SS, Huh JY, Hwang IJ, Kim JI, Kim JB. Adipose Tissue Remodeling: Its Role in Energy Metabolism and Metabolic Disorders. Front Endocrinol (Lausanne) 2016;7:30.

269. Chen YS, Wu R, Yang X et al. Inhibiting DNA methylation switches adipogenesis to osteoblastogenesis by activating Wnt10a. Sci Rep 2016;6:25283.

270. Benton MC, Johnstone A, Eccles D et al. An analysis of DNA methylation in human adipose tissue reveals differential modification of obesity genes before and after gastric bypass and weight loss. Genome Biol 2015;16:8.

271. Nie B, Nie T, Hui X et al. Brown Adipogenic Reprogramming Induced by a Small Molecule. Cell Rep 2017;18(3):624-635.

272. Khan S, Ullah MW, Siddique R et al. Role of Recombinant DNA Technology to Improve Life. Int J Genomics 2016;2016:2405954.